THE INITIATION OF YIELDING AND BRITTLE FRACTURE IN ANNEALED MILD STEEL

Thesis by

James A. Hendrickson

In Partial Fulfillment of the Requirements

for the Degree of

Doctor of Philosophy

California Institute of Technology

Pasadena, California

1957

ACKNOWLEDGEMENTS

Acknowledgement is made to the Union Carbide and Carbon Corporation for the fellowship granted to the author during the latter stages of this research. Acknowledgement is also made to the Office of Naval Research and the Office of Ordnance Research, U.S. Army, whose financial support made this work possible. Particular appreciation is expressed to Professor D. S. Wood of the California Institute of Technology for his guidance and personal encouragement to the author.

Appreciation is also expressed to Professors D. S. Clark and G. W. Housner of the California Institute of Technology for their invaluable suggestions and comments during the course of this research. Thanks are extended to Mr. Wilfred D. Iwan of the California Institute of Technology for his assistance in many phases of the experimental work, and his assistance in the preparation of many of the figures appearing in this thesis.

ABSTRACT

The initiation of brittle fracture and the transition between ductile and brittle behavior of an annealed mild steel has been investigated. A theoretical and experimental investigation has been made on notched tensile specimens to determine the state of stress beneath a notch which governs the initiation of a brittle fracture. The experimental investigation was conducted for constant rates of stress application of from 10^2 to 10^7 lb/in.^{2} sec at temperatures of -110° F (-79° C) and -200° F (-129° C). The stress analysis of the notched specimen includes the effect of limited plastic deformation known to precede brittle fracture.

The true tensile stress at the position and instant of initiation of brittle fracture in the notched tensile specimens is determined from the experimental results, a knowledge of the yielding behavior of the material, and the elastic-plastic stress analysis. In this manner it is shown that brittle fracture occurs when a critical value of the maximum tensile stress is attained. This critical value of the tensile stress is found to be constant, independent of rate and temperature, and is shown to occur at the elastic-plastic boundary beneath the root of the notch.

The information gained from the investigation of the initiation of brittle fracture in notched tensile specimens is applied to the prediction of the transition temperature in the case of the Izod impact test. The prediction is checked by experiment and the agreement is found to be good.

TABLE OF CONTENTS

TABLE OF CONTENTS (Cont'd)

LIST OF FIGURES

LIST OF FIGURES (Cont'd)

LIST OF FIGURES (Cont'd)

LIST OF TABLES

I. INTRODUCTION

Structural steel has become of ever increasing importance since Bessemer first introduced his steelmaking process in 1856. Steel is readily available, economical and under normal conditions it possesses excellent mechanical qualities. One of these qualities of particular importance is the fact that structural or mild steel will normally undergo a large amount of plastic deformation before it fractures. This property is known as ductility. A high local stress in a structure of ductile material will cause local plastic flow or yielding to occur, if this stress is in excess of the yield point of the material. This local yielding may act to redistribute the high stresses in such a way that no further yielding will occur. Hence, the normal ductile properties of mild steel would seem to make it ideally suited as a structural material.

Shortly after the introduction of mild steel as a structural material, however, a strange property of the material was reported. In certain instances steel structures were observed to suffer sudden and catastrophic failure without apparent prior plastic deformation. However, when material from the fractured structure was subjected to a standard tensile test, it was found to possess a normal amount of ductility. The reports of cases of these catastrophic failures are not isolated. Such failures have been recorded for bridges, pressure vessels, pipe lines, ships, etc. (1)*. Some of the more recent and spectacular of these failures involve the breaking up of T-2 tankers and Liberty ships

---

*Figures appearing in parentheses refer to references listed at the end of this thesis.

during the second World War. Such failures have become known as "brittle", as opposed to "ductile" fractures, due to the apparent lack of plastic deformation.

Investigations of cases of brittle fractures showed that in each case the structure failed during, or soon after, a condition of low temperature existed. The fractures were found to be of the cleavage type, instead of failure in shear which is normal to ductile materials. Often the fracture surfaces exhibited herringbone markings. The apex of these markings were found to point to a common origin, presumably the origin of fracture. In this manner, it was found that the brittle crack originated at a place of high stress concentration, such as a notch or sharp corner. Also, in many instances, the occurrence of a brittle type fracture was identified with a high rate of stress rise, such as an impact.

Extensive experimental research on the problem of brittle fracture has been in progress since the latter part of the nineteenth century. The vast majority of this research has been connected with notched bar impact tests of materials such as mild steel. The purpose of these tests is to determine the amount of energy absorbed by the material as a function of the temperature. Impact tests on mild steel, for instance, show that at high temperatures a large amount of energy is absorbed. However, as the temperature is decreased the amount of energy absorbed decreases until at low temperatures an extremely small amount of energy is absorbed, i.e., brittle behavior is observed.

The transition from ductile to brittle behavior in notched bar impact tests is not sudden, rather, there is a gradual transition.

However, investigators have come to accept a certain amount of absorbed energy as indicating the temperature at which transition from ductile to brittle behavior occurs. This temperature has been called the "transition temperature".

A transition from ductile to brittle behavior in conventional notched bar impact tests has been found to occur in many, if not all, of the metals which exhibit the body-centered cubic crystal structure. While some of the hexagonal close-packed metals also exhibit a transition temperature, the face-centered cubic metals do not (1). It is significant that the classification of metals on the basis of their crystal structure also differentiates those which do and do not exhibit distinct yield points or discontinuous yielding in their conventional stress-strain relations. The metals that crystallize in the body-centered cubic structure and some of those that have hexagonal structure exhibit distinct yield points, while the face centered cubic metals do not. Those metals that exhibit a transition temperature and distinct yield points also exhibit delayed yielding (2), (3), (4), (5), (6). The probability is thus strong that the existence of a ductile to brittle transition temperature and delayed yielding are closely related.

Many attempts have been made by engineers to find a remedy to the brittle fracture problem. Much of the progress in the brittle fracture field has come about by studying the effects of metallurgical variables such as chemical composition, grain size, etc., on the suppression of the transition temperature in notched bar impact tests of structural materials. By proper metallurgical

control, engineers have to a certain extent been able to reduce the susceptibility of structures to the initiation of brittle fracture. Other means have also been used in an attempt to lessen the susceptibility of a structure to brittle fracture. One of the earliest attempts in this line was to install crack arrestors, or extra material, near places of high stress concentration. However, these attempts were only moderately successful because of the extremely fast speed with which a brittle crack progresses (several thousand ft/sec), thus allowing the crack to travel through regions of low stress.

The study of the brittle fracture phenomenon has so far not led to a basic understanding of its mechanism. Various suggestions as to the cause of brittle fracture have been made. For instance, earlier investigators thought that a brittle fracture was truly brittle, i.e., that no plastic deformation occurred. The role of the notches in the impact tests was then thought to be due to the triaxial stress state existing beneath the notch, tending to inhibit plastic flow. The reason for the transition phenomenon was not satisfactorily explained. Recent investigations have definitely shown that a brittle fracture is not truly brittle. In fact, even in the presence of the most severe notches, a small but perceptible amount of plastic flow occurs (7).

Hence, it seems that the factors that must be considered in obtaining a basic understanding of the brittle fracture and transition phenomenon are low temperature, rate of stress rise, notches or stress raisers and the yielding behavior of the material. An understanding of the interdependence of these parameters is of importance

from two points of view. First, such an understanding is necessary for the establishment of quantitative methods by which the susceptibility of structures to brittle fracture in service may be predicted from the results of laboratory fracture tests. Second, quantitative knowledge and control of these macroscopic parameters is a prerequisite to the planning and interpretation of experimental investigations concerning the microscopic or atomistic mechanisms of the initiation of brittle fracture. Investigations of the latter type are the means by which a fundamental understanding of the influence of metallurgical variables such as grain size, chemical composition, heat treatment, etc. upon the initiation of brittle fracure may be obtained. An understanding of the mechanism by which brittle fracture is initiated may require new, rather than traditional, avenues of approach, as has been indicated by Shank (1) in an excellent summary of progress in the field of brittle fracture.

The study of the phenomenon of brittle fracture may be broken up into two main fields of endeavor. First, the initiation of brittle fracture, i.e., what factors combined give rise to the formation of the crack. Second, the study of the propagation of the crack. This thesis will be concerned only with the first of these two aspects. Furthermore, the material investigated will be limited to an annealed mild steel.

The purpose of this investigation is to determine quantitatively the inter-relationship between temperature, loading rate and notch geometry which governs the initiation of brittle fracture. A further purpose is to determine the relationship of these parameters to the transition temperature, and what relationship, if any, exists

between the transition from ductile to brittle behavior and the delayed yield phenomenon.

The first section of this thesis is devoted to a study of the yielding behavior of mild steel when subjected to different temperatures and different constant rates of loading. This information is necessary to the study of the effect of limited plastic deformation on the brittle fracture phenomenon. The second section of the thesis is concerned with the effect of temperature, loading rate and limited plastic deformation on the brittle fracture behavior of notched tensile specimens.

The purpose of the tests on notched specimens is to investigate the true stress state, including the effects of limited plastic deformation, that exists beneath the notch at the instant of initiation of fracture. The true stress state is obtained by combining experimental results of fracture tests with an elastic-plastic stress analysis of the notched specimen. The yielding behavior of the annealed mild steel for different rates of loading and temperatures must be known in order that quantitative results may be obtained from the elastic-plastic stress analysis of notched specimens. The information obtained from the investigation of the yielding and brittle fracture behavior of the material will be applied in the final part of this thesis to a study of the transition temperature as obtained from notched bar Izod impact tests.

An understanding of the basic mechanism underlying the transition temperature and brittle fracture behavior of structural materials such as steel is of great engineering importance. Such

an understanding may enable future investigations to be directed in a more fruitful manner than in the past toward a final solution to the problem of initiation of brittle fracture in structures. Also the problem as to the propagation of a brittle fracture may be more readily attacked if the mechanism of initiation is understood.

II. THE EFFECT OF RATE OF STRESS APPLICATION AND TEMPERATURE ON THE UPPER YIELD STRESS

2:1 Introduction

The yielding behavior of the annealed mild steel of this investigation must be known so that the effect of limited plastic deformation on the brittle fracture behavior of the material may be taken into account. The brittle fracture phenomenon is investigated under conditions of different constant rates of stress application and temperature. Hence, the yielding behavior of the material must be known for the same test conditions.

An experimental investigation of the effect of rate of stress application on the upper yield stress of an annealed mild steel has been made by Morrison (8). Morrison's investigations were made at room temperature for a steel of slightly different composition than the steel used in the brittle fracture investigation of this thesis. The results of Morrison's investigation show that the upper yield stress of the steel increases above the static value as the rate of stress application is increased beyond a lower limiting value.

The experimental results of Morrison, however, are too limited to allow any definite conclusions to be drawn. Hence, it is necessary to perform an experimental investigation in order to determine the effect of rate of stress application and temperature on the upper yield stress. Moreover, the temperatures and rates must cover the range of these variables that are to be investigated in studying the brittle fracture phenomenon. Also, it is desirable to obtain a theoretical understanding of the effect of rate and temperature on the yield stress so that the yielding phenomenon may be

better understood.

Extensive investigations have been conducted on the yielding behavior of annealed mild steel, of the type used in this investigation, when subjected to rapidly applied constant tensile stresses in excess of the static upper yield stress (2), (3), (9). These investigations have shown that a well defined period of time is required for the initiation of plastic deformation. This period of time has been defined as the "delay time for yielding", and is a function of both the magnitude of the applied stress and the temperature.

The experimental observations of delayed yielding have been quantitatively described in terms of the generation and motion of dislocations by means of a theoretical model of a yield nucleus (10), (11). This model is based upon the concept of the thermally activated release of dislocations from carbon and nitrogen "atmospheres" as proposed by Cottrell and Bilby (12), the Frank-Read dislocation source (13), and the obstruction of dislocation motion by grain boundaries proposed by Cottrell (14). Such a model of a yield nucleus should also be capable of predicting the effect of rate and temperature on the yield phenomenon in mild steel.

This section of the thesis presents the results of the determination of the upper yield stress of an annealed mild steel as a function of rate of stress application and temperature. The purpose of this phase of the investigation is to provide necessary information to the study of the brittle fracture phenomenon. A further purpose is to show that these results can be predicted from delay time data by the use of the dislocation model of yielding.

2:2 Material Tested and Test Specimen

The material used in this investigation is the same 0.17% carbon steel employed in previous studies (2), (3). This steel was obtained from the Columbia Steel Company, Torrance, California Works. The steel was hot rolled to 5/8 inch diameter bars from one billet of heat number 32882. The analysis as given by the mill is as follows:

Carbon	0.17%
Manganese	0.39%
Phosphorus	0.017%
Sulfur	0.040%

The material was tested in the same annealed condition employed previously (2), namely, the specimens were annealed by heating at 1600°F for 50 minutes followed by slow cooling in the furnace. The entire annealing treatment was done in an atmosphere of dry hydrogen after all machining operations on the specimens had been completed. The average grain size of the material is ASTM number 6.5.

The design of the specimens is shown in Figure 1. This is the same specimen design as that used in a previous investigation of delayed yield phenomena (3).

2:3 Equipment, Test Procedure, and Experimental Results

The applied loading rates were obtained by means of a hydropneumatically operated rapid load tensile testing machine described previously (2). This machine is capable of rates of load application up to about 10^6 lb/sec and provides a maximum possible specimen

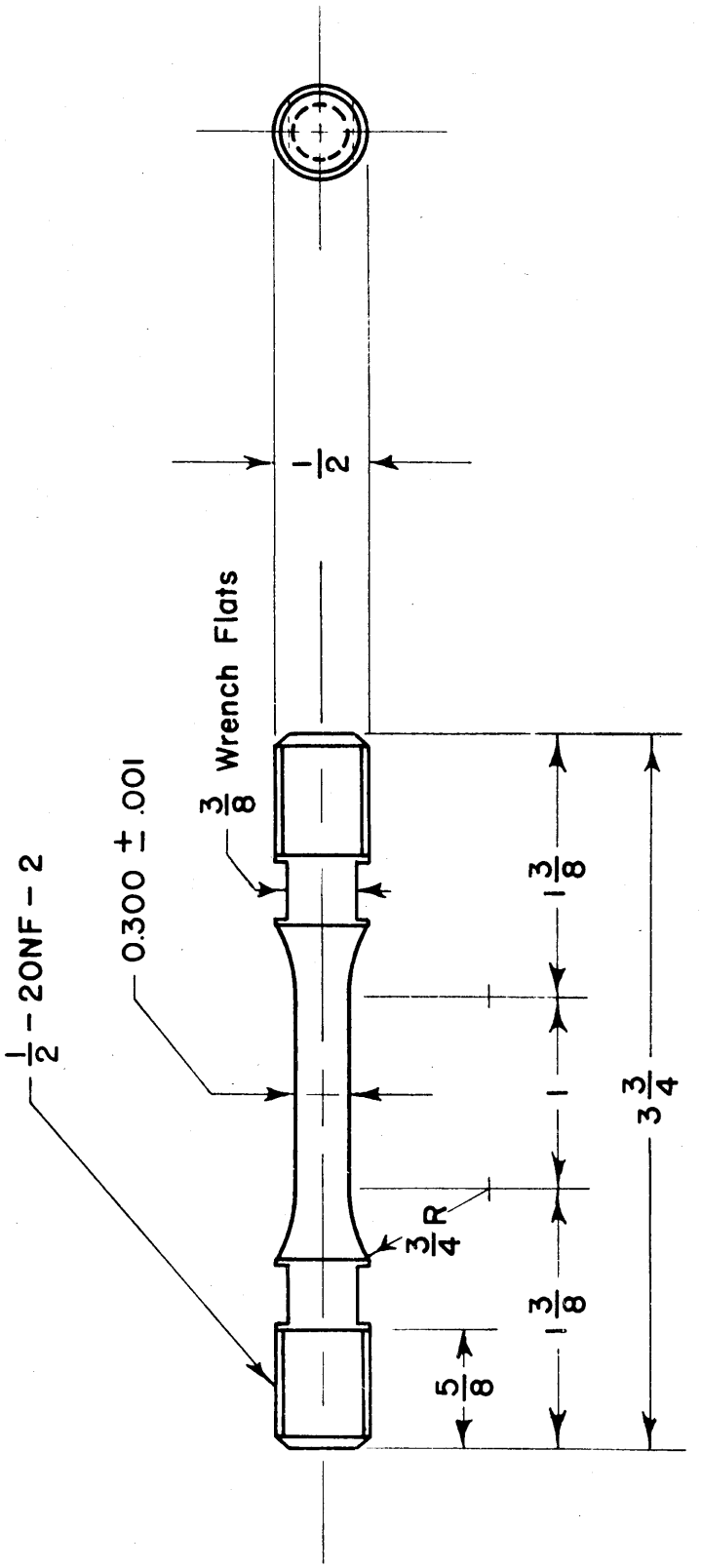

Figure 1 Tensile Test Specimen

extension of 0.05 in. The maximum load of 10^4 can be applied in a minimum time of about 10 millisec. The minimum loading rate attainable with automatic operation of the machine is about 7×10^3 lb/sec. Lower rates of loading from about 10 lb/sec to about 7×10^3 lb/sec may be obtained through proper manipulation of various manually operated valves associated with the machine. These loading rates are reproducible and, for all practical purposes, are constant with respect to time. The diameter of the gage section of the test specimen is 0.300 in. Hence, the maximum stress is limited to about 140,000 lb/in.^{2} and the range of rate of stress application attainable is from about 10^2 to 10^7 lb/in.^{2} sec.

The applied load was determined as a function of time during each test by means of a dynamometer, described previously (15), employing type AB-14, SR-4 wire strain gages. The signal from the dynamometer was recorded on photographic paper by means of a recording oscillograph, manufactured by the Consolidated Electrodynamics Corporation, Pasadena, California. A 3000 cycle/sec carrier bridge amplification system was used in conjunction with the recording oscillograph. The time resolution of the recording system is about $\pm$ 1 millisec at the maximum recording rate. The load acting on the specimen at any time could be determined to within an estimated overall error of about 4 per cent. The onset of macroscopic yielding is characterized by a sudden decrease of load which is readily detectable on the test record.

The specimens were tested at the temperatures where brittle fracture in notched tensile specimens was observed, as will be described in a later section of this thesis, namely, -110° F (-79° C) and -200° F (-129° C). The test temperature of -110° F (-79° C) was achieved with dry ice and Freon 12 placed in a hard rubber container surrounding the specimen and attached to the grips. The specimen grips, described previously (16), are thermally insulated so as to minimize the heat flux into the specimen. Prior to the beginning of tests at a temperature of -110° F (-79° C), the specimen and grip assembly were pre-cooled in dry ice so that the equilibrium temperature of the dry ice and Freon could be attained quickly.

The test temperature of -200° F (-129° C) was secured by means of the arrangement shown in Figure 2. The specimen is surrounded by liquid Freon 12 contained within the inner brass cylinder of this device. A 250 watt electric heater is also placed in this cylinder. Liquid nitrogen is placed in the annular space between the inner and outer brass cylinders. The entire outer surface of the arrangement is insulated with cork. The desired specimen temperature is obtained by adjusting the voltage applied to the heater coil.

The temperatures were measured with three copper constantan thermocouples. A thermocouple was attached to each of the specimen fillets and one was attached to the center of the specimen gage length. Temperature measurements made during the tests indicated that the total temperature difference along the specimen gage length was less than $\pm$ 5° F for the tests at a temperature of

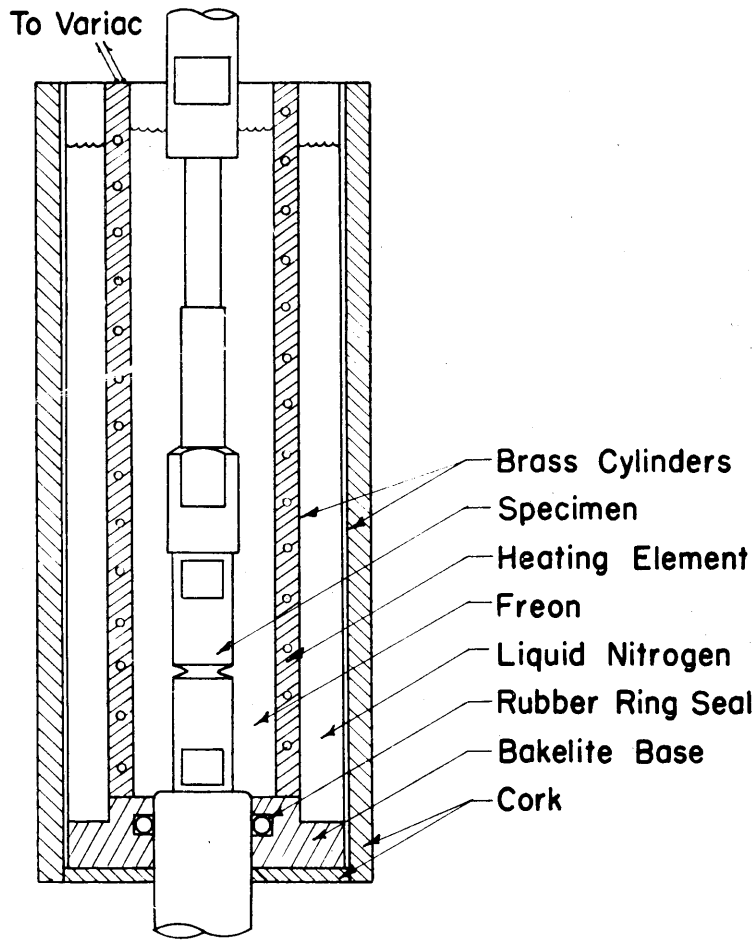

Figure 2 Container for Thermostatic Bath Employed at -200°F (-129°C)

-200° F (-129° C) and less than $\pm 1^{\circ}$ F during the tests at a temperature of -110° F (-79° C). The temperature variation was $\pm 10^{\circ}$ F or less during the tests at a temperature of -200° F (-129° C) and less than $\pm 1^{\circ}$ F during the tests at a temperature of -110° F (-79° C).

The rates of load application were measured from the photographic record of the test. A typical test record is shown in Figure 3 for one of the tests performed at a temperature of -110° F (-79° C). The rate of load application is taken to be the average slope of the load vs. time trace prior to yielding, as indicated in Figure 3. The rate of stress application is then taken to be the rate of load application divided by the initial cross sectional area of the test specimen. Enough tests were performed at each temperature so as to reasonably define the variation of yield stress with rate of stress application.

The experimentally determined relationship between the yield stress and the logarithm of the rate of application of stress is shown in Figure 4 for temperatures of -110° F (-79° C) and -200° F (-129° C). The experimental results are given by the plotted points, and the average trend of these points is represented by the full lines.

2:4 Theoretical Considerations

The dislocation model of a yield nucleus employed in this thesis has been discussed previously (10). Briefly, this model consists of a Frank-Read source, which is a dislocation segment with fixed end points, lying on a slip surface bounded by a grain boundary. The dislocation segment is bound along its length by interstitial solute atoms such as carbon and nitrogen. This Frank-

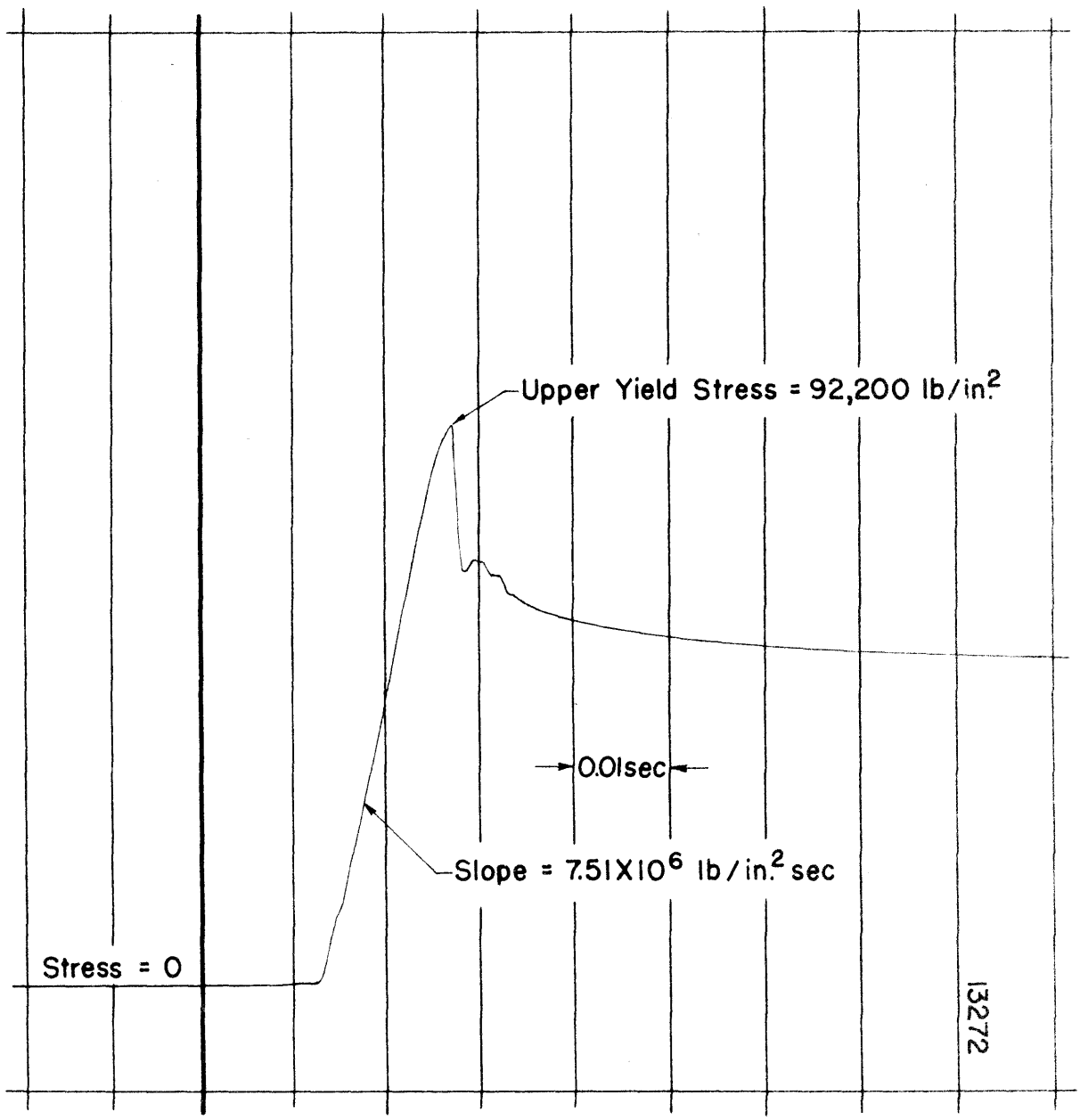

Figure 3. Typical Test Record of Load vs. Time at a Temperature of -110° F (-79° C)

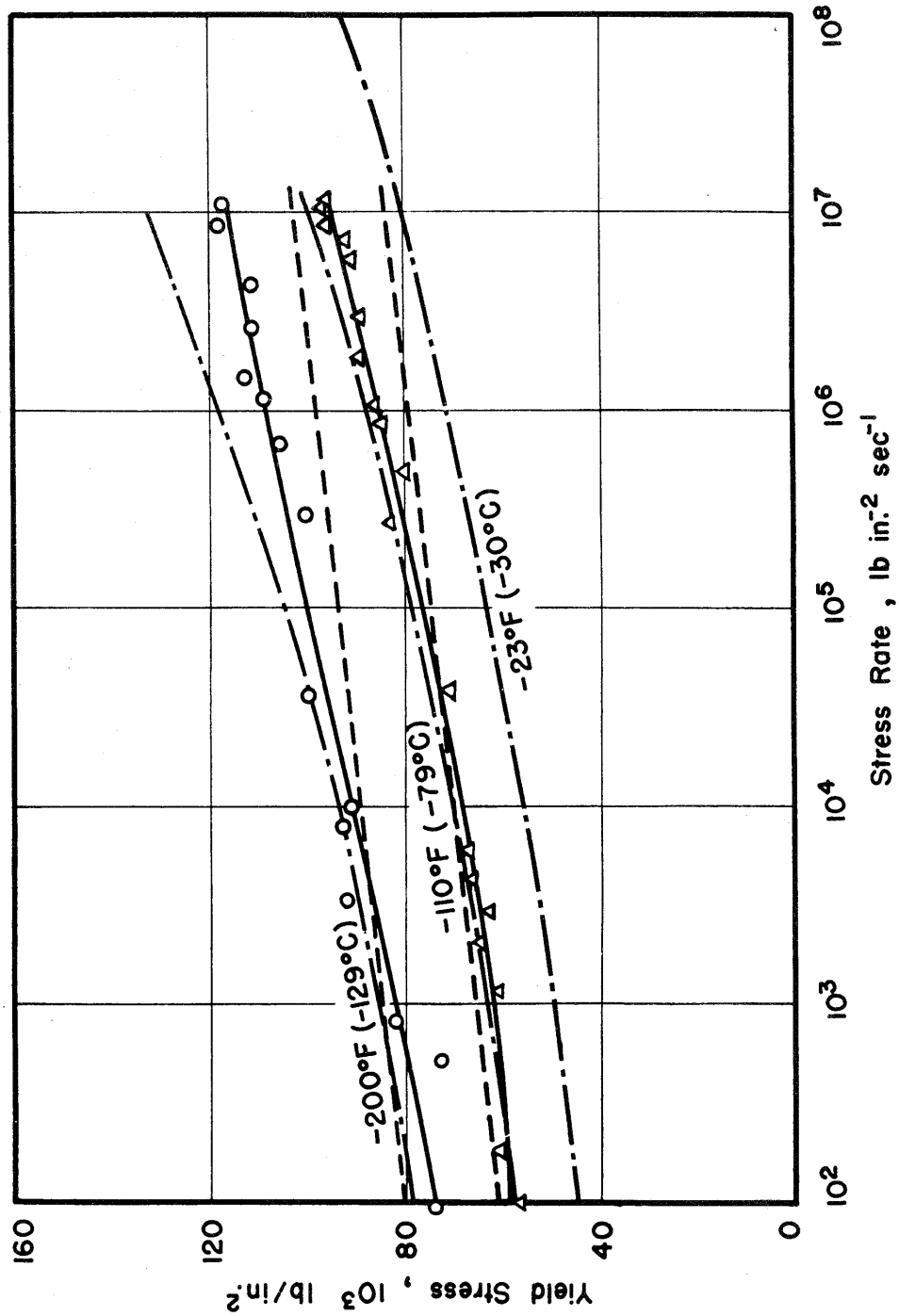

Figure 4 Upper Yield Stress vs. Applied Stress Rate for Unnotched Specimens Tested at -110°F (-79°C) and -200°F (-129°C)

Read dislocation source may generate dislocation loops under the action of applied stress. A generated dislocation loop will then expand causing a very small amount of plastic deformation, until an obstacle, such as the grain boundary or a previously generated dislocation loop, prevents the loop from expanding further. The piling up of these loops at the grain boundary concentrates the stress acting on that boundary to a much higher value than the stress that acts on the dislocation source. The assumption is made that general yielding occurs when the concentrated stress acting on the grain boundary reaches a critical value.

An expression may be derived for the yield stress as a function of the rate of load application and temperature on the basis of the dislocation model of a yield nucleus described above. The rate of generation of dislocation loops at the Frank-Read source is assumed to be controlled by the thermally activated release of the source dislocation from its "atmosphere". The expression for the rate of generation of dislocation loops from a single source, given previously by Fisher (17) is:

$$\frac{dn}{dt} = \dot{n} = \nu \exp\left(-\frac{W}{kT}\right), \quad \tau_s \geq \frac{Gb}{\ell}$$

$$\dot{n} = 0 \qquad\qquad , \quad \tau_s < \frac{Gb}{\ell} \tag{1}$$

where

n is the number of dislocations generated,

t is the time,

ν is the frequency of the appropriate form of thermal fluctuations,

τ_s is the resolved shear stress at the Frank-Read source,

k is Boltzmann's constant,

T is the absolute temperature,

W is the thermal activation energy required for the release of a dislocation from an "atmosphere" of solute atoms,

G is the shear modulus

b is the atomic slip distance or Burger's vector, and

ℓ is the distance between the end points of the Frank-Read source.

Fisher's (17) expression for the activation energy is:

$$W = \frac{\gamma_0^2}{b\tau_s} f\left(\frac{\gamma}{\gamma_0}\right), \tag{2}$$

where

$$f\left(\frac{\gamma}{\gamma_0}\right) = \cos^{-1}\left(\frac{\gamma}{\gamma_0}\right) - \frac{\gamma}{\gamma_0}\left[1-\left(\frac{\gamma}{\gamma_0}\right)^2\right]^{\frac{1}{2}} \approx \frac{4\sqrt{2}}{3}\left(1-\frac{\gamma}{\gamma_0}\right)^{3/2} \text{ for } \frac{\gamma}{\gamma_0} \approx 1 ,$$

γ_o is the energy per atomic distance of a dislocation without an "atmosphere",

and γ is the energy per atomic distance of a dislocation with an "atmosphere".

Equation 1 may be put in the following form through the use of Equation 2:

$$\dot{n} = \nu \exp\left(-\frac{B}{2\tau_s T}\right) ,$$

where

$$B = \frac{2\gamma_0^2 f\left(\frac{\gamma}{\gamma_0}\right)}{bk}$$

Further, if the applied shear stress at the source, τ_s, is assumed to be independent of the number of loops generated, and equal to one half the applied tensile stress, σ, then

$$\dot{n} = \nu \exp\left(-\frac{B}{\sigma T}\right) . \tag{3}$$

For tests at constant rates of stress rise, $\sigma = \dot{\sigma} t$, where $\dot{\sigma}$ is the constant applied stress rate. The number of dislocation loops present at any instant is then obtained by using this relation in Equation 3 and integrating with respect to time. The result is

$$n = \nu t \exp\left(-\frac{B}{\dot{\sigma} t T}\right) + \frac{B\nu}{\dot{\sigma} T} E_i\left(-\frac{B}{\dot{\sigma} t T}\right) , \tag{4}$$

where $E_i\left(-\frac{B}{\dot{\sigma} t T}\right)$ is the exponential integral of the indicated argument.

The assumption will now be made that macroscopic yielding occurs when the critical resolved shear stress at the grain boundary reaches the theoretical strength of a perfect crystal. This is the same condition for yielding used previously (11) and implies that yielding occurs when

$$n\tau_s = \frac{G}{2\pi} . \tag{5}$$

Thus, by using Equation 4 to eliminate n from Equation 5 and setting $\tau_s = \frac{\dot{\sigma} t}{2} = \frac{\sigma_{yd}}{2}$, the following relation between the upper yield stress, σ_{yd}, the stress rate, and the temperature is obtained:

$$\frac{G}{2\pi} = \frac{\nu}{2\dot{\sigma}} \left[(\sigma_{yd})^2 \exp\left(-\frac{B}{\sigma_{yd} T}\right) + \frac{B\sigma_{yd}}{T} E_i\left(-\frac{B}{\sigma_{yd} T}\right)\right] . \tag{6}$$

An expression for the delay time for yielding, t_d, under conditions of rapidly applied constant stress, may be derived by employing the same dislocation model and assumptions as those used

in the derivation of Equation 6. The expression for the delay time, t_d, is obtained by integrating Equation 3, while holding the stress, σ, constant and using the yield condition expressed by Equation 5 to eliminate n. Hence, if the time, t, is set equal to the delay time, t_d, and the applied shear stress, τ_s, is set equal to one half the applied tensile stress, σ, there results:

$$t_d = \frac{G}{\pi \nu \sigma} \exp\left(\frac{B}{\sigma T}\right) . \tag{7}$$

The undetermined constants, B and ν, are common to both Equations 6 and 7. Their numerical values have been determined by fitting Equation 7 to the experimental relationship between delay time, stress, and temperature found in previous investigations (2), (3) on the same steel. This fit covers the ranges of the variables

$$3 \times 10^{-5} \text{ sec} \leq t_d \leq 10^3 \text{ sec},$$
$$40 \times 10^3 \text{ lb/in.}^2 \leq \sigma \leq 115 \times 10^3 \text{ lb/in.}^2 ,$$
$$141^\circ\text{K } (-205^\circ\text{F}) \leq T \leq 394^\circ\text{K } (250^\circ\text{F}) .$$

The values of the constants obtained in this manner are

$$B = 1.67 \times 10^{-6} \, G^2 \text{ lb/in.}^2 \, ^\circ\text{K},$$
$$\nu = 6.77 \times 10^{10} \text{ sec}^{-1} .$$

The values of the shear modulus, G, as a function of temperature are obtained from the results of Köster's (18) measurements of Young's modulus and the assumption that Poisson's ratio is independent of temperature. Thus,

$$G = (13.30 - 0.003T) \times 10^6 \text{ lb/in.}^2 .$$

The fit of Equation 7 to the experimental relationship between delay time, stress, and temperature is shown in Figure 5. The solid lines in Figure 5 indicate the logarithm of the delay time vs. stress as given by Equation 7 and the above values of B, ν, and G. The plotted points represent the experimental data.

These values of B, ν, and G have been used in Equation 6 to obtain the "dash-dot" curves of upper yield stress vs. applied stress rate shown in Figure 4 for temperatures of -110° F (-79° C) and -200° F (-129° C). The variation of yield stress with rate of stress application for a temperature of -23° F (-30° C) has been computed from Equation 6 and is plotted in Figure 4 for use in the investigation of the initiation of brittle fracture in notched tensile specimens of the same steel.

Yokobori (19) has developed a theoretical relationship for the yield stress as a function of the rate of stress application and temperature based on the work of Campbell (20). Yokobori has expressed this relationship in the form

$$\sigma_{yd} = \sigma_0 \left[\frac{\dot{\sigma} C}{mkT\sigma_0}\right]^{mkT}, \quad mkT << 1, \tag{8}$$

where m and C are constants for the material, $\dot{\sigma}$, k, and T have the same meaning as described previously, and σ_o is the yield stress at absolute zero. The constants m and C may be determined by fitting the delay time results on mild steel (2), (3), using Campbell's theory of the delay time vs. applied stress for constant stress tests (20). The value, 1/m, determined in this manner, is found to be 0.63 ev. The constant, C, is found to be about 10^{-16} seconds.

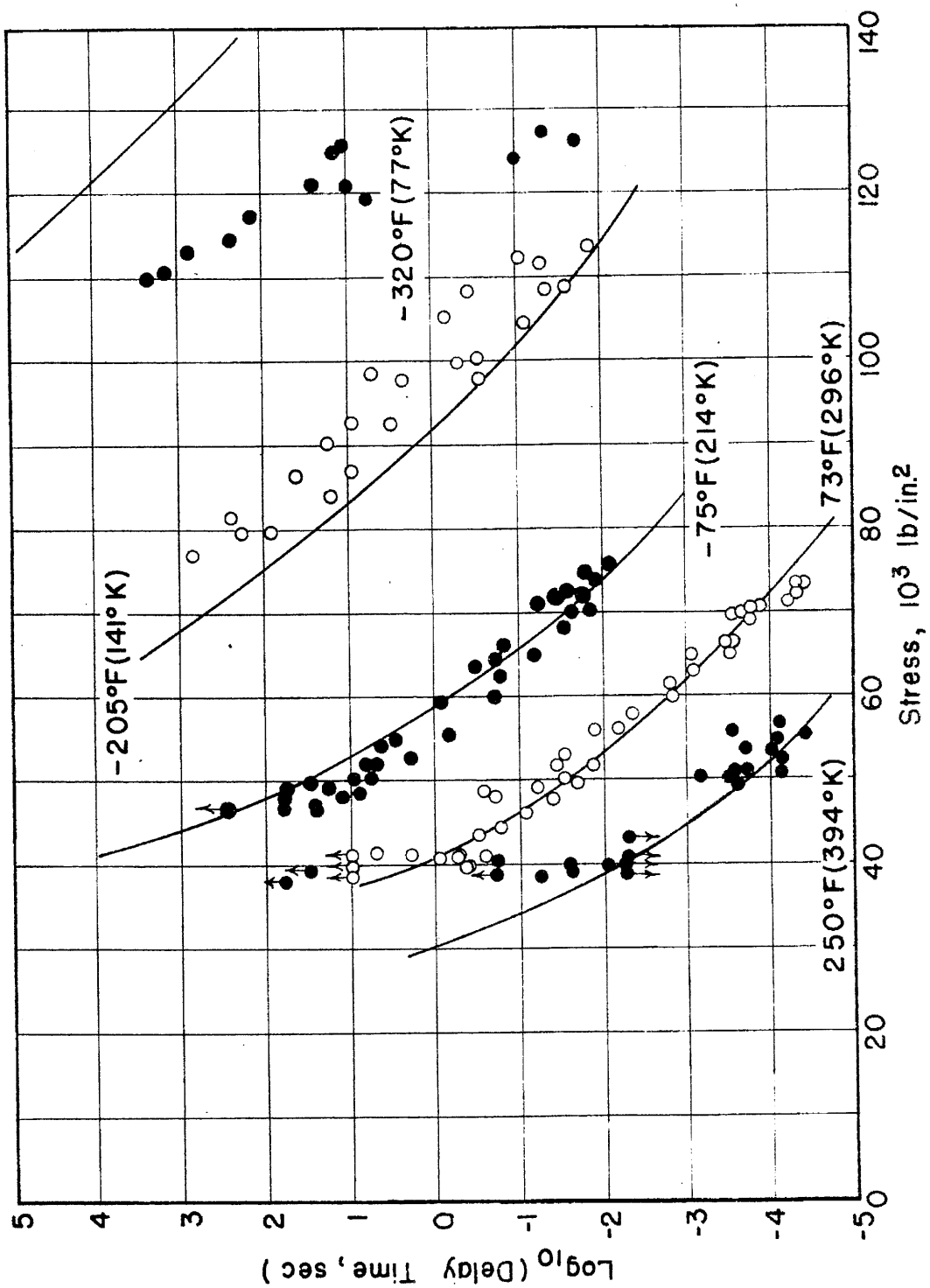

Figure 5. Logarithm of the Delay Time vs. the Tensile Stress at Five Temperatures from -320° F (77° K) to 250° F (394° K)

The yield stress at absolute zero, σ_o, is taken to be 1.25×10^{10} dynes/cm^2 or 181.5×10^3 lb/in.^{2} (21).

The yield stress as a function of stress rate for temperatures of -110° F (-79° C) and -200° F (-129° C) given by Equation 8 is shown by the dashed curves in Figure 4 together with the results as derived in this thesis (dash-dot curves).

2:5 Discussion

The relatively good agreement between theory and experiment, shown in Figure 4, indicates that the yield stress as a function of applied stress rate is directly related to the delay time for yielding at constant stress. Also, the agreement between theory and experiment further substantiates the dislocation theory of yielding.

The only significant divergence of the theory derived in this investigation from the experimental results occurs at a temperature of -200° F (-129° C) for stress rates greater than about 10^6 lb/in.^{2} sec. The deviation of the theory from experimental results may become greater at higher temperatures for stress rates greater than those obtainable with the present equipment, namely for stress rates exceeding about 10^7 lb/in.^{2} sec. The maximum stress rate for which the theory is accurate seems to be less for lower temperatures. The reason for the failure of the theory at low temperatures and high rates is not understood.

The present theory differs in two respects from the theory of Campbell and Yokobori. First, the expression for the activation energy required for the release of a dislocation from its "atmosphere" differs. Second, the conditions assumed for the onset of

yielding differ for the two theories. For instance, Campbell (20) assumes that yielding occurs when a critical number of dislocation loops are generated, whereas the present theory assumes that a critical stress acting on the grain boundary is required to produce yielding. However, since both theories fit the experimental data with about the same accuracy for the range of temperatures and rates investigated, no definite conclusion can be reached as to which theory is more apt to be correct for other conditions of rate and temperature.

Fisher (17) has proposed a different combination of the expression for the activation energy and the yield condition than that used in this thesis or by Campbell and Yokobori. Fisher suggests that the activation energy is given by the expression used in this thesis. However, Fisher suggests that yielding occurs when a critical number of dislocation loops are generated in accordance with Campbell's theory. A third expression for the activation energy has been proposed by Cottrell and Bilby (12). This latter expression, however, is much more complicated than those proposed by Yokobori and Fisher. Hence, there are three existing expressions for the activation energy and two suggested yield conditions. The combination of the form of the activation energy and the yield condition that is correct is not known. However, the results of the present investigation indicate that at least two combinations lead to approximately equivalent results.

2:6 Summary and Conclusion

The upper yield stress of an annealed low carbon steel

has been determined as a function of rate of stress application within the range from 10^2 to 10^7 lb/in.^{2} sec at temperatures of -110° F (-79° C) and -200° F (-129° C).

A theoretical expression has been obtained to relate yield stress to rate of stress application for different temperatures. The constants appearing in the theoretical expression have been evaluated by means of data obtained in tests to determine delay time of yielding at constant stress. This theoretical expression agrees very well with the experimental results within the range of temperature and rate of stress application investigated.

The expressions proposed by Campbell (20) and Yokobori (19) have been evaluated and compared with the results of this investigation. These expressions are also in reasonably good agreement with the experimental results.

III. BRITTLE FRACTURE IN NOTCHED TENSILE SPECIMENS

3:1 Introduction

The initiation of brittle fracture in a material such as mild steel is known to be related to such factors as low temperature, a high rate of stress rise, and the presence of a tri-axial stress condition such as exists beneath a notch. Investigations have also shown that a small amount of plastic deformation is involved in brittle type fractures (7). An understanding of the initiation of a brittle fracture requires that the role of all of these factors be known. Of particular importance is the understanding of the state of stress at the instant and position of brittle fracture initiation.

This section of the thesis presents the results of an investigation of the behavior of notched tensile specimens subjected to different constant rates of loading at different temperatures. The purpose of this investigation is to determine quantitatively the effect of rate of loading, temperature, and limited plastic deformation on the stress state beneath a notch which governs the initiation of brittle fracture in an annealed mild steel.

Notched specimens subjected to tensile loading were chosen in preference to the more conventional notched bar bending tests because of the availability of a rapid load tensile testing machine (2). The use of this machine allows a large range of applied rates of loading to be studied. Furthermore, these rates of loading are controllable and reproducible.

3:2 Theoretical Considerations

The stress condition beneath a notch, in a tensile specimen, includes triaxial tensile stresses. Such a stress condition suppresses general yielding of the material and hence is conducive to fracture with greatly reduced plastic flow or brittle fracture. The fact that some plastic deformation in a local region near the notch root precedes brittle fracture, even in the case of extremely sharp notches is rather well established (7). Brittle fracture appears to be initiated at some distance beneath the notch surface (22), presumably at some point near the boundary between the region of elastic behavior and the plastically deformed region. Since plastic deformation occurs prior to the initiation of brittle fracture, the stress distribution beneath the notch at the instant of initiation of fracture cannot be determined solely by means of the theory of elasticity. Thus a suitable form of the theory of plastic deformation must be employed in the region of plastic flow, while the theory of elasticity is employed for the remainder of the specimen.

The stress solutions for the elastic and plastic regions must be such that the conditions of continuity of both stresses and displacements are satisfied at the boundary between the two regions. The solutions in both the elastic and plastic regions must also satisfy the external boundary conditions. That is, normal and tangential stresses on the free (notch) surface are zero and the appropriate integral of the stresses over the other external surfaces (assumed to be at infinity) is equal to the applied load.

An elastic-plastic stress analysis appropriate for application to the experimental results obtained in this investigation will

now be presented. The stress analysis has been made for a solid body having the cross-section shown in Figure 6. The notch surfaces are formed by the two sheets of an hyperbola having an included angle of 29^{o} between the asymptotes. The ratio of the half width at the minimum cross-section, a, to the radius of curvature at the root of the notch, ρ, is $a/\rho = 15$. The body is of infinite extent in the plane of Figure 6 and in the direction normal to that plane. All cross-sections parallel to the plane of the figure are the same. Thus the problem to be solved is one of plane strain.

The tensile load, P, per unit thickness normal to the plane of the figure acts in the direction perpendicular to the plane of the minimum cross-section. This load is assumed to be applied by suitably distributed surface forces acting on the body at an infinite distance from the minimum cross-section. The load may be expressed in terms of the nominal stress, σ_n, acting on the minimum cross-section by the relation $P = 2a\sigma_n$.

This elastic-plastic body does not coincide with the actual specimen shape employed in the experimental portion of this investigation. The specimen shape is axially symmetric with the notch surface in the form of an hyperboloid of revolution. However, the results of the stress analysis are believed to provide a close approximation to the stress state in the test specimen, as will be discussed later. The plane strain approximation is employed in the analysis because a method of solution for this problem is available while a method applicable to the axially symmetric case is not.

The stress analysis for the elastic-plastic body in plane

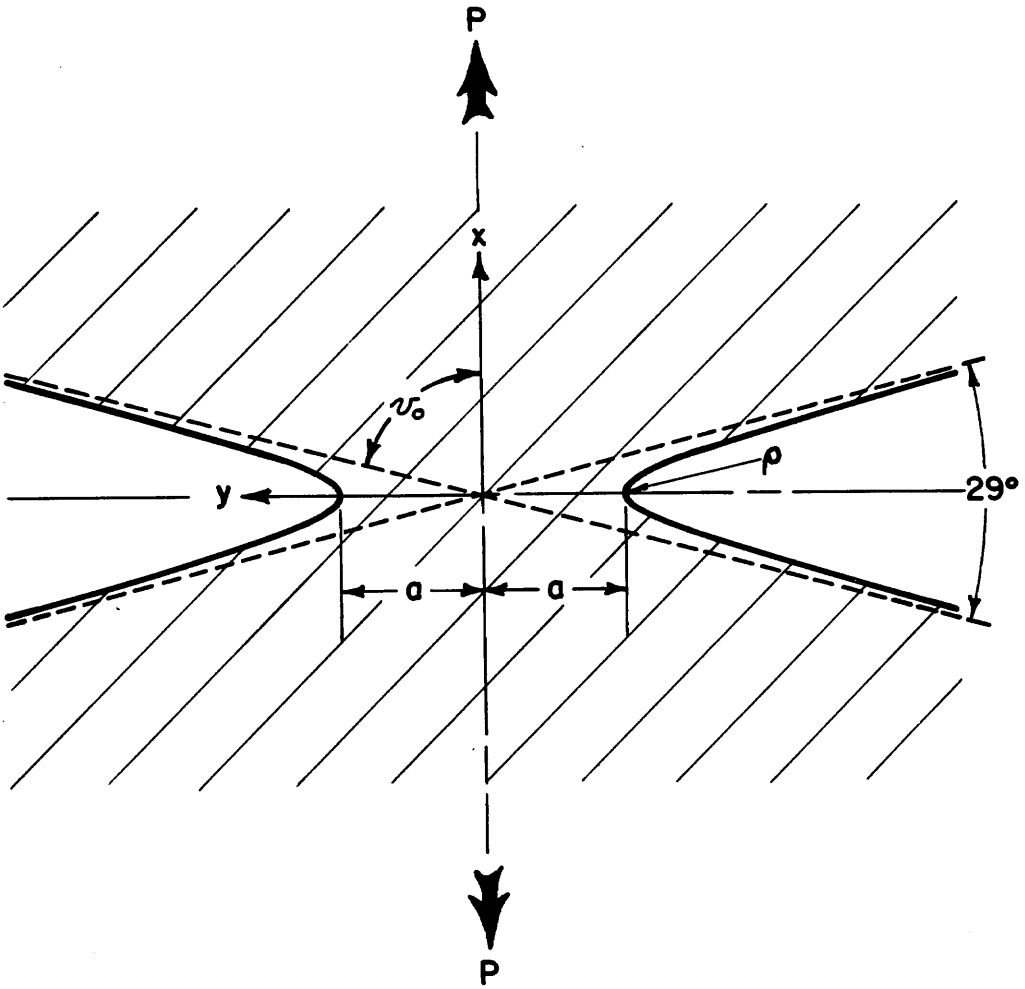

$$P = 2a\sigma_n$$

Figure 6 Elastic-Plastic Solid with Hyperbolic Notches

strain is based upon the following assumptions:

(1) The material (mild steel) is assumed to be homogeneous and isotropic in both the elastic and plastic regions. This assumption means, in effect, that the stresses and strains are only considered as average values over regions larger than the grain size of the material.

(2) Hook's Law, implying a linear relation between stress and strain, is assumed to apply at any point in the elastic region.

(3) Plastic deformation occurs when the maximum shear stress, τ_{max}, reaches a critical value, τ_c. This is the commonly used Tresca Yield condition and holds quite well for steel which exhibits a distinct yield point.

(4) The material is non-strain hardening. This assumption holds true in mild steel for small plastic strain. The inclusion of strain hardening considerations in this investigation would require a modification of the yield condition with an attendant increase in mathematical complexity.

(5) The direction of the maximum shear stress, τ_{max}, is assumed to always lie in the plane of Figure 6. Hence the component of plastic strain in the direction normal to the plane of Figure 6 is always zero. When plastic deformation is first initiated at the root of the notch, this condition is satisfied. Thus it may also be expected to hold true for a small penetration of the plastic region beneath the notch.

(6) The displacements at the free (notch) surface are small enough that the change in shape of the notch contour during plastic deformation need not be taken into account. The justification of this assumption comes from the solution of the problem. Namely, the plastic region existing at the instant of initiation of brittle fracture is always small and confined to the immediate vicinity of the notch root. Thus the plastic strains are small (of the order of elastic strains), and therefore the displacements of the free surface are negligible.

(7) The load is applied in a monotonically increasing manner and the strain in any element of the body increases monotonically. This corresponds with the type of loading employed in the experimental work.

The origin of the coordinate system employed in the stress analysis is at the center of symmetry of the body as shown in Figure 6. The z coordinate is normal to the plane of the figure. The x axis is in the direction of the applied load and the y axis passes through the notch root.

The equations of equilibrium of an element of the material are the same in both the plastic and elastic regions. These equations may be satisfied by expressing the stresses in terms of appropriate derivatives of a stress function which is single valued and analytic everywhere within the body. These expressions for the stresses may be written in the following form:

$$\frac{\sigma_x}{\sigma_{yd}} = \frac{\partial^2 \Psi}{\partial y^2} \; ; \; \frac{\tau_{xy}}{\sigma_{yd}} = - \frac{\partial^2 \Psi}{\partial x \partial y} \; ; \; \frac{\sigma_y}{\sigma_{yd}} = \frac{\partial^2 \Psi}{\partial x^2} \tag{9}$$

where Ψ is the stress function,

σ_{yd} is the upper yield stress in simple tension,

σ_x is the direct stress in the x direction,

σ_y is the direct stress in the y direction,

and

τ_{xy} is the shear stress in the x-y plane.

The requirement that the displacements be single valued and continuous in the elastic region (compatibility of the strains) is satisfied provided that the stress function is a solution of the equation

$$\nabla^4 \Psi = \frac{\partial^4 \Psi}{\partial x^4} + 2 \frac{\partial^4 \Psi}{\partial x^2 \partial y^2} + \frac{\partial^4 \Psi}{\partial y^4} = 0 \; . \tag{10}$$

The differential equation for the stress function in the plastic region is determined by the yield condition, namely, in view of assumption 3 above,

$$(\sigma_x - \sigma_y)^2 + 4\tau_{xy}^2 = 4\tau_c^2 \; . \tag{11}$$

Since τ_c is one-half the yield stress in simple tension, σ_{yd}, Equation 11 may be written in the dimensionless form

$$\left[\frac{\sigma_x - \sigma_y}{\sigma_{yd}}\right]^2 + 4 \left[\frac{\tau_{xy}}{\sigma_{yd}}\right]^2 = 1. \tag{12}$$

Equation 12 may be written in terms of the stress function, Ψ, by substituting for the stresses their equivalent form from Equation 9. Hence the yield condition may be written as

$$\left[\frac{\partial^2\Psi}{\partial y^2} - \frac{\partial^2\Psi}{\partial x^2}\right]^2 + 4\left[\frac{\partial^2\Psi}{\partial x \partial y}\right]^2 = 1. \tag{13}$$

The boundary conditions of the problem are as follows: the normal and tangential stresses must be zero at all points on the free surface (notch surface). The stresses must be continuous across the boundary separating the regions of elastic and plastic deformation, and the integral of the axial stress component over the minimum cross-section of the notched bar must be equal to a specified value of the total load. The continuity of stresses at the elastic-plastic boundary is satisfied by requiring that the stress function and its derivatives up to the second order be continuous at that boundary.

The stress function and its first derivatives may be determined on the boundary of the notched bars by means shown in Appendix 1 at the end of this thesis. The boundary conditions are satisfied provided $\partial\Psi/\partial x$ and $\partial\Psi/\partial y$, at any point on the free surface, s, are given by

$$\left.\frac{\partial\Psi}{\partial x}\right|_s = 0; \quad \left.\frac{\partial\Psi}{\partial y}\right|_s = \frac{a\sigma_n}{\sigma_{yd}}, \quad y > 0$$
$$\left.\frac{\partial\Psi}{\partial y}\right|_s = -\frac{a\sigma_n}{\sigma_{yd}}, \quad y < 0 . \tag{14}$$

The value of the stress function, Ψ, on the free surface, s, is given by the expression

$$\Psi|_s = C + a\left(\frac{\sigma_n}{\sigma_{yd}}\right)|y| \tag{15}$$

where C is an arbitrary constant of integration. The value of the stress function at the root of the notch, $y = a$, is taken to be zero for convenience. Thus the stress function at any point on the free (notch) surface is given by

$$\Psi\Big|_s = -a^2 \left(\frac{\sigma_n}{\sigma_{yd}}\right) \left(1 - \left|\frac{y}{a}\right|\right), \tag{16}$$

where $|y|$ is the absolute value of y.

The specification of the boundary conditions may be completed by choosing the values of the stress function within the body at $x = \pm \infty$ in such a way that the net resultant of the stresses at $x = \pm \infty$ is equal to the applied load, $P = 2a\sigma_n$. This may be done for the present problem by using the stress function determined by Neuber (23) in his stress analysis of elastic bodies of this shape subjected to the same type of loading. This is possible since plastic deformation in a region limited to the vicinity of the notch does not influence the state of stress at an infinite distance from that region. The problem has thus been reduced to the problem of finding the stress function, Ψ, as a function of the coordinates, x, and y, which satisfies the differential Equations 10 and 13 in the regions of elastic and plastic deformation respectively, subject to the boundary conditions expressed by Equations 14 and 16, and the requirements of continuity at the elastic-plastic boundary.

There are two fundamental mathematical difficulties in obtaining the desired solution to this problem. The first is that differential Equation 13 is non-linear. The second is that the position of the boundary separating the elastic and plastic regions is unknown and must be obtained as a part of the solution of the problem. For

these reasons no general methods are known by which solutions for such problems may be obtained in analytical form.

Fortunately, numerical solutions may be obtained for problems of this type by a technique of step by step numerical iteration known as the "relaxation method" due to Southwell (24). Allen and Southwell (25) have successfully applied the relaxation method in the investigation of problems of plane elastic-plastic deformation similar to the present problem.

The procedure in the relaxation method is to replace the differential equations that the stress function must satisfy by finite difference approximations in which the differential equations are expressed in terms of the values of the stress function at a finite number of points within the body. These points are arranged in the form of a regular lattice. The lattice spacing must be chosen small enough so that the second differences of the stress function (finite difference approximations for the stresses) do not change by excessive amounts between adjacent lattice points, in order to achieve a reasonable accuracy in the values of the stresses.

The lattice points used for the relaxation procedure in this investigation are equally spaced in both the x and y coordinate directions, thus forming a square net. The following formulae, reproduced from Southwell (24), are the finite difference expressions for the required differentials of the stress function evaluated at a typical point "O" in terms of the values of the stress function at neighboring points, as shown in Figure 7, for a square net having a side of length "d".

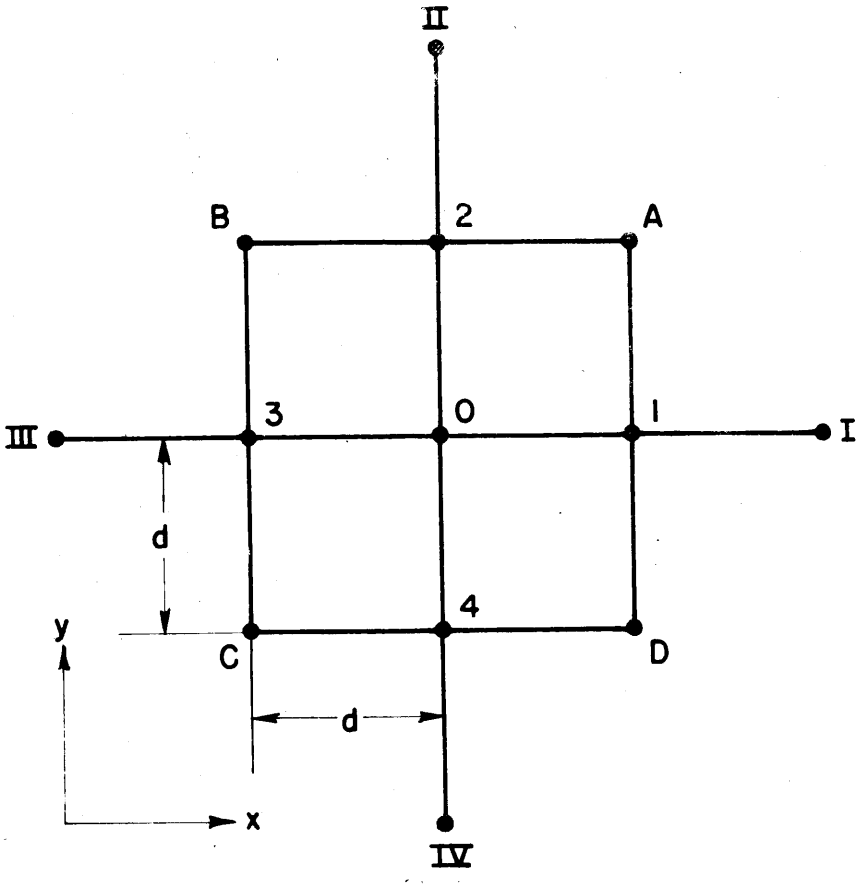

Figure 7 Portion of Square Net Pattern Used in Relaxation Method

$$\left(\frac{\partial \Psi}{\partial x}\right)_0 \cong \frac{1}{2d}\left[\Psi_1 - \Psi_3\right]$$

$$\left(\frac{\partial \Psi}{\partial y}\right)_0 \cong \frac{1}{2d}\left[\Psi_2 - \Psi_4\right] \tag{17}$$

$$\left(\frac{\sigma_y}{\sigma_{yd}}\right)_0 = \left(\frac{\partial^2 \Psi}{\partial x^2}\right)_0 \cong \frac{1}{d^2}\left[\Psi_1 - 2\Psi_0 + \Psi_3\right]$$

$$\left(\frac{\sigma_x}{\sigma_{yd}}\right)_0 = \left(\frac{\partial^2 \Psi}{\partial y^2}\right)_0 \cong \frac{1}{d^2}\left[\Psi_2 - 2\Psi_0 + \Psi_4\right] \tag{18}$$

$$-\left(\frac{\tau_{xy}}{\sigma_{yd}}\right)_0 = \left(\frac{\partial^2 \Psi}{\partial x \partial y}\right)_o \cong \frac{1}{4d^2}\left[\Psi_A - \Psi_B + \Psi_C - \Psi_D\right]$$

$$\left(\frac{\partial^4 \Psi}{\partial x^4}\right)_0 \cong \frac{1}{d^4}\left[\Psi_I - 4\Psi_1 + 6\Psi_0 - 4\Psi_3 + \Psi_{III}\right]$$

$$\left(\frac{\partial^4 \Psi}{\partial y^4}\right)_0 \cong \frac{1}{d^4}\left[\Psi_{II} - 4\Psi_2 + 6\Psi_0 - 4\Psi_4 + \Psi_{IV}\right] \tag{19}$$

$$\left(\frac{\partial^4 \Psi}{\partial x^2 \partial y^2}\right)_0 \cong \frac{1}{d^4}\left[\Psi_A + \Psi_B + \Psi_C + \Psi_D - 2(\Psi_1 + \Psi_2 + \Psi_3 + \Psi_4) + 4\Psi_0\right]$$

The finite-difference approximation for the yield criterion, Equation 13, may then be written in the form:

$$\frac{1}{d^2}\left\{\left[\Psi_2 + \Psi_4 - \Psi_1 - \Psi_3\right]^2 + \frac{1}{4}\left[\Psi_A + \Psi_C - \Psi_B - \Psi_D\right]^2\right\}^{1/2} = 1 \tag{20}$$

and the finite difference approximation for the differential equation that holds in the elastic region, Equation 10, becomes

$$(\nabla^4\Psi)_0 \approx \frac{1}{d^4}\Big\{(\Psi_I+\Psi_{II}+\Psi_{III}+\Psi_{IV})+2(\Psi_A+\Psi_B+\Psi_C+\Psi_D)-8(\Psi_1+\Psi_2+\Psi_3+\Psi_4) +20\Psi_0\Big\} = 0 \qquad (21)$$

Values of the stress function at lattice points within the body at a distance from the minimum cross-section greater than 10ρ may be computed from Neuber's (23) solution for the elastic problem which is summarized in Appendix 2. These values of the stress function are not varied during the relaxation process. This is an approximation which is justified by the observation that in the cases of interest for this investigation the regions of plastic deformation never extend a distance of more than 6ρ from the root of the notch.

The initial values of the stress function at interior lattice points less than 10ρ from the minimum cross-section are also chosen to be Neuber's values for the elastic case. These do not satisfy Equation 13 in the plastic region. However, they represent the best available first approximation for the correct values. Thus this initial choice of the values of the stress function at interior lattice points minimizes the computational labor required in the relaxation process.

Equations 20 and 21 express the mathematical condition of the problem at interior lattice points in the plastic and elastic regions respectively. Equation 21 is satisfied at the outset since the elastic stress solution is used as a starting point. However, Equation 20 is initially violated within a certain region of the body.

This region is the first approximation of the region of plastic deformation. The region of plastic deformation is confined to the immediate vicinity of the root of the notch for values of the applied load of interest in this investigation. The true plastic region, determined at the completion of the relaxation procedure, is slightly larger in extent than this first approximation.

The amount by which the left side of Equation 20 exceeds the value of unity, is called the plastic residual, $(F_p)_0$, at the point "O" in the plastic region. Thus

$$(F_p)_0 = \frac{1}{d^2}\left\{\left[\Psi_2+\Psi_4-\Psi_1-\Psi_3\right]^2+\frac{1}{4}\left[\Psi_A+\Psi_C-\Psi_B-\Psi_D\right]^2\right\}^{1/2}-1. \qquad (22)$$

The plastic residual is never negative. Any lattice point at which Equation 22 gives a negative result lies in the elastic region and hence is subject to Equation 21 rather than Equation 20. The values of the stress function at lattice points within and adjoining the plastic region must be altered so as to reduce the residuals at all lattice points in the plastic region to an acceptably low value. This relaxation of values of the stress function so as to reduce plastic residuals as given by Equation 22 leads to a violation of Equation 21 at lattice points which lie in the elastic region near the elastic-plastic boundary. Hence elastic residuals, $(F_e)_0$ exist, the values of which are just the amount by which Equation 21 is violated. Elastic residuals may be either positive or negative. The elastic residuals must be eliminated or sufficiently reduced in value by altering the values of the stress function in the elastic region. This in turn re-introduces residuals in the plastic region. Hence the relaxation process involved

will alternate between reducing residuals in the plastic region and then the elastic region until the desired reduction of all residuals is attained. During this process the elastic-plastic boundary expands slightly from the first approximate position. The position of the elastic-plastic boundary at any stage in the relaxation process is given by those lattice points at which the plastic residual is just slightly negative. Such points are in the elastic region immediately adjacent to the boundary.

The boundary condition at the free (notch) surface must be put in finite difference form before the actual process of relaxation of the elastic and plastic residuals can be accomplished. Values of the stress-function for lattice points which are less than one-half the net spacing, d, from the actual free surface in either coordinate direction (either inside or outside the actual surface) are computed by means of Equation 16, and these values remain fixed during the relaxation process. Typical lattice points of this type are those marked α in Figure 8, which is a schematic representation of a portion of the relaxation net in the region of the notch surface.

The values of the stress function at those lattice points designated β and γ in Figure 8, which are at a distance greater than one-half and less than one and one-half the lattice spacing from the actual free boundary in either coordinate direction, must be varied during the relaxation process. This must be done in such a way that the conditions expressed by the finite difference form of Equation 14 are satisfied. For example, the second of Equations 14 and 17 give

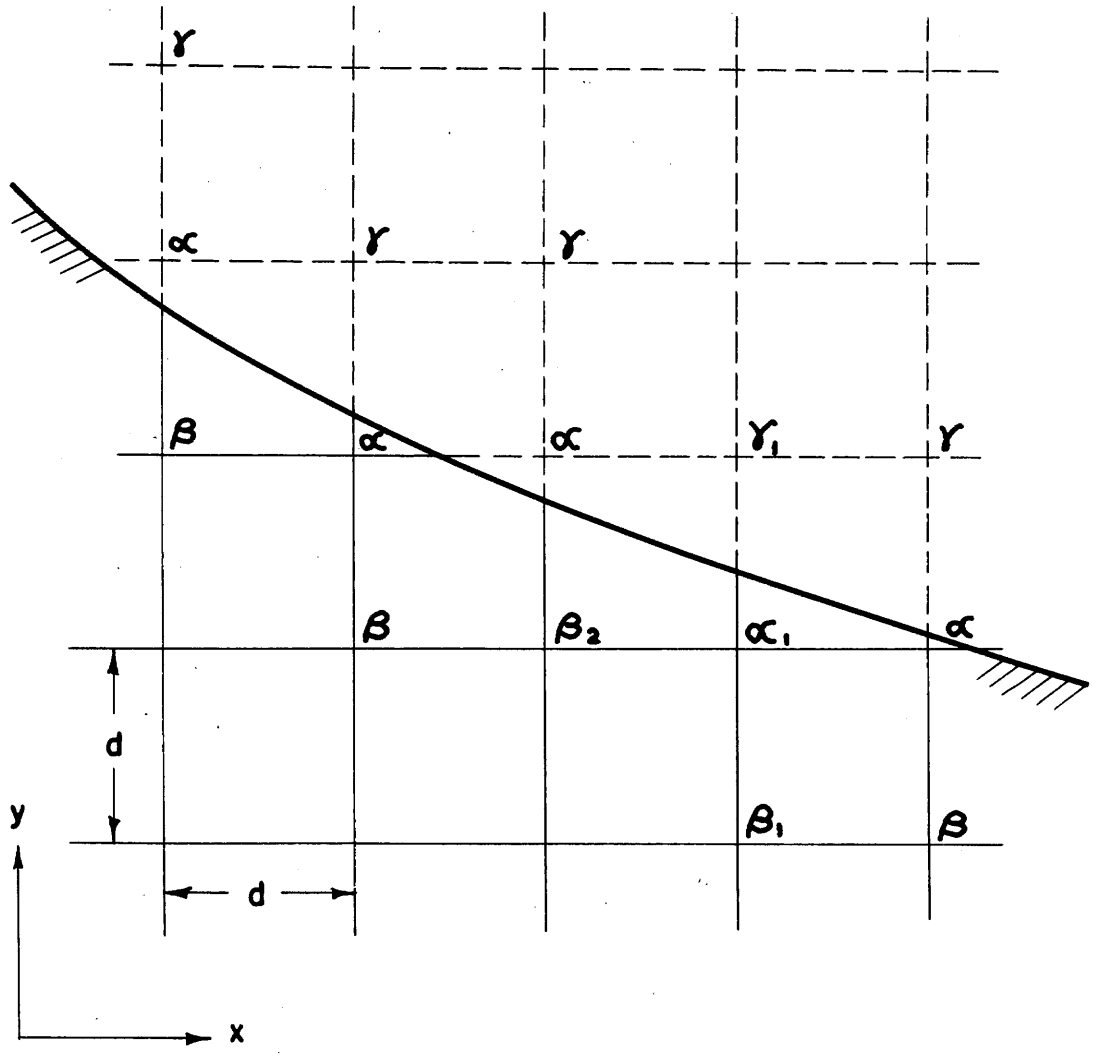

Figure 8 Typical Lattice Points Near the Free Surface in the Relaxation Method

$$\frac{1}{2d}\left[\Psi_{\gamma_1} - \Psi_{\beta_1}\right] = a\left(\frac{\sigma_n}{\sigma_{yd}}\right) .$$

Thus when the value of the stress function, Ψ_{β_1}, at the lattice point β_1, is varied during the relaxation procedure, the value of the stress function, Ψ_{γ_1}, at the point γ_1 (outside the actual body) is given by

$$\Psi_{\gamma_1} = 2ad\left(\frac{\sigma_n}{\sigma_{yd}}\right) + \Psi_{\beta_1} .$$

This value of the stress function at the point γ_1, must be computed, even though the point is outside the actual body, because it enters the expression for the residual at the points β_1 and β_2 as may be seen from Equation 21 or Equation 22 and Figure 7.

The reduction of residuals is systematized by the use of "relaxation patterns". Consider a typical lattice point, "O", in the elastic region. The effect of a unit change in the stress function at this point is to change the residuals at "O" and surrounding points by the amounts shown in Figure 9, as may be seen from Equation 21. Figure 9 is thus the "relaxation pattern" for the elastic region. This relaxation pattern serves two purposes. First, it aids in judging which lattice points should be relaxed first and the amount by which the stress function should be changed in order to obtain the most rapid convergence of the relaxation process. Second it provides the means by which the residuals at all lattice points in the elastic region are continuously corrected as changes in the stress function are made.

A single relaxation pattern applicable to any point in the plastic region does not exist in view of the quadratic form of Equation 22. However, an approximate pattern may be used in the plastic

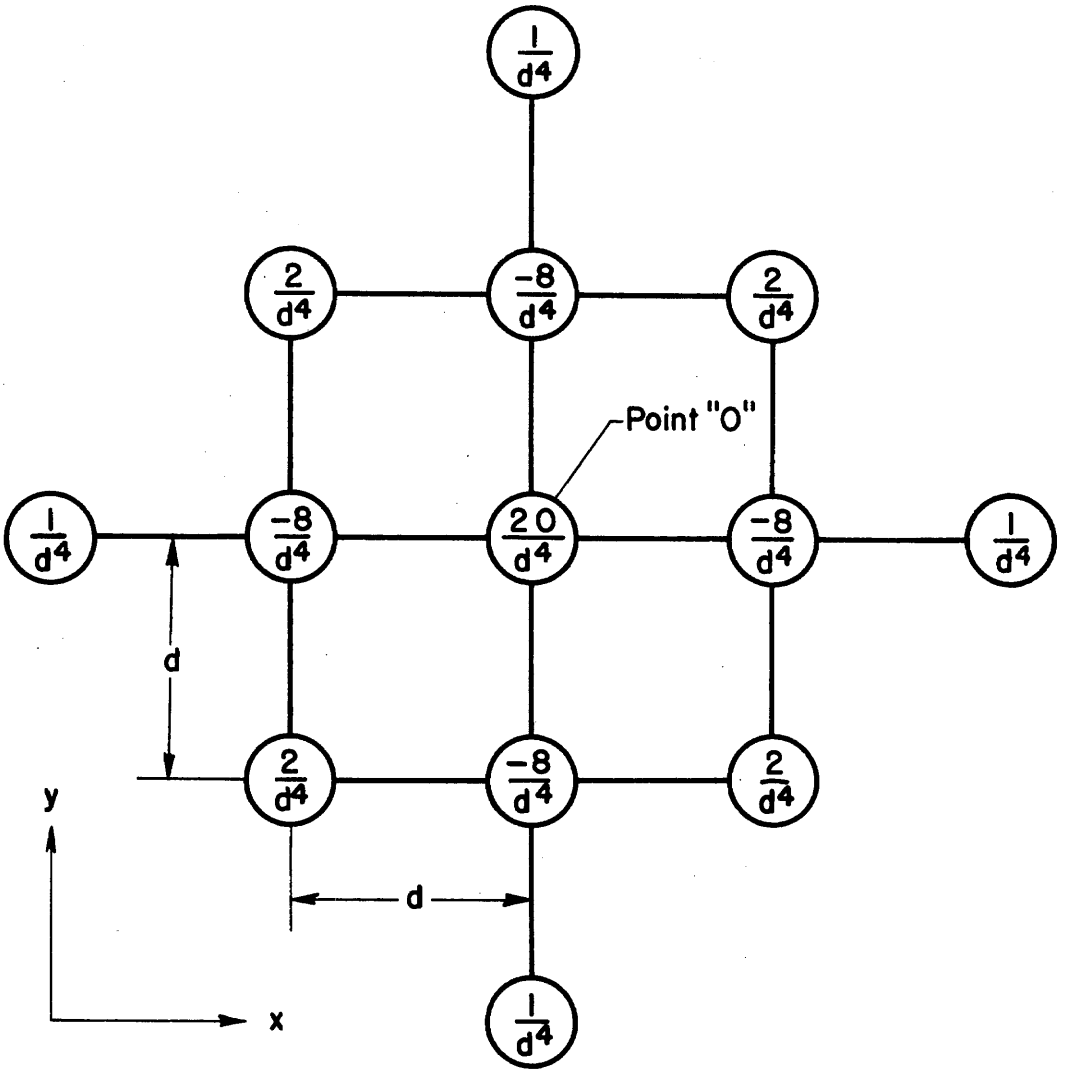

Figure 9 Changes of Residuals in the Vicinity of a Typical Point, "O", in the Elastic Region due to a Unit Change of the Stress Function at "O"

region if $(\sigma_x - \sigma_y)$ is large compared to τ_{xy}. Neglecting τ_{xy} compared with $(\sigma_x - \sigma_y)$ in the expression for the yield condition, Equation 12, the plastic residual becomes

$$(F_p)_0 \cong \frac{1}{d^2} [\Psi_2 + \Psi_4 - \Psi_1 - \Psi_3] - 1, \qquad (23)$$

instead of Equation 22. Since this expression is linear in the values of the stress function it provides the basis for the approximate plastic relaxation pattern shown in Figure 10. This pattern serves to indicate which lattice points in the plastic region should be relaxed first and the approximate amount by which the stress function should be changed in order to achieve the most rapid convergence of the process. However, since Equation 23 may be appreciably in error, the plastic relaxation pattern shown in Figure 10 may not be employed to keep a continuous account of the residuals in the plastic region. After a set of changes has been made in the values of the stress function at the lattice points in the plastic region, the residuals are recalculated using the correct expression given by Equation 22. Thus the use of the approximate relaxation pattern does not introduce errors in the values of the stress function obtained at the completion of the relaxation process. This method of carrying out the relaxation in the plastic region has been employed by Allen and Southwell (25).

The relaxation calculations for this investigation were conducted in the following manner for each of four values of the ratio between the nominal stress on the minimum cross-section and the yield stress, namely, $\sigma_n/\sigma_{yd} = 0.70,\ 0.81,\ 1.12,$ and 1.35. The

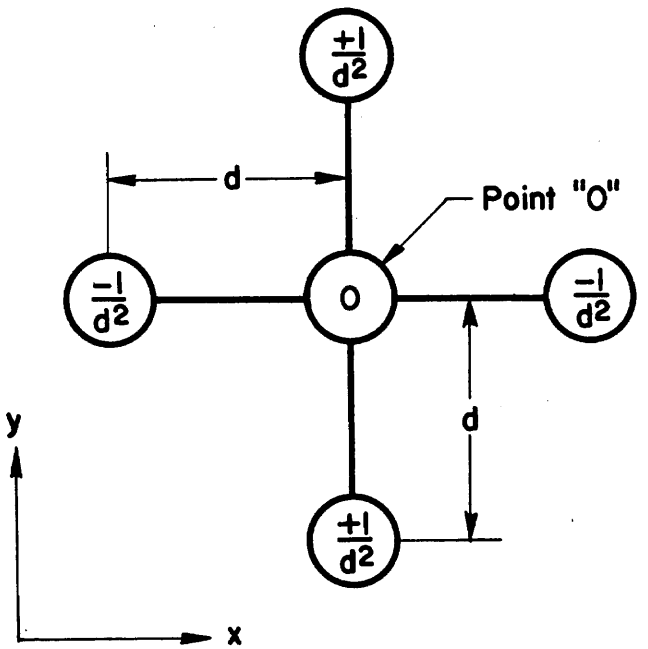

Figure 10 Approximate "Relaxation Pattern" for the Plastic Region

coordinates x and y were made dimensionless by choosing the value $a = 1$ for the half width of the body at the minimum cross-section. An initial spacing of the lattice points of $d = \rho = 1/15$ was chosen. This net of lattice points covered that region of the body bounded by the lines $x = 0$, $y = 0$, $x = 12\rho$, $y = 22\rho$ and the notch surface. The values of the stress function at the lattice points lying on the lines $x = 11\rho$, $x = 12\rho$, $y = 21\rho$, and $y = 22\rho$ were maintained constant during the relaxation calculations and equal to the values given by the solution for purely elastic deformation.

After the residuals at all lattice points of this net had been reduced to acceptably low values, additional lattice points having a spacing of $d = 1/2\rho = 1/30$ were introduced in a region near the notch root somewhat larger than the region of plastic deformation. Residuals for this net were then reduced by the relaxation procedure. Finally a third net of lattice points having a spacing of $d = 1/4\rho = 1/60$ was employed in the region extending a distance of $1-1/2\rho$ from the root of the notch in both the x and y directions. This was done in order to improve the accuracy in the determination of the stresses in this critical region. The relaxation for all the grid sizes was continued until the residuals at all lattice points were reduced to sufficiently low values that the stresses could be obtained to an accuracy of 5 per cent of the yield stress.

The values of the stress function obtained at the lattice points for the case $\sigma_n/\sigma_{yd} = 0.81$ are shown in Figures 11 and 12. Figure 11 shows the entire region within which the relaxation calculations were made, except for a sub-region near the notch root.

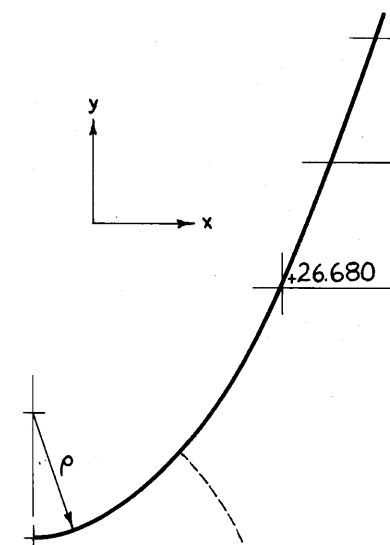

			+53.450	+53.650	+54.220	+54.850	+55.700	+56.600
			+40.050	+40.540	+41.360	+42.530	+43.700	+44.800
		+26.680	+26.980	+27.680	+28.790	+30.240	+31.980	+34.000
				+15.210	+16.630	+18.400	+20.550	+23.000
				+3.350	+5.020	+7.010	+9.220	+11.800
				-7.920	-5.990	-3.750	-1.340	+1.310
				-18.640	-16.320	-13.840	-11.280	-8.480
-34.266	-33.941	-32.675	-30.700	-28.420	-25.945	-23.282	-20.531	-17.680
-43.203	-42.886	-41.430	-39.360	-37.120	-34.730	-32.020	-29.260	-26.765
-51.268	-50.968	-49.270	-47.010	-44.790	-42.550	-39.920	-37.180	-34.180
-58.563	-58.263	-56.330	-54.170	-51.840	-49.660	-47.240	-44.620	-41.600
-65.158	-64.858	-62.760	-60.360	-58.000	-55.900	-53.600	-51.000	-48.000
-71.103	-70.803	-68.500	-66.000	-63.500	-61.400	-59.200	-56.700	-53.700

Figure 11 Relaxation Net with Values of the Stress Function, Ψ , Multiplied by 225, for the Case $\frac{\sigma_n}{\sigma_{yd}} = 0.81$

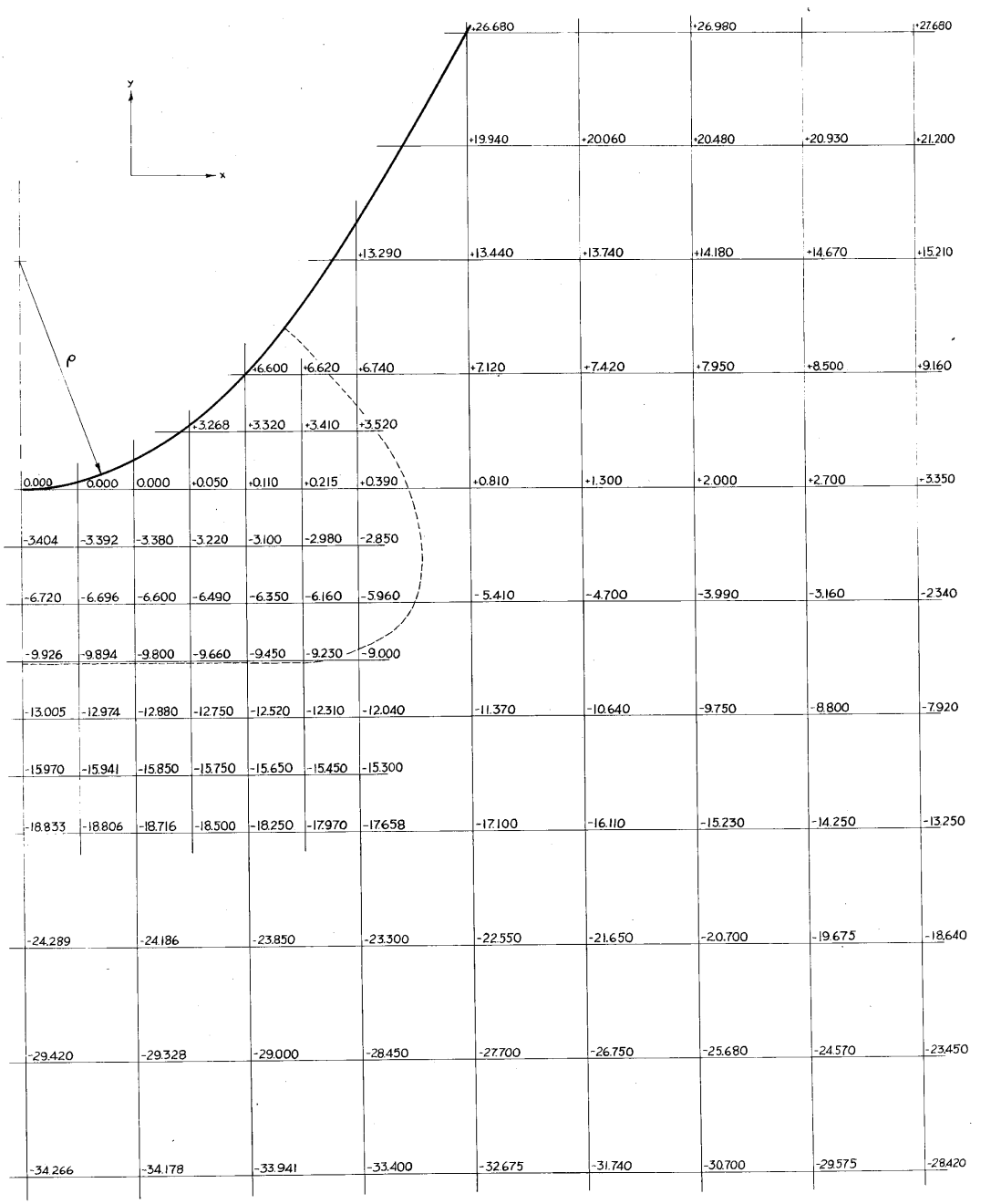

Figure 12 Relaxation Net in the Region of the Notch Root with Values of the Stress Function, Ψ, Multiplied by 225

This sub-region is shown on a larger scale in Figure 12, and contains the lattice points at spacings of d = 1/30 and d = 1/60 as well as those of d = 1/15.

The principal stresses at the minimum cross-section, computed by means of Equation 18, are shown as a function of position, $(a - y)/\rho$, near the root of the notch in Figure 13 for the case $\sigma_n/\sigma_{yd} = 0.81$. The full lines represent the stresses for elastic-plastic deformation and the dashed lines show the stresses for purely elastic deformation. The maximum stress, $(\sigma_a)_{max}$, in the case of elastic-plastic deformation is the stress in the x direction at the elastic-plastic boundary. The value of this maximum tensile stress in the notched bar has been determined for the several values of nominal stress for which the elastic-plastic stress analysis has been made. The relationship between $(\sigma_a)_{max}/\sigma_{yd}$ and σ_n/σ_{yd} for the notch considered in this investigation is shown in Figure 14.

The elastic stress concentration factor for the particular notch investigated is 4.96. Hence, at a value of $\sigma_n/\sigma_{yd} = 1/4.96$ yielding will just begin at the root of the notch at which point $(\sigma_a)_{max}/\sigma_{yd} = 1$. The body deforms purely elastically for any value of $\sigma_n/\sigma_{yd} < 1/4.96$ as indicated in Figure 14. The regions of plastic deformation which occur for values of $1/4.96 < \sigma_n/\sigma_{yd} < 1.35$ are similar to the region of plastic deformation shown in Figure 12, in that they are confined to the immediate vicinity of the root of the notch. However, when σ_n/σ_{yd} exceeds about 1.35, narrow regions of plastic deformation extend toward the axis of the specimen but away from the minimum cross-section. This mode of plastic deformation is very similar to that found by Allen and Southwell (25)

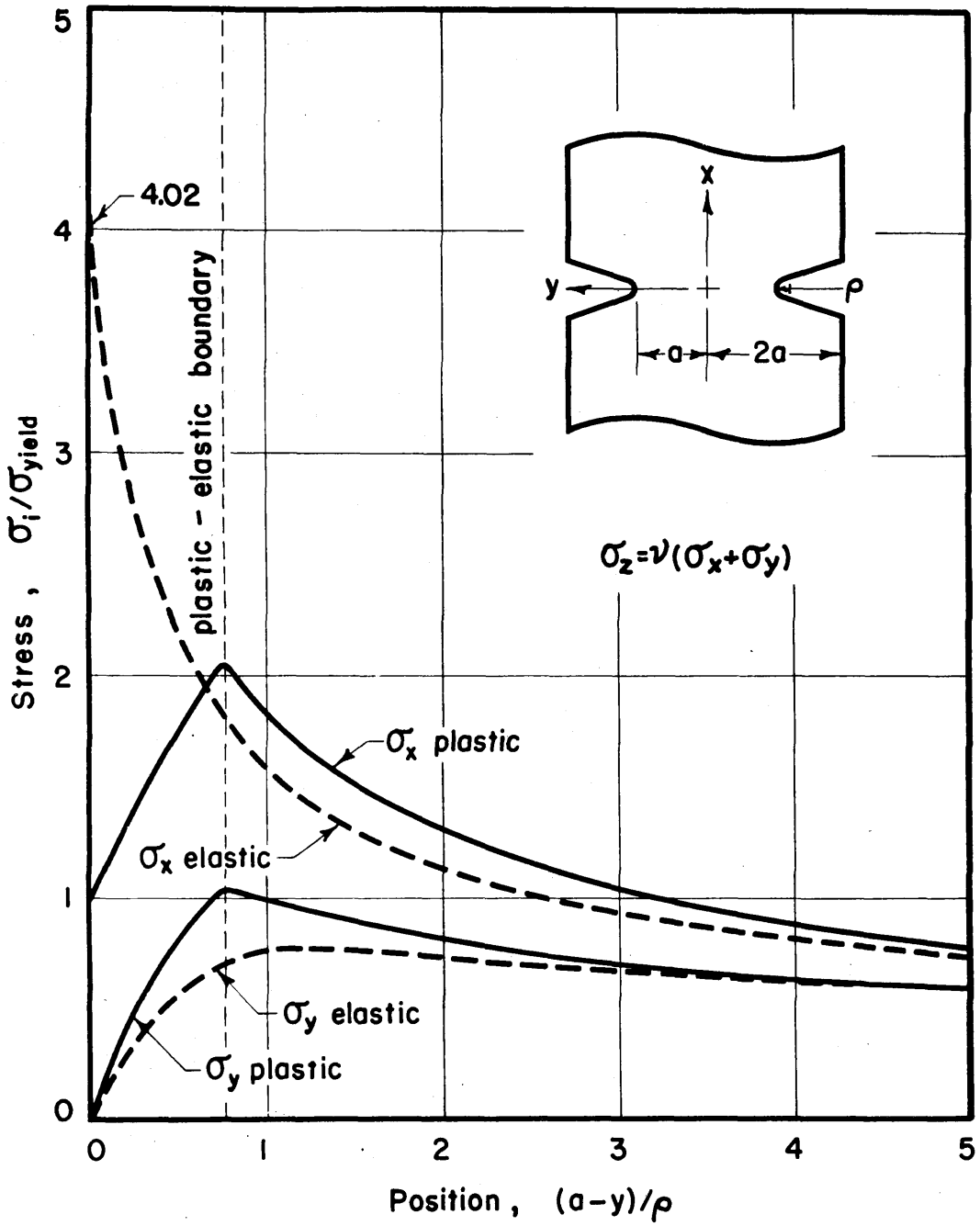

Figure 13 Principal Stresses vs. Position on the Minimum Cross-Section of a Plane Notched Bar with $\frac{a}{\rho} = 15$ under a Nominal Tensile Stress of $\frac{\sigma_n}{\sigma_{yd}} = 0.81$

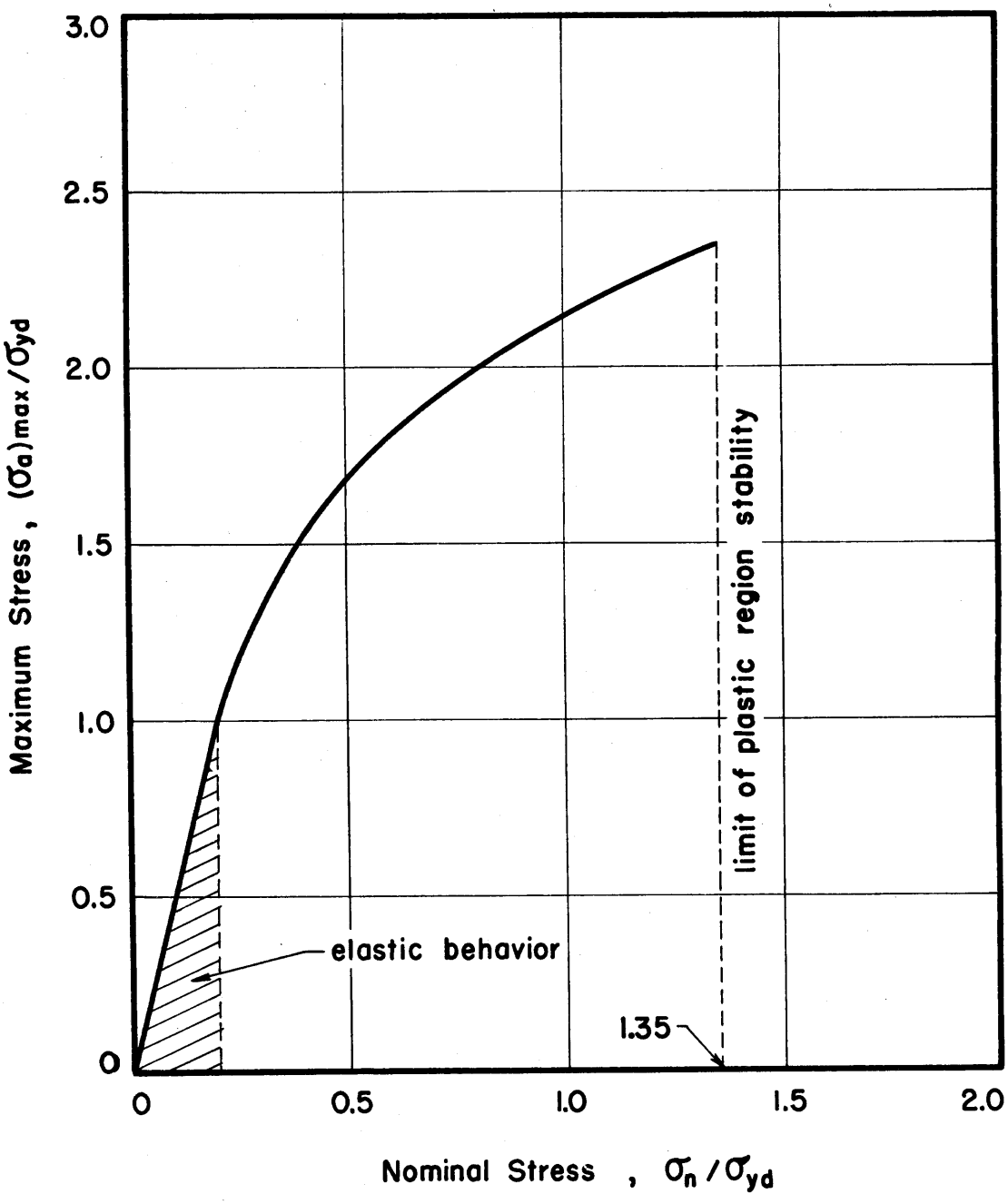

Figure 14 Maximum Stress Ratio, $\frac{(\sigma_a)_{max}}{\sigma_{yd}}$ vs. Nominal Stress Ratio, $\frac{\sigma_n}{\sigma_{yd}}$, for a Plane Notched Bar with $\frac{a}{\rho}=15$

for "v" notched specimens when a critical load is exceeded. The extended regions of plastic deformation join with small isolated plastically deformed regions which form on the axis of the specimen away from the center of symmetry. Thus for the notch considered in this investigation the confined plastic regions at the root of the notch become unstable at a nominal stress of $\sigma_n = 1.35\sigma_{yd}$, and plastic deformation extends completely across the body for very little further increase in the applied load. As Hill (26) has pointed out, the present method of solution is no longer strictly valid for loads which exceed this critical value. For this reason the relation between $(\sigma_a)_{max}/\sigma_{yd}$ and σ_n/σ_{yd} shown in Figure 14 is terminated at the value $\sigma_n/\sigma_{yd} = 1.35$

A consistent definition of "brittle" as opposed to "ductile" fracture in notched specimens may be made on the basis of the foregoing results. Namely, "brittle" fracture is a fracture which takes place while the plastically deformed regions are confined to the vicinity of the notch root. Thus any fracture which occurs in the particular notched specimen employed in this investigation, at a nominal stress, σ_n, such that $\sigma_n/\sigma_{yd} < 1.35$ is a "brittle" fracture. Conversely any fracture which occurs after plastic deformation has progressed to the axis of the specimen, i.e., when $\sigma_n/\sigma_{yd} > 1.35$, is a "ductile" fracture. This definition of the distinction between brittle and ductile fractures should correlate well with the transition in the amount of energy absorbed by the notched specimen, since the total energy absorbed will increase markedly

when the plastically deformed region extends to the specimen axis.

The results of the theoretical investigation provide a means for computing the maximum stress beneath the root of the notch at the instant of initiation of brittle fracture. These calculations can be made provided the values of the nominal fracture stress, σ_{nf}, and the yield stress, σ_{yd}, are determined experimentally, for different constant rates of stress application and temperatures. The variation of the yield stress with rate of stress application and temperature has been determined in the previous section of this thesis. Hence, it remains to determine the nominal fracture stress, σ_{nf}, as a function of rate and temperature.

3:3 Material Tested and Test Specimen

The material used in this investigation is the same 0.17 per cent carbon-steel employed in previous studies (2), (3). Thus its delayed yield behavior under rapidly applied constant stress in the absence of notches is known for extensive ranges of stress and temperature. The details as to annealing treatment and metallurgical analysis have been given in part 2:2 of this thesis.

The form of notch chosen for the experimental investigation is a hyperboloid of revolution. This form was chosen for two principal reasons: First, a complete elastic stress analysis is available from the work of Neuber (23), and second, a notch of this type may be accurately machined by a generating process.

The use of a specimen in the form of a wide plate with two symmetric hyperbolic notches on the faces would be preferable for the purpose of affording a direct relationship between the experimental results and the theoretical elastic-plastic stress analysis.

However, this was not feasible with the available rapid load testing machine. This machine has a maximum load capacity of 10,000 lb. Therefore the thickness of a sufficiently wide flat plate specimen at the minimum cross-section and the radius of curvature at the root of the notch would be about 0.150 in. and 0.005 in. respectively. Such specimens would be quite difficult to manufacture, since a notch in a plate cannot be generated. Furthermore, experimental errors due to bending stresses would be about doubled as compared with the axially symmetric specimen having a diameter at the minimum section of 0.300 in. Thus the theoretical advantage of a wide plate specimen would be offset by its practical disadvantages.

The profile of the experimental notch is the same as the notch considered in the stress analysis. The ratio between the radius of the specimen at the minimum cross-section and the radius of curvature of the root of the notch is $a/\rho = 15$, since $a = 0.150$ in. and $\rho = 0.010$ in.

The notches are cut in a cylindrical specimen of 0.600 in. diameter. Thus the stress analyses for an infinitely deep notch does not strictly apply. However, since the notch root radius is small compared with the notch depth, the errors introduced in this way are negligible.

The specimen design is shown in Figure 15. The notch was ground with a generating type of operation. The principle involved in this grinding operation is based on the fact that a hyperboloid of revoluation can be generated by straight lines. The method of grinding the notches is as follows. A carborundum grinding disc,

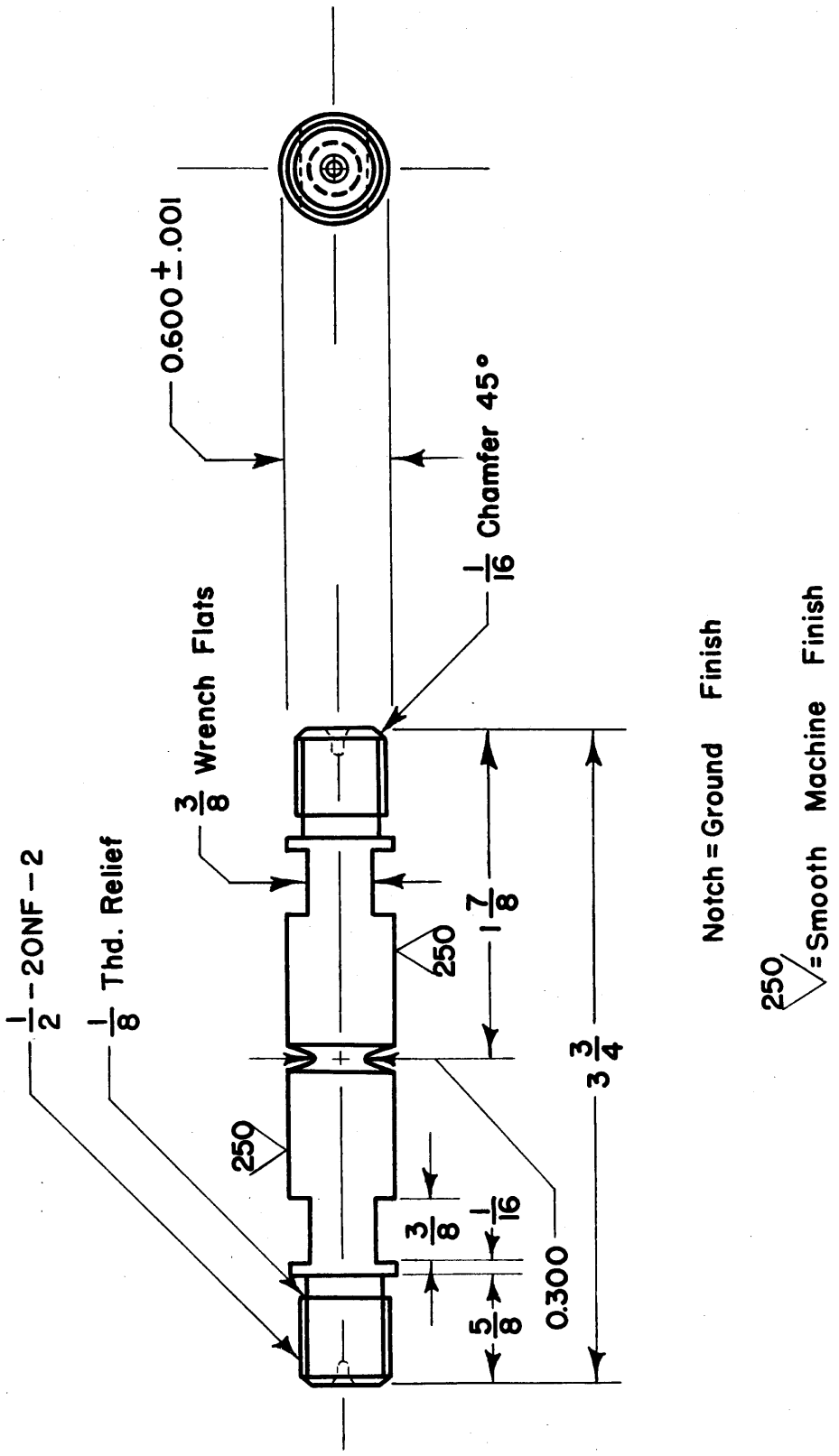

Figure 15 Notched Test Specimen

6 in. in diameter and 0.020 in. thick was faced to a sharp edge. The specimen was rotated about its cylindrical axis at a speed of about one r.p.m. by means of a suitable mechanism. This mechanism with the specimen was placed on the table of a No. 2 Cincinnati tool and cutter grinder with the axis of the specimen at $12\frac{1}{2}^{o}$ to the axis of rotation of the grinding disc. The table of the grinding machine was given an oscillatory motion parallel to the plane of the grinding disc. The sharp edge of the grinding disc together with the oscillatory motion of the grinding machine table serves as the straight line generator of the hyperboloid of revolution. The rotation of the specimen about its own axis causes this line to generate the desired notch surface. The depth of the notch is controlled by the feed of the table into the grinding disc. The finite thickness of the edge of the grinding disc and the unavoidable small wobble of the disc, causes the generation of a notch corresponding to an angle of $14\frac{1}{2}^{o}$. The latter value is the angle associated with a notch for which $a/\rho = 15$.

The dimensions of the notches produced by this method were determined by means of an optical comparator. The measurements show that the notches correspond quite well to the theoretical shape as indicated in Figure 16. The radius of curvature at the root of the notch is reproducible to within 10 per cent from specimen to specimen. The details of the measurement of the notch shape and the determination of the notch root radius of curvature therefrom are given in Appendix 3.

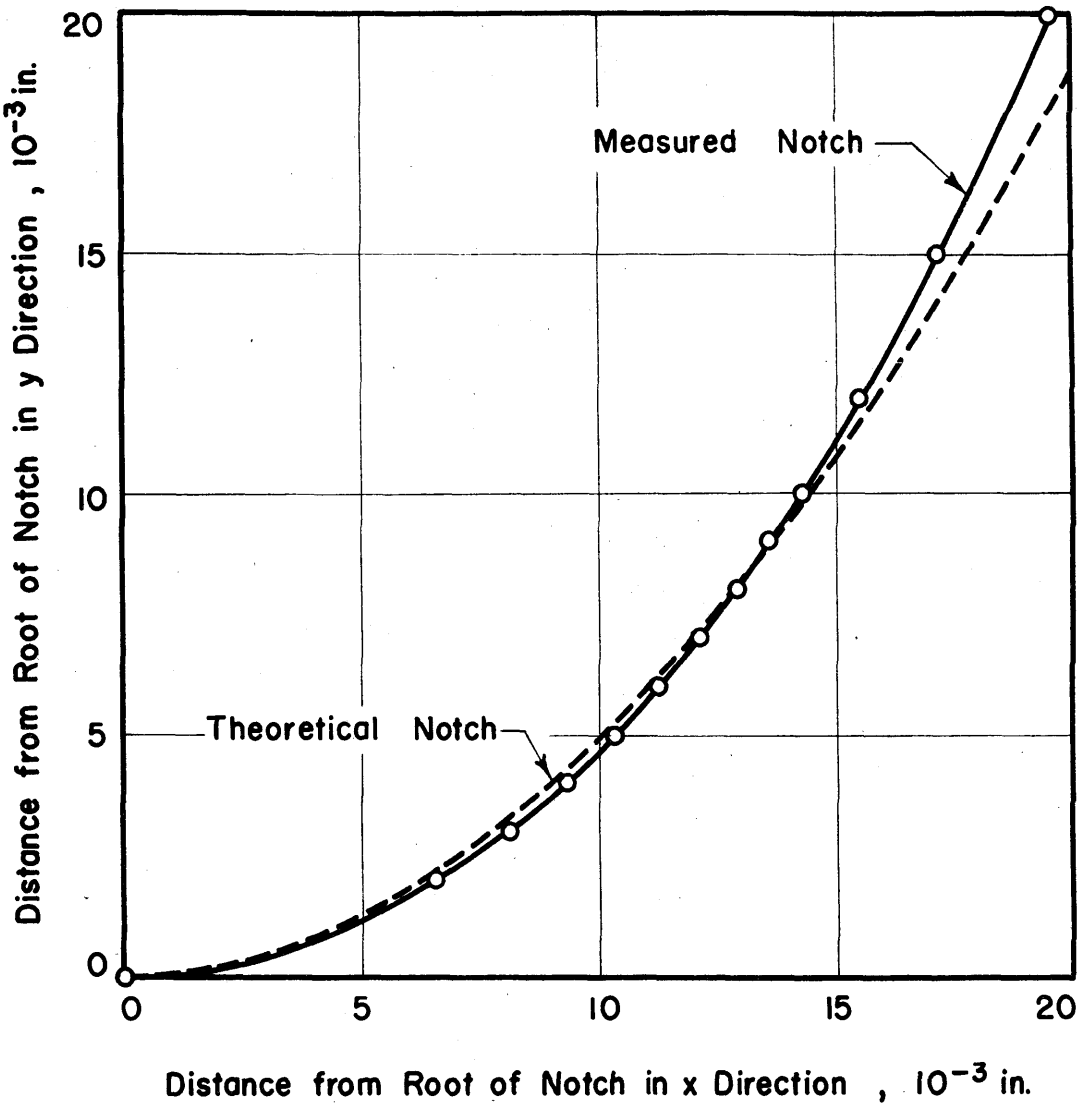

Figure 16 Comparison of the Ground Specimen Notch with the Theoretical Notch

3:4 Equipment and Test Procedure

1. Rapid Load Tests on Notched Specimens

The means of obtaining and measuring the rates of load application are the same as described previously in part 2:3 of this thesis. The diameter of the minimum section of the notched test specimen is the same as the gage section diameter of the unnotched test specimen described in part 2:2, namely 0.300 in. Hence the maximum nominal stress at the minimum section of the notched specimen and the range of rate of nominal stress application attainable at the minimum section is the same as was obtainable for the tests on unnotched specimens, namely, 140,000 lb/in.^{2} and from about 10^2 to 10^7 lb/in.^{2} sec respectively.

The notched mild steel specimens were tested at temperatures of -23° F (-30° C), -110° F (-79° C), and -200° F (-129° C). The test temperature of -23° F (-30° C) was accomplished by placing liquid Freon 12, previously liquefied by the use of dry ice, into a hard rubber container surrounding the specimen and attached to the grips. The boiling of the Freon provides a simple and stable thermostatic bath. The test temperatures of -110° F (-79° C) and -200° F (-129° C) were secured in the fashion described in part 2:3 of this thesis.

The temperature of the notched specimens was determined by means of copper constantan thermocouples secured to the specimen by "Scotch" electrical tape. A thermocouple was secured to the specimen at each of two positions about 1/4 in. on each side of the notch. Readings during tests indicated that the total temperature

difference across the notch was less than $\pm$ 4°F for the tests at a temperature of -200° F (-129° C), and negligible for the other two test temperatures. The temperature variation during a test and from test to test was about $\pm$ 3°F at -200° F (-129° C) and negligible at temperatures of -110° F (-79° C) and -23° F (-30° C).

2. Static Tests on Notched Specimens

Static tests were performed to check the theoretical prediction that macroscopic yielding occurs at a critical value of the ratio between the nominal stress and the yield stress. The static tests were performed at room temperature and at -23° F (-30° C). The tests at a temperature of -23° F (-30° C) were made in the rapid load testing machine with the same grips and means of obtaining test temperatures as for the tests at higher loading rates. These tests were performed by controlling the applied load with the various manually operated valves associated with the machine in such a manner that the load was applied in steps. The static test at room temperature was performed on a 150,000 lb Olsen Universal Testing Machine having a least reading of 1 lb. The head of the rapid load testing machine was mounted in the static testing machine so as to provide for the gripping of the specimen in such a manner that the bending stesses in the specimen were minimized.

The extension of the specimen in the static tests was measured by means of type AD-7 SR-4 wire strain gages. The gages were bonded to strips of steel shim stock 0.001 in. thick, 0.4 in. wide and long enough to bridge the notch in the specimen. Two

such strips with gages attached by Duco cement were placed diametrically opposite one another on the specimen such that the gage section of the wire strain gages bridged the notch on the specimen. The steel strips were held to the specimen by means of specially designed small aluminum clamps.

Temperature compensation was obtained by means of strain gages attached to an unstrained specimen maintained at the same temperature as the test specimen. These strain gages were connected in the same bridge circuit with the strain gages on the test specimen. The extensions across the notch of the specimen were obtained from the measurements on the assumption that the strain in the steel strips was uniform. Thus the extension was taken as the strain indicated by the strain gages multiplied by the gage length of the steel strip.

The extension of the specimen in the static test at room temperature was also determined by a second method which permitted the determination of greater extensions than those obtained by means of the strain gages. Two extensometers, mounted diametrically opposite to one another, were attached to the specimen grips. The extensometers, employing SR-4 wire strain gages, have been described previously (2). A correction factor, based upon the strain gage indications, was applied to the extensometer measurement to account for the elastic extension of the specimen grips and the part of the specimen away from the notch.

The load in the static tests was measured by the same dynamometer employed in the dynamic tests. The signals from

the strain gages, extensometers and dynamometer were recorded with the same oscillograph used in the dynamic tests after a period of about five minutes at each load increment.

3. Location of the Elastic-Plastic Boundary

The position of the elastic-plastic boundary may be determined theoretically. Hence, the theory can be checked by comparing the elastic-plastic boundary determined theoretically against that determined experimentally. The position of this boundary was determined experimentally for several of the notched specimens that fractured at test temperatures of -110° F (-79° C) and -200° F (-129° C).

The fractured specimens were sectioned longitudinally along the axis of symmetry and mounted in lucite. The specimens were then alternately polished and etched to remove the cold worked surface layer. A micro-hardness survey was then made in the vicinity of the root of the notch. The hardness determinations were made with a Tukon Hardness Tester, using a 136° diamond penetrator and a 0.2 kg load. Hardness readings were taken at a sufficient number of points to establish the position of the elastic-plastic boundary. All hardness readings were taken in regions of ferrite grains, since the pearlite is harder than the ferrite and any overlap of the penetrator between the two structures would give a misleading hardness indication. The positions of penetration of the diamond were such that the distance of closest approach between any two indentations, or between any indentation and the boundary of the notch was not less than the width of the indentation.

3:5 Experimental Results

1. Rapid Load Tests on Notched Specimens

The results of the tests on notched specimens are shown in Figure 17 for temperatures of -110° F (-79° C) and -200° F (-129° C). These results are also listed in Table I (see page 76), together with the results obtained at a temperature of -23° F (-30° C). Figure 17 shows the relation between the nominal fracture stress, σ_{nf}, and the logarithm of the rate of nominal stress application (nominal stress rate). The trend of the test points is represented by straight lines for both test temperatures. The specimens tested at a temperature of -110° F (-79° C) fractured when the nominal stress rate at the minimum section was greater than about 10^6 lb/in.^{2} sec. Nominal stress rates of less than about 10^6 lb/in.^{2} sec did not produce fractures at a temperature of -110° F (-79° C) within the range of maximum obtainable nominal stress (140,000 lb/in.^{2}) and maximum attainable specimen extension (0.05 in.). The results of tests at a temperature of -110° F (-79° C) in which fracture did not occur are shown with arrows in Figure 17 indicating that fracture would eventually occur if there were no restrictions on specimen extension or applied load.

Fractures occurred in the notched specimens tested at a temperature of -200° F (-129° C) within the entire range of applied nominal stress rates (1.4×10^2 to 1.4×10^7 lb/in.^{2} sec). Fractures did not occur in any of the four tests at a temperature of -23° F (-30° C) which included the range of stress rates from 5.7×10^6 to 1.49×10^7 lb/in.^{2} sec.

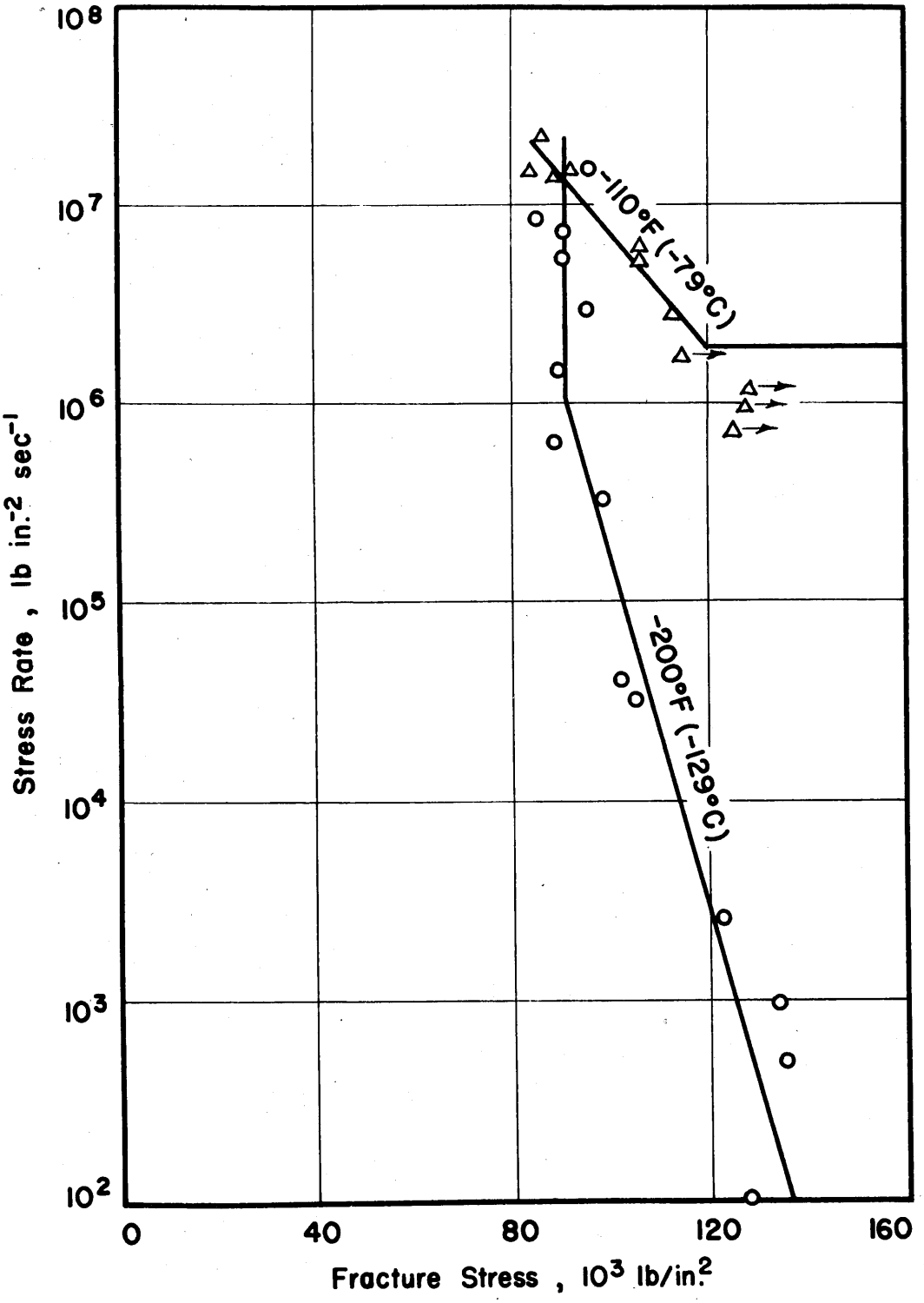

Figure 17 Nominal Stress Rate vs. Nominal Fracture Stress for Notched Specimens Tested at -110°F (-79°C) and -200°F (-129°C)

2. Static Tests on Notched Specimens

The relations between the nominal stress on the minimum section and the extension under load in the static tests of notched specimens at room temperature and -23° F (-30° C) are shown in Figures 18 and 19, respectively. The scales of extension on these curves terminate prior to fracture because of the limited ranges of the means employed for extension measurements. However, the tests were continued until the specimens fractured. The nominal stress at the minimum section at the instant of fracture was about 100,000 lb/in.^{2} at room temperature and 125,000 lb/in.^{2} at a temperature of -23° F (-30° C). The periphery of the fracture surface, in each case, was composed of a small "shear lip" indicating ductile behavior of the material immediately below the root of the notch. The actual fracture surface, aside from the shear lip, had the general appearance of a brittle type fracture. However, a large amount of plastic deformation preceded fracture so that the fractures in the static tests are not considered to be of the brittle type according to the definition used in this thesis.

3. Location of the Elastic-Plastic Boundary

The results of the surveys of micro-hardness on the cross-sections of notched specimens that fractured are shown in Figures 20, 21, 22 and 23 for values of σ_{nf}/σ_{yd} equal to 0.79, 0.9, 1.25 and 1.64, respectively. The means of obtaining the ratio σ_{nf}/σ_{yd} will be explained in a subsequent section of this thesis. The boundary delineating the regions of plastic and elastic behavior is also shown. The values of the hardness in the region of elastic

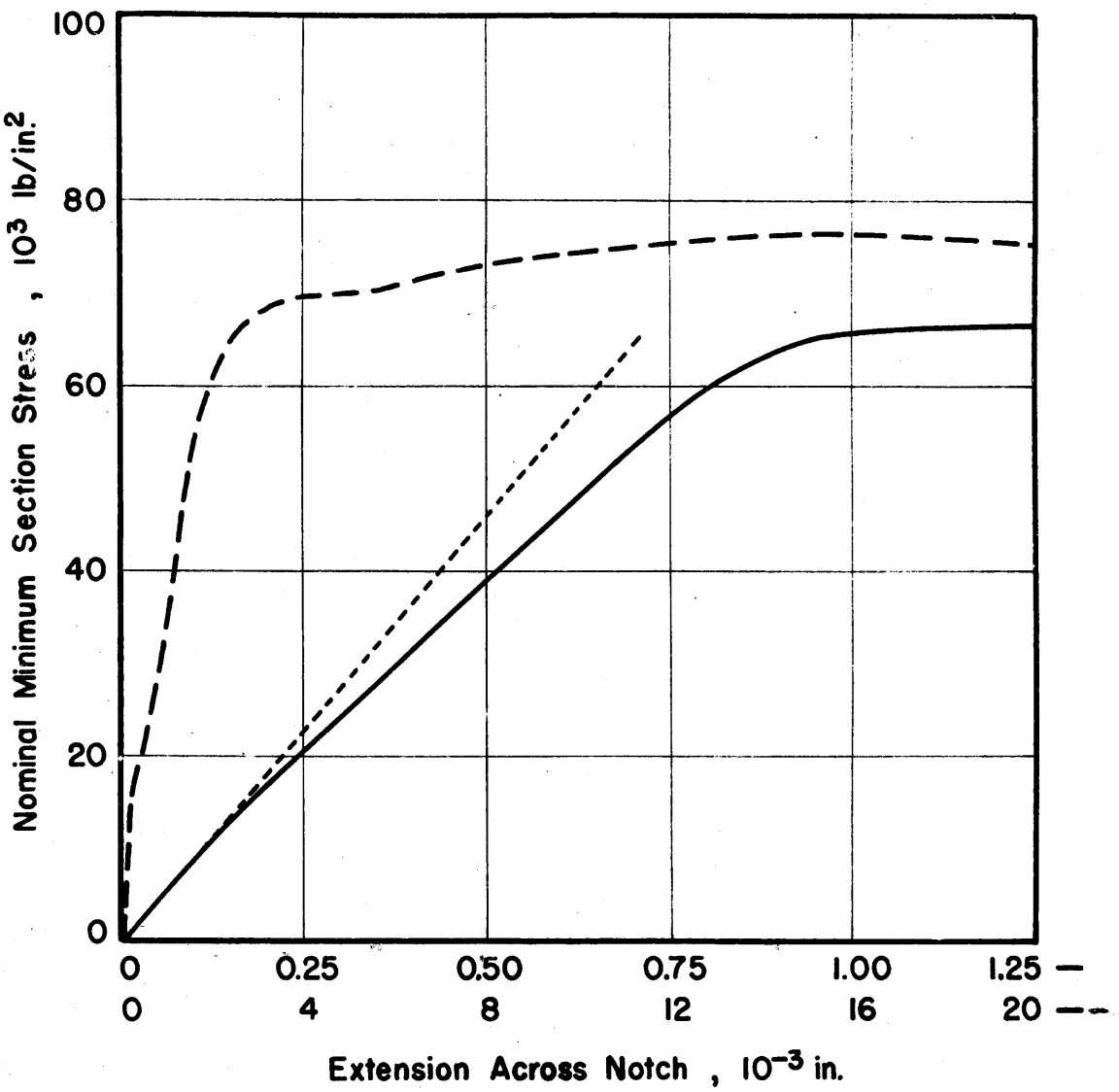

Figure 18 Nominal Stress vs. Extension Across the Notch for Static Test at Room Temperature

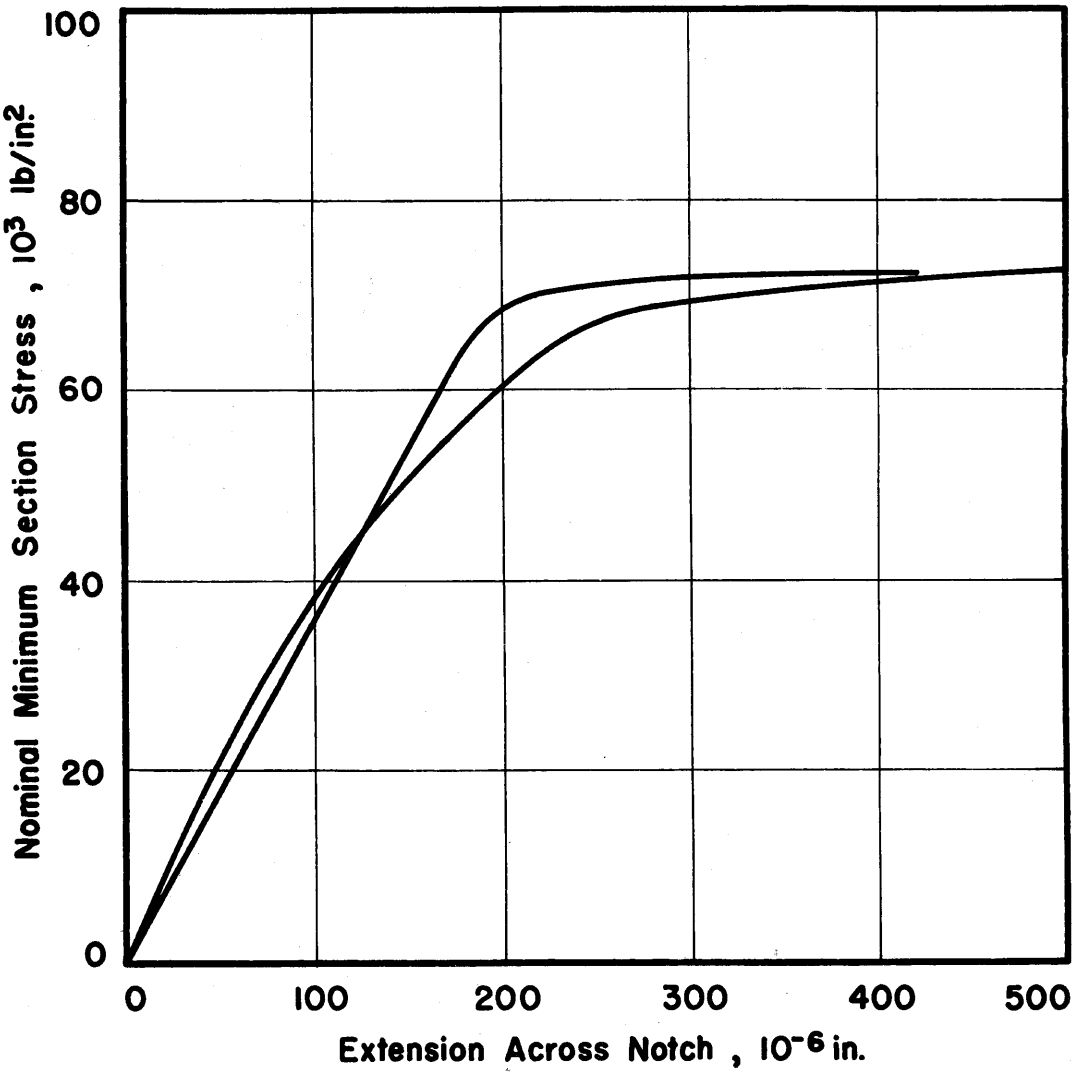

Figure 19 Nominal Stress vs. Extension Across the Notch for Static Tests at -23°F (-30°C)

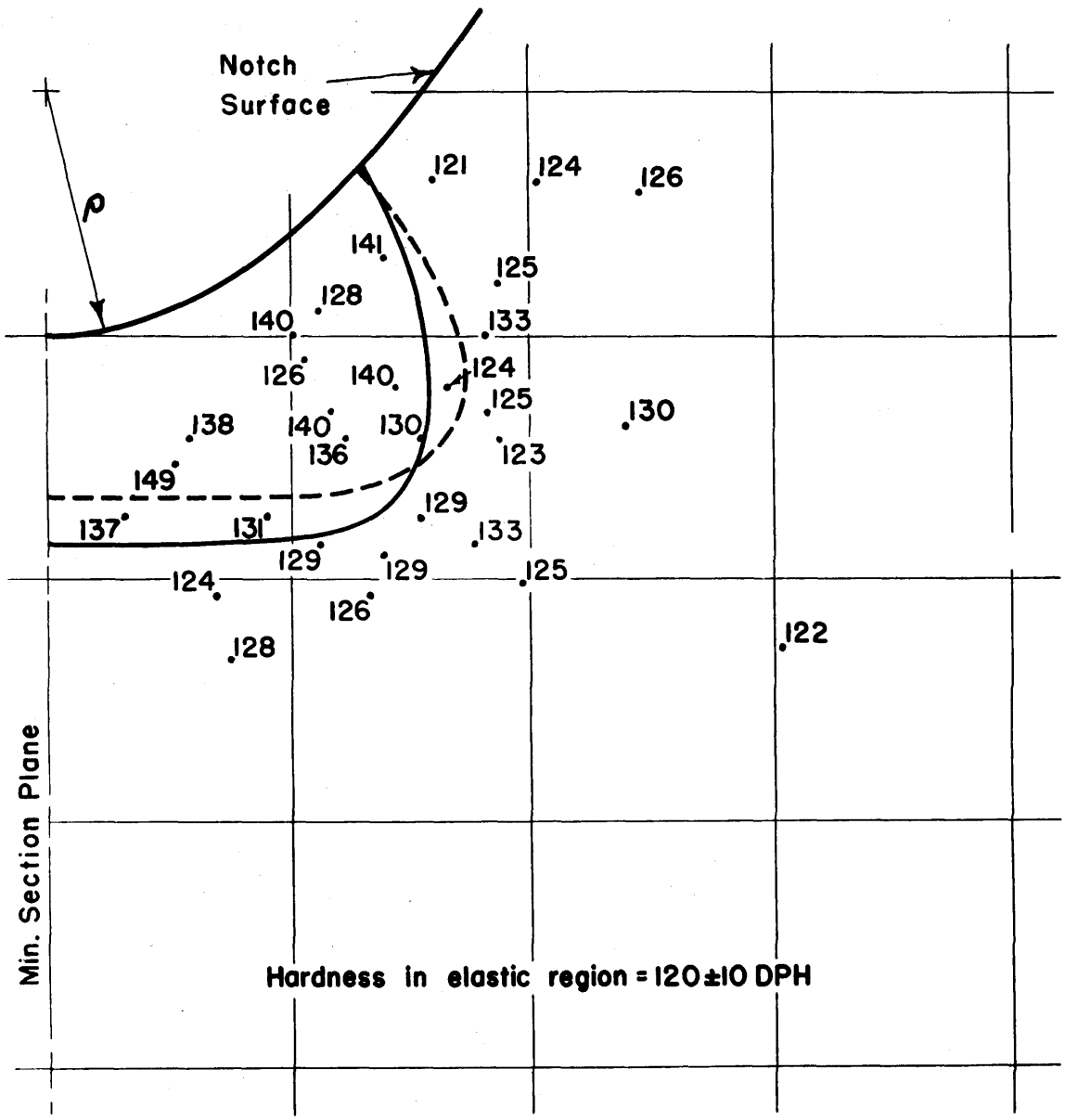

Figure 20 Diamond Penetration Hardness vs. Position and Elastic-plastic Boundary for a Test at -200°F (-129°C) with Fracture at $\frac{\sigma_{nf}}{\sigma_{yd}} = 0.78$

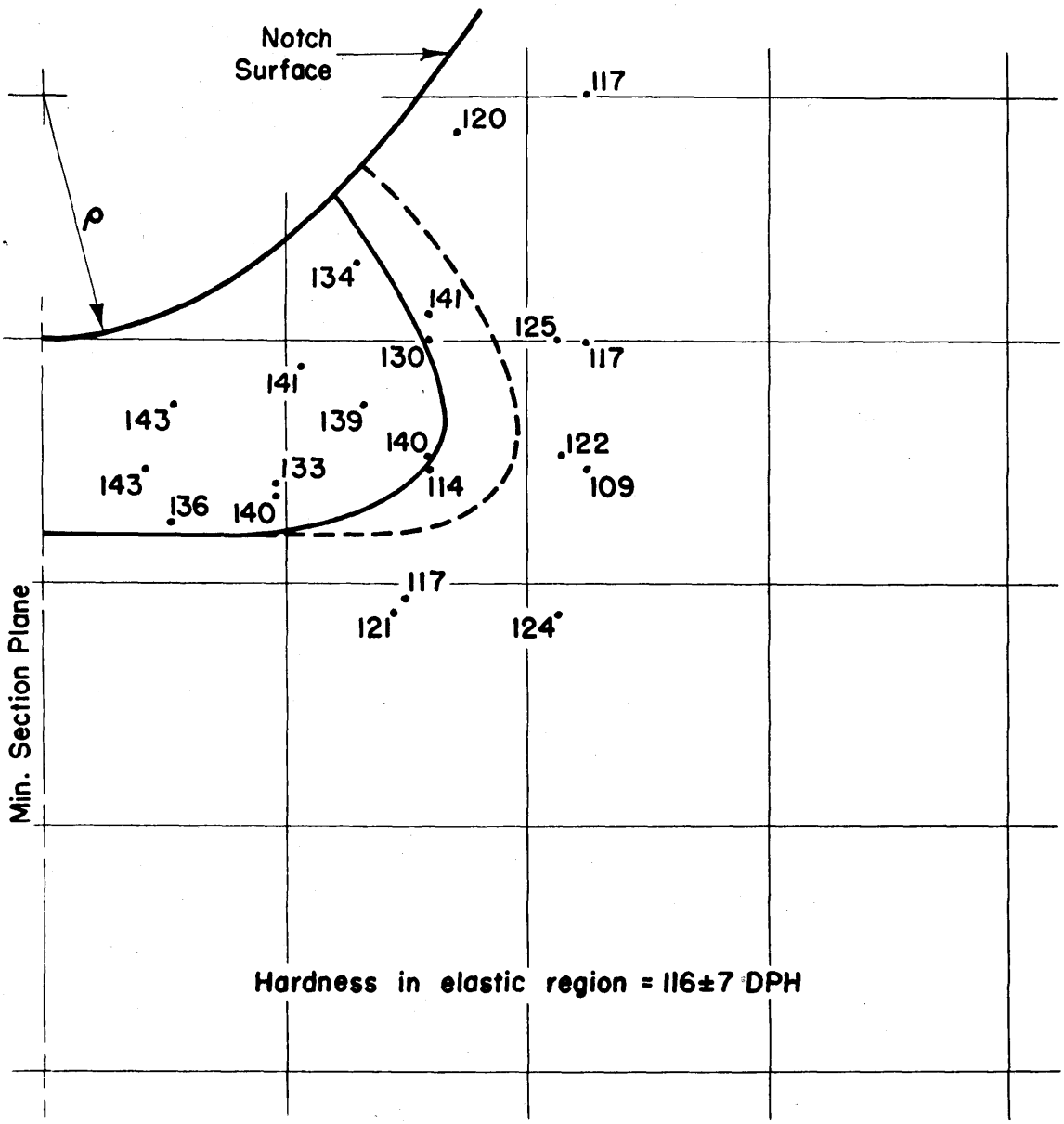

Figure 21 Diamond Penetration Hardness vs. Position and Elastic-Plastic Boundary for a Test at -110°F (-79°C) with Fracture at $\frac{\sigma_{nf}}{\sigma_{yd}} = 0.90$

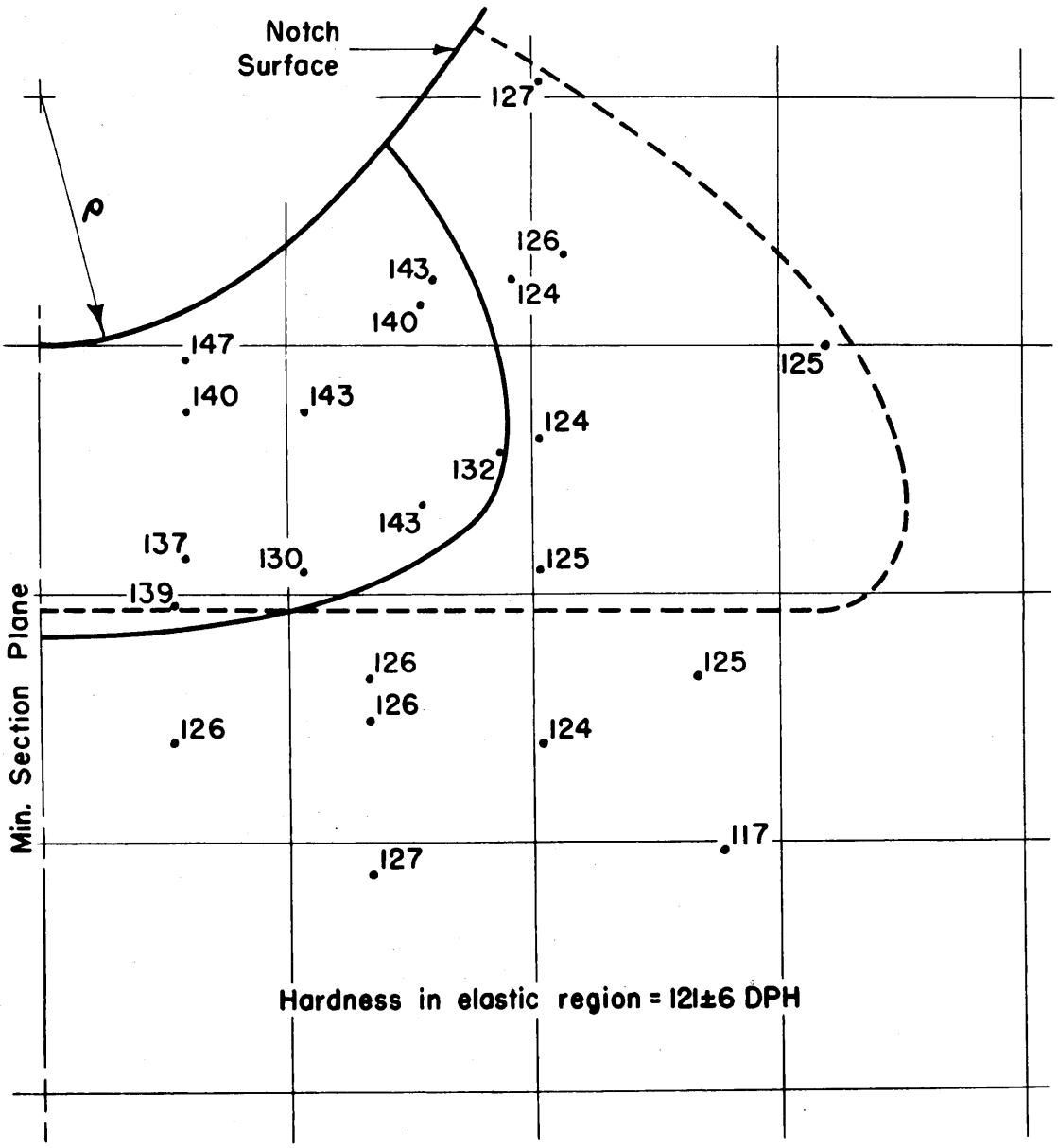

Figure 22 Diamond Penetration Hardness vs. Position and Elastic-Plastic Boundary for a Test at -110°F (-79°C) with Fracture at $\frac{\sigma_{nf}}{\sigma_{yd}} = 1.25$

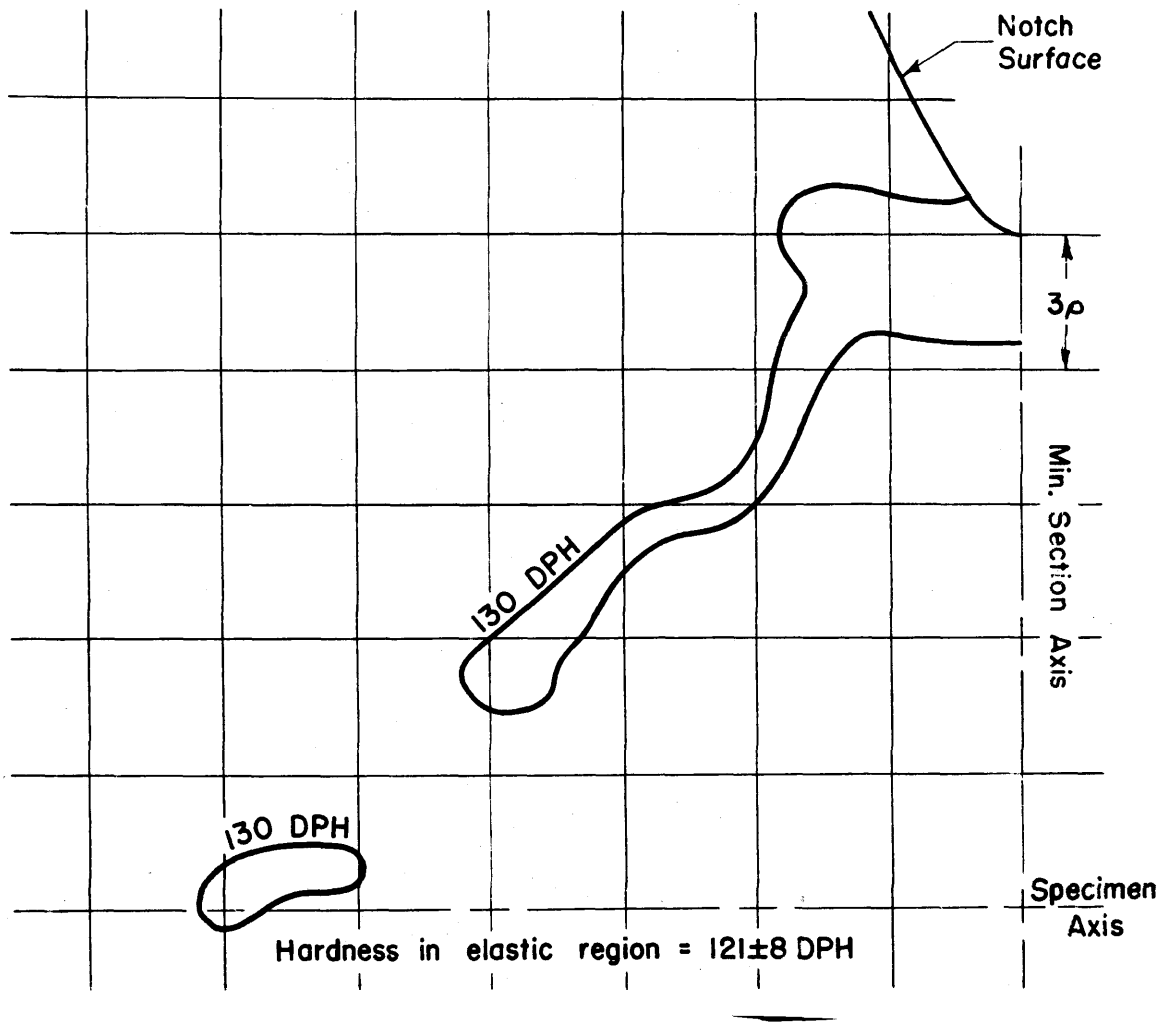

Figure 23 Elastic-Plastic Boundary for a Test at -200°F (-129°C) with Fracture at $\frac{\sigma_{nf}}{\sigma_{yd}} = 1.64$

behavior given on these figures were determined by 10 measurements taken at positions remote from the notch root. The elastic-plastic boundary, shown by the solid lines in Figures 20, 21, 22 and 23 bounds the region within which the hardness is greater than the maximum hardness obtained in the elastic region. The dashed boundaries shown in Figs. 20, 21 and 22 are the elastic-plastic boundaries as predicted by theory. The theory is not applicable to values of $\sigma_{nf}/\sigma_{yd} > 1.5$, hence there is no theoretical elastic-plastic boundary shown in Figure 23. The experimental elastic-plastic boundary for $\sigma_{nf}/\sigma_{yd} = 1.64$, shown in Figure 23 is based on the results of about 140 hardness readings.

3:6 Discussion

The maximum stress within the notched test specimens at the instant of initiation of brittle fracture may be determined by application of the elastic-plastic stress analysis to the experimental results. However, it is necessary to consider the fact that the stress analysis is made for plane strain deformation whereas the experiments were performed on axially symmetric specimens. An exact comparison between the stresses in axially symmetric and plane bodies of the shape considered in this thesis may be made in the case of purely elastic deformation. This is possible since Neuber (23) has obtained analytical solutions for both of these problems. These analytical solutions are listed in Appendix 2 and the comparison is shown in Figure 24.

This shows that in the region extending a distance of about one root radius, ρ, below the root of the notch, the elastic stresses,

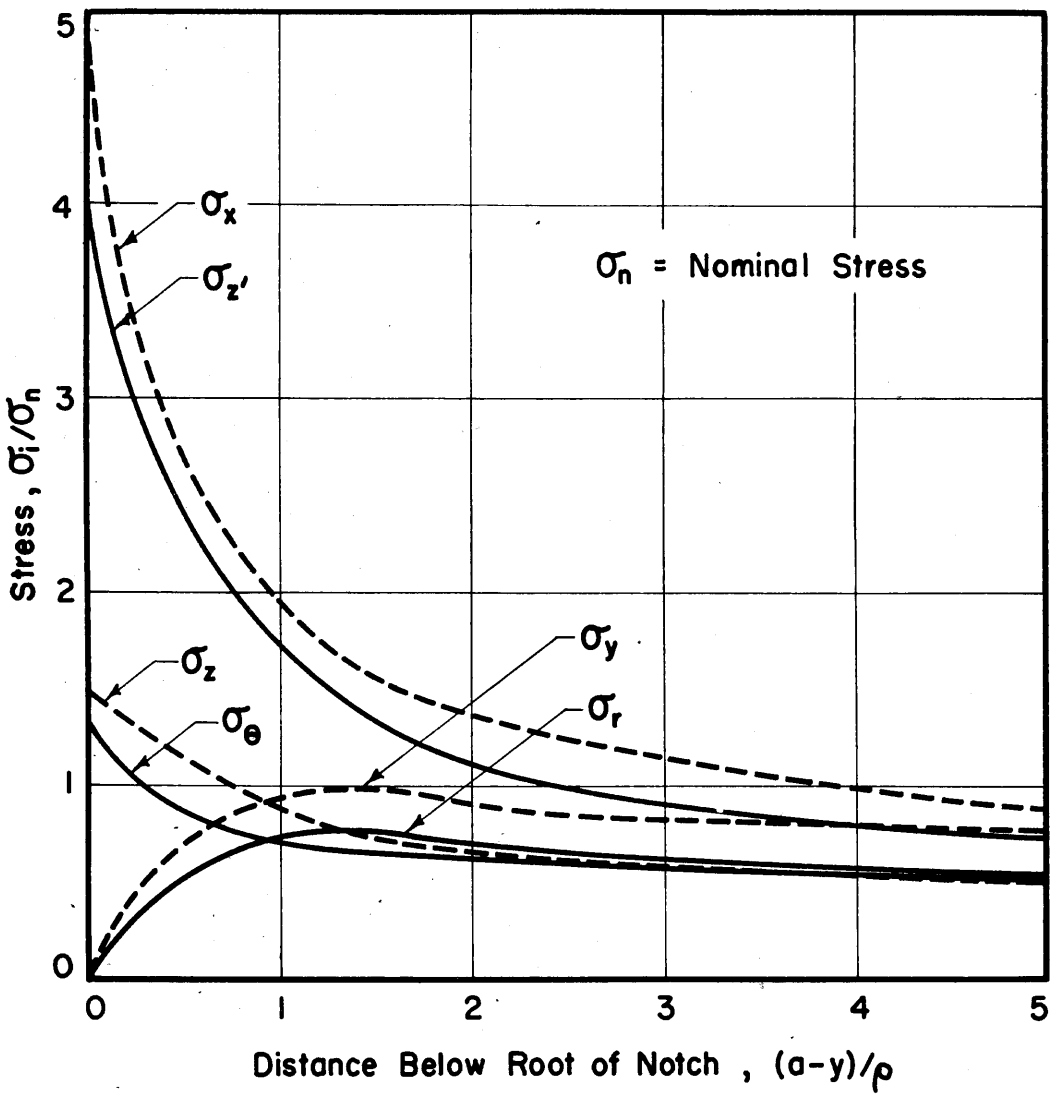

Figure 24 Comparison of Elastic Stresses at the Minimum Cross-Section of Axially Symmetric $(\sigma_{z'}, \sigma_n, \sigma_\theta)$ and Plane $(\sigma_x, \sigma_y, \sigma_z)$ Bars with Hyperbolic Notches

$\sigma_{z'}$, σ_r, and σ_θ in the axial, radial, and circumferential directions respectively, are smaller in the axially symmetric body than the corresponding stresses, σ_x, σ_y, and σ_z in the plane body under the same nominal stress, σ_n. For example, the axial stress $\sigma_{z'}$, at the root of the notch in the axially symmetric body is 4.03 times the nominal stress while the axial stress at the root of the notch in the plane body is 4.96 times the nominal stress.

The region extending for a distance of about one root radius of curvature below the root of the notch is the region of primary interest for this investigation. This is true because the depth of penetration of the plastic deformation which occurs prior to the initiation of brittle fracture is limited to this region, as shown in Figures 20, 21 and 22. The elastic stresses in this region in the axially symmetric bar are nearly equal to those in the plane bar when the nominal stress in the axially symmetric bar is ten per cent greater than the nominal stress in the plane bar. This should also be the case when small plastic strains take place in the immediate vicinity of the notch root. Therefore in the application of the elastic-plastic stress analysis to the experimental results it will be assumed that the nominal stress acting on the test specimen for a given state of stress is ten per cent greater than the nominal stress which is required to produce the same state of stress in the plane bar. Thus the value of the nominal stress ratio, σ_n/σ_{yd}, which produces a given maximum axial stress ratio, $(\sigma_a)_{max}/\sigma_{yd}$, in the test specimen is taken to be ten per cent greater than the value shown by the curve in Figure 14. For example, the critical nominal stress ratio which produces instability of the region of plastic deformation in the

test specimens will be taken as $(\sigma_n/\sigma_{yd})_{crit.} = 1.5$ rather than the value 1.35 shown in Figure 14.

The application of the elastic-plastic stress analysis to the experimental results requires that the value of the yield stress, σ_{yd}, be known as a function of the rate of load application and temperature. The yield stress vs. stress rate has been established in part II of this thesis, the results being shown in Figure 4.

The relationship between the yield stress in unnotched specimens and the yield stress in notched specimens is now required. This relationship may be obtained as follows: the rate of increase of the axial stress at the root of the notch during the period of purely elastic deformation, $\dot{\sigma}_a$, in the notched specimen is equal to the product of the nominal rate of stress application, $\dot{\sigma}_n$, and the axial stress concentration factor, $k = 4.03$. Thus yielding in the notched specimen will begin when the axial stress at the root of the notch is equal to the yield stress as determined from tests on unnotched specimens for the same temperature but for a rate of stress application in the unnotched specimen equal to k times the nominal stress rate, $\dot{\sigma}_n$, for the notched specimen. The yield stress actually varies as yielding spreads from the root of the notch toward the axis of the specimen since the rate of stress rise at the elastic-plastic boundary varies as the boundary moves inward. However, the assumption will be made that the yield stress remains constant and equal to the initial value. The error introduced by this assumption is expected to be small in the case of brittle fracture since the plastic strain is confined to a small depth of penetration beneath the root of the notch.

Thus the ratio of the measured nominal fracture stress to the yield stress, σ_{nf}/σ_{yd}, may be computed for each test on notched specimens in which brittle fracture occurred. These values are given in Table I. A knowledge of the value of σ_{nf}/σ_{yd} for a particular fracture test allows the results of that test to be compared with theoretical predictions.

The validity of the application of the elastic-plastic stress analysis to the experimental results may be checked in two ways. First, the position of the elastic-plastic boundary determined from micro-hardness measurements may be compared with the position calculated by the analysis for different values of $\sigma_{nf}/\sigma_{yd} < 1.5$. This comparison is shown in Figures 20, 21, and 22 and substantiates the validity of the assumptions and the accuracy of the relaxation calculations made in the elastic-plastic stress-analysis.

Second, the results of the static tests on notched specimens may be used to check the theoretical prediction that yielding progresses to the axis of the notched specimen when the ratio between the nominal stress and the yield stress (σ_n/σ_{yd}) equals 1.5. The static tests should exhibit a marked increase in permanent extension at the nominal applied stress at which the instability of the plastic region is predicted because large plastic deformation would be expected when the plastic region reaches the axis of the specimen. The value of the static upper yield stress at room temperature for the steel used in this investigation is about 42,000 lb/in.^{2} (2). Hence the nominal stress corresponding to large scale plastic deformation in the static testing of the notched specimen at room temperature is predicted by the analysis to be 1.5 x 42,000 or 63,000 lb/in^2.

TABLE I

Experimental Results and Computed Values of the Maximum Tensile Stress, $(\sigma_a)_{max}$.

Specimen Number	Nominal Fracture Stress σ_{nf}, lb/in.^{2}	Nominal Stress Rate $\dot{\sigma}_n$, lb/in.^{2} sec	$\frac{\sigma_{nf}}{\sigma_{yd}}$	Temperature °F	$(\sigma_a)_{max}$, 10^{-3} lb/in.^{2}
58	128.0×10^3	1.03×10^2	1.64	-200 (1)	--
54	135.5×10^3	4.91×10^2	1.62	-200 (1)	--
57	133.8×10^3	9.97×10^2	1.54	-200	206
6	122.1×10^3	2.59×10^3	1.34	-200	207
3	105.6×10^3	3.27×10^4	1.04	-200	213
9	102.2×10^3	4.08×10^4	1.00	-200	211
27	98.35×10^3	3.41×10^5	0.89	-200	219
1	89.32×10^3	6.57×10^5	0.79	-200	215
7	89.27×10^3	1.41×10^6	0.77	-200	218
37	94.70×10^3	3.19×10^6	0.80	-200	226
29	90.60×10^3	5.50×10^6 (2)	--	-200	--
38	90.22×10^3	7.35×10^6 (2)	--	-200	--
4	85.30×10^3	8.84×10^6 (2)	--	-200	--
18	95.67×10^3	1.57×10^7 (2)	--	-200	--
44	No fracture	7.74×10^5	--	-110	--
33	No fracture	9.80×10^5	--	-110	--
10	No fracture	1.22×10^6	--	-110	--
52	No fracture	1.70×10^6	--	-110	--
26	113.0×10^3	2.88×10^6	1.17	-110	210
17	106.0×10^3	5.24×10^6 (3)	1.07	-110	209
28	106.0×10^3	6.46×10^6 (3)	1.06	-110	210
DI	88.59×10^3	1.45×10^7 (3)	0.86	-110	202
36	92.20×10^3	1.56×10^7 (3)	0.90	-110	206
DII	83.23×10^3	1.60×10^7 (3)	0.81	-110	200
34	85.90×10^3	2.20×10^7 (3)	0.82	-110	203
22	No fracture	3.62×10^6	--	-23	--
32	No fracture	4.35×10^6	--	-23	--
13	No fracture	5.70×10^6	--	-23	--
53	No fracture	1.49×10^7	--	-23	--

(1) Not obtainable since $\sigma_n/\sigma_{yd} > 1.5$ (Not brittle fracture)
(2) Not obtainable since yield stress not established for these rates.
(3) Based on extrapolation of yield stress vs. stress rate curves to higher rates than experimentally established.

Figure 18 shows that the corresponding experimental stress is actually about 67,000 lb/in^2. The static test results for notched specimens at a temperature of -23° F (-30° C), presented in Figure 19, show that a nominal stress of about 72,000 lb/in^2. produces a large plastic deformation. Hence the static yield stress for unnotched specimens at a temperature of -23° F (-30° C) should be 72,000/1.5 or about 48,000 lb/in^2. Although the static yield stress of an unnotched specimen of this steel at a temperature of -23° F (-30° C) has not been obtained, interpolation of values from the work of Wood and Clark (2) shows the yield stress to be close to the above value. The results of the static tests thus tend to further substantiate the theoretical results and the validity of the assumptions made in deriving the theory.

The elastic-plastic stress analysis shows that the axial tensile stress is a maximum at the elastic-plastic boundary on the minimum section of the notched specimens. The value that the maximum axial stress attains at the instant of brittle fracture may be computed by applying the analysis to the experimental results obtained in this investigation. The method of determining this stress may best be illustrated by reference to Figure 25. Figures 25 a and 25 b are schematic representations of Figures 17 and 4 respectively. Figure 25 c is a schematic representation of Figure 14. The latter represents the theoretical relation between the maximum axial stress ratio, $(\sigma_a)_{max}/\sigma_{yd}$, and the nominal stress ratio, σ_n/σ_{yd}. The values of σ_n/σ_{yd} in Figure 25 c are considered to be values in Figure 14 plus ten per cent, as discussed previously.

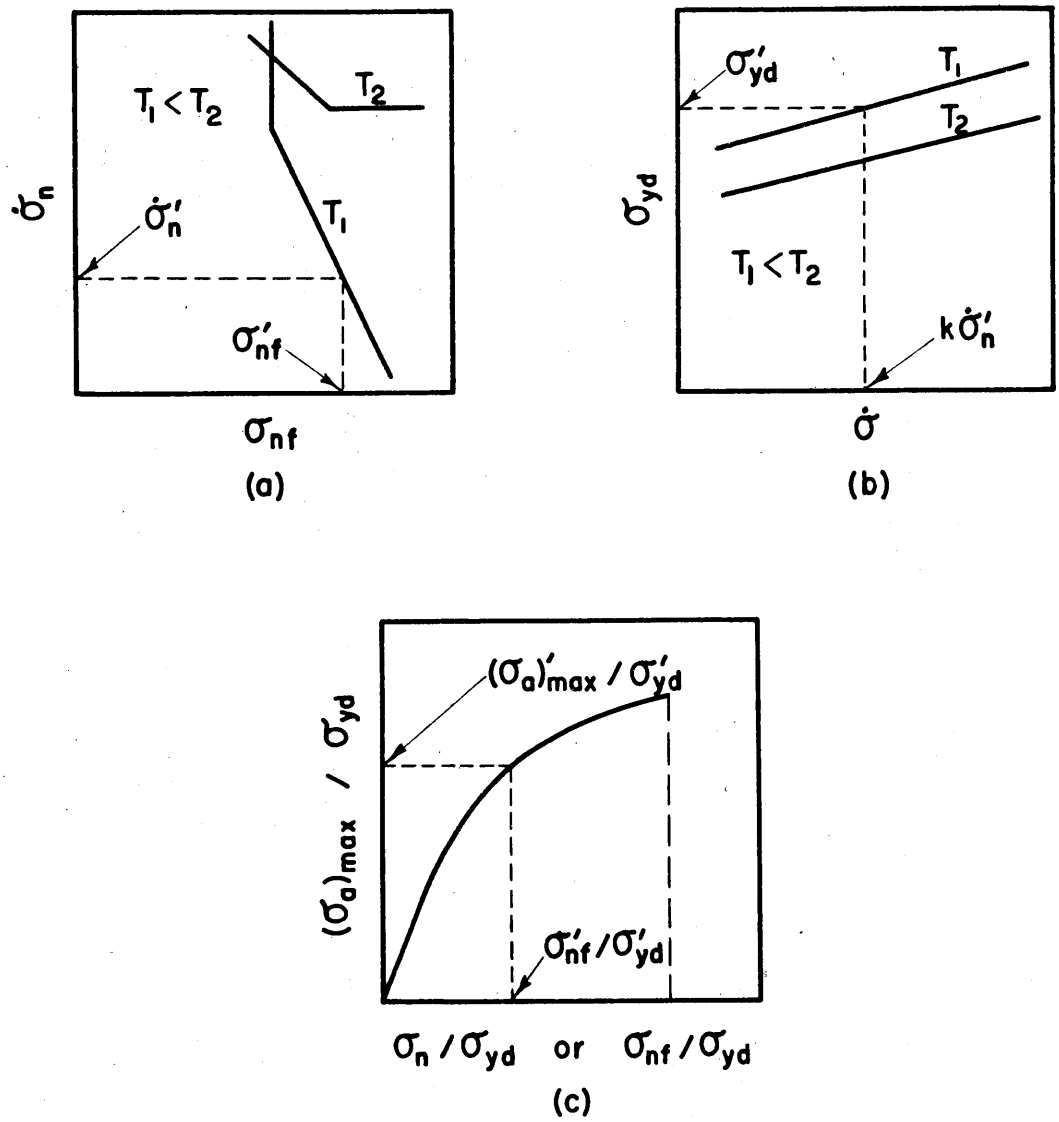

Figure 25 Schematic Presentation of Figures 4, 14, and 17.

Fracture occurs at a nominal stress of σ'_{nf} when a nominal rate of stress rise $\dot{\sigma}'_n$ is applied to the notched specimen at a temperature T_1, as shown in Figure 25a. The yield stress, σ'_{yd}, is obtained from Figure 25b for a stress rate of $k\dot{\sigma}'_n$ and the temperature T_1. Now the ratio $\sigma'_{nf}/\sigma'_{yd}$ may be obtained and if this ratio is less than 1.5 the ratio of $(\sigma'_a)_{max}/\sigma'_{yd}$ can be determined as indicated in Figure 25c. Hence the value of the maximum axial stress beneath the notch at the instant of brittle fracture, $(\sigma_a)_{max}$, may be obtained.

Table I shows the value of $(\sigma_a)_{max}$ computed for each brittle fracture observed at temperatures of -110° F (-79° C) and -200°F (-129° C) in all cases where the necessary information is available. The values of $(\sigma_a)_{max}$ presented in Table I are constant within the probable experimental and theoretical errors, namely within the range from 200,000 to 226,000 lb/in^2. with the average value of 210,000 lb/in^2. Thus the results of this investigation show that brittle fracture is initiated at a point in the material when the stress at that point attains a critical value (210,000 lb/in^2.). The results also show that this critical stress is independent of temperature and rate of loading.

The evidence obtained thus far indicates that a necessary and sufficient condition for the occurrence of brittle fracture in the notched steel specimens of this investigation is that a critical value of the tensile stress of about 210,000 lb/in^2. is reached before plastic deformation extends to the axis of the specimen. The critical value of tensile stress is never reached in some tests on notched

specimens before plastic deformation progresses to the axis of the specimen ($\sigma_n / \sigma_{yd} > 1.5$). The fracture which ultimately occurs in such tests is ductile rather than brittle. Thus transition from brittle to ductile behavior, for the particular notch investigated occurs when $\sigma_{nf}/\sigma_{yd} = 1.5$ at the instant $(\sigma_a)_{max} = 210,000$ lb/in^2. Figure 14 shows that the transition from brittle to ductile behavior for this notch occurs when $(\sigma_a)_{max}/\sigma_{yd} = 2.34$ or for $\sigma_{yd}^* = 210,000/2.34 \approx 90,000$ lb/in^2. Hence these notched specimens behave in a ductile fashion when the yield stress is less than 90,000 lb/in^2.

The transition from ductile to brittle behavior in the notched specimens may be located on Figure 17. Figure 4 shows that a yield stress of 90,000 lb/in^2. occurs in unnotched specimens at temperatures of -110° F (-79° C) and -200° F (-129° C) when the rate of stress application is about 4×10^6 and 10^4 lb/in^2. sec respectively. Hence the transition from ductile to brittle behavior in notched specimens should occur at nominal stress rates of about 10^6 and 2×10^3 lb/in.^{2} sec ($\dot{\sigma}_a = k\dot{\sigma}_n$) for temperatures of -110° F (-79° C) and -200° F (-129° C) respectively (rates greater than these correspond to brittle behavior). Figure 17 shows that a discontinuous change occurs in the relationship between the nominal fracture stress and the nominal stress rate at a rate of 10^6 lb/in^2. sec for the tests at -110° F (-79° C). This is in agreement with the prediction. However the results obtained at -200° F (-129° C) do not exhibit a discontinuity at a nominal stress rate of 2×10^3 lb/in^2. sec. Nevertheless the hardness surveys of specimens

tested at -200° F (-129°C) at nominal stress rates less than 2×10^3 lb/in.^{2} sec shows that these specimens exhibit greater ductility than those tested at rates greater than 2×10^3 lb/in.^{2} sec. An example is given by the results of the hardness survey of the specimen tested at a rate of 1.03×10^2 lb/in.^{2} sec shown in Figure 23. This shows that plastic deformation has progressed very nearly to the axis of the specimen as expected.

Figure 17 indicates that at a temperature of -200° F (-129° C) there may be a change in the fracture behavior for nominal stress rates greater than about 10^6 lb/in.^{2} sec. The fractures occurring in notched specimens at a temperature of -200° F (-129° C) for nominal stress rates greater than 10^6 lb/in.^{2} sec are of the brittle type since $\sigma_{nf}/\sigma_{yd} < 1.5$. However, Figure 17 indicates that at a temperature of -200° F (-129° C) the nominal fracture stress is constant for nominal stress rates exceeding 10^6 lb/in.^{2} sec. This behavior is probably attributable to an independence of the yield stress upon stress rate in this range. This range in notched specimens corresponds to stress rates greater than 4×10^6 lb/in.^{2} sec in unnotched specimens.

Figure 4 indicates that if the yield stress is constant for rates of stress application greater than about 10^7 lb/in.^{2} sec at a temperature of -200° F (-129° C) the maximum value of the yield stress would be about 120,000 lb/in^2. A stress of 120,000 lb/in.^{2} corresponds approximately to the upper limiting stress in the stress vs. log delay time relationship for this material at a temperature of -320° F (-196° C) (3). An upper limiting stress was

not observed in the stress vs. log delay time relationship at a temperature of -200° F (-129° C) at the shortest delay time investigated, namely 10^{-2} sec. However, it is not unreasonable to expect that such an upper limiting stress exists at delay times shorter than 10^{-2} sec. Therefore the constancy of nominal fracture stress with respect to nominal stress rate for rates exceeding 10^6 lb/in.^{2} sec at a temperature of -200° F (-129° C) may be attributable to this upper limiting yield stress.

Brittle fractures were not observed in the tests at a temperature of -23° F (-30° C), within the range of stress rates investigated. This behavior is consistent with the criterion for the occurrence of brittle fracture deduced from the results obtained at lower temperatures. This consistency may be shown by considering the conditions existing at the maximum nominal stress rate, 10^7 lb/in.^{2} sec, for tests on notched specimens. Lower stress rates are less conducive to brittle fracture. This nominal stress rate in a notched specimen corresponds to a stress rate of 4×10^7 lb/in.^{2} sec in unnotched specimens ($\dot{\sigma}_a = k\dot{\sigma}_n$). The theoretically derived relation between yield stress and stress rate for a temperature of -23° F (-30° C) is shown in Figure 4. The yield stress corresponding to a stress rate of 4×10^7 lb/in.^{2} sec is about 85,000 lb/in.^{2} Ductile behavior of the material is expected since this yield stress is less than 90,000 lb/in.^{2} (σ_{yd}*). The transition from ductile to brittle behavior at a temperature of -23° F (-30° C) should occur when the stress rate is such that $\sigma_{yd} = \sigma_{yd}^* = 90{,}000$ lb/in^2. Figure 4 shows that the stress rate

corresponding to a yield stress of 90,000 lb/in.^{2} is about 2×10^8 lb/in.^{2} sec. This stress rate is produced in a notched specimen by applying a nominal stress rate of about 5×10^7 lb/in.^{2} sec. Hence to produce brittle fracture in the notched specimen of this investigation at a temperature of -23° F (-30° C) requires that the nominal stress rate be greater than 5×10^7 lb/in.^{2} sec.

3:7 Summary and Conclusions

The true state of stress at the minimum cross-section of a notched specimen subjected to tensile loading has been determined by means of an elastic-plastic stress analysis. This analysis takes into account plastic deformation which is limited to the immediate vicinity of the root of the notch. The analysis provides a theoretical prediction of the position of the boundary between the regions of plastic and elastic deformation. The load at which general yielding in the region of the notch occurs is also predicted.

An experimental investigation has been conducted on notched specimens subjected to tensile loading at different temperatures and rates of loading. The experimental results are found to be in agreement with the position of the elastic-plastic boundary and the level for general yielding predicted by the stress analysis.

The nominal stress at the instant of fracture in notched specimens as a function of nominal stress rate has been determined experimentally at two temperatures, -110° F (-79°C) and -200° F (-129° C). The true tensile stress at the position and at the instant of initiation of brittle fracture has been determined from the experimental results by the application of the stress analysis. The results show that brittle fracture is initiated in

the material employed in this investigation when a critical tensile stress of about 210,000 lb/in.^{2} is attained. This value is found to be independent of stress rate and temperature.

Brittle fracture in notched specimens depends on the notch acuity, the stress rate, and the temperature. This investigation shows that the influence of temperature and stress rate on the initiation of brittle fracture is associated entirely with the dependence of the yield stress on temperature and stress rate.

The results of static tests on notched specimens show that yielding just reaches the axis of the specimen when the ratio between the nominal stress and the yield stress reaches a critical value, in agreement with theoretical prediction. Hence it is shown that a necessary condition for brittle fracture, or fracture preceded by limited plastic deformation, is that the ratio between the nominal applied stress and the yield stress never attains the critical value which would cause yielding to progress to the axis of the specimen.

IV. THE TRANSITION TEMPERATURE IN THE IZOD IMPACT TEST

4:1 Introduction

The results obtained in parts II and III of this thesis indicate that it should be possible to predict the conditions under which brittle fracture will occur in specimens of mild steel having any notch geometry. This is possible, provided the influence of stress rate and temperature on the yield stress and the true fracture stress is known for the particular steel. A method has been presented whereby the yield stress may be obtained theoretically for certain ranges of applied stress rates and temperatures. Also, a method has been presented whereby the true stress state beneath the notch may be computed. The next logical step is to apply these results to the prediction of brittle fracture behavior for some case of practical engineering interest.

One such case of practical interest is the prediction of the temperature at which a transition from ductile to brittle behavior occurs for standard notched bar impact tests. This temperature is known as the "transition" temperature and has become accepted by engineers as an indication of a material's susceptibility to brittle failure under service conditions.

Several types of notched bar impact tests have become accepted and standardized. One of these tests is the Izod or cantilever beam test (ASTM designation E23-56T). The purpose of the Izod test is to measure the amount of energy which a test specimen absorbs in fracturing as a function of temperature. In this manner the range of temperature over which the material exhibits a transition

from ductile to brittle behavior may be obtained. The transition temperature for a material such as mild steel is usually taken to be that temperature corresponding to an energy absorption of 15 ft lb (Charpy "v" notch).

The Izod test is conducted with a test specimen of the design shown in Figure 26. The test specimen is clamped as a cantilever beam in the vertical position, and is given an impact on the notched side of the specimen. This impact is delivered by a weight, attached to a pendulum arm, at a fixed distance from the root of the notch. The position of impact is shown in Figure 26, where the instantaneous value of the force transmitted to the specimen is denoted by the symbol "P".

This section of the thesis presents the results of an investigation of the transition temperature as determined by the Izod impact test for the same steel employed in parts II and III. The purpose of this investigation is to show that the transition temperature in the Izod impact test can be predicted from a knowledge of the yielding and brittle fracture behavior of the material. Hence, the results obtained in the previous sections of this thesis will be used as a basis for the prediction of the transition temperature for the annealed mild steel in the Izod test.

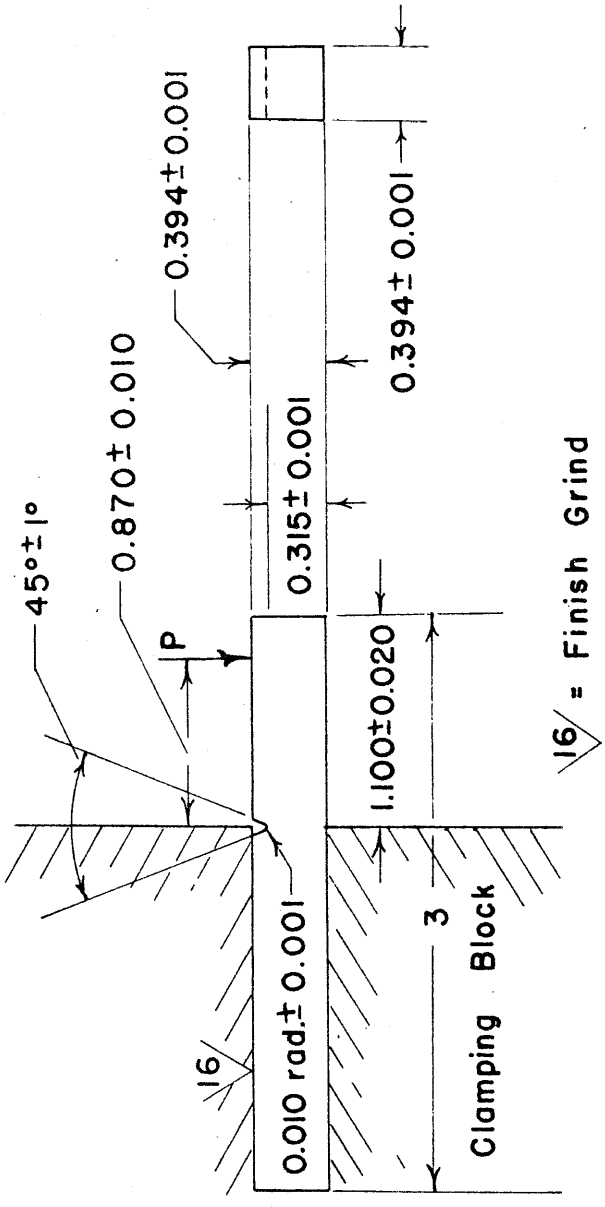

Figure 26. Izod Test Specimen

4:2 Theoretical Considerations

The preceding section of this thesis has shown that brittle behavior in notched tensile specimens of the mild steel investigated is governed by two conditions. First, the region of plastic deformation must be limited to the vicinity of the root of the notch, i.e., general yielding must not occur. Second, the maximum tensile stress occurring beneath the notch must reach a critical value. The results of the previous section show that the amount of plastic deformation that occurs beneath the notch is a function of the applied load, and the upper yield stress of the steel. In particular, it is shown that plastic deformation is no longer confined to the region of the notch when a critical value of the ratio between the applied load and the upper yield stress is exceeded.

A transition from ductile to brittle behavior occurs in the notched tensile specimens investigated when the two conditions are simultaneously satisfied. Namely, the ratio between the applied load and the upper yield stress must reach the critical value to produce full scale yielding at the instant the maximum tensile stress reaches the critical value to produce a brittle fracture.

The transition from ductile to brittle behavior for the Izod specimen may be expected to be governed by conditions similar to those found for the tensile test. Hence, the prediction of the transition temperature for the Izod test requires that an elastic-plastic stress analysis be made similar to that made for the tensile specimen. This analysis will consist of several parts. First, it is necessary to obtain an elastic-plastic stress solution corresponding to the

critical ratio between the applied load and the yield stress (i.e., a ratio greater than the critical will produce yielding which is no longer confined to the region near the notch root). Second, this elastic-plastic stress solution will be used to calculate the upper yield stress corresponding to the transition between ductile and brittle behavior. Third, the rate of stress application in the case of the Izod specimen must be computed. Finally, the transition temperature may be computed from a knowledge of the stress rate, yield stress, and the relationship relating these parameters described previously.

A stress analysis appropriate for investigating the Izod test has been made for a solid body having the cross section and loading shown in Figure 27. All cross sections parallel to the plane of the figure are the same and the body is assumed to extend to a sufficient extent in the direction normal to the plane so that the problem is one of plane strain.

The origin of the coordinate system employed lies beneath the notch at a distance from the side opposite the notch equal to one-half the maximum height of the body as shown in Figure 27. The z coordinate is normal to the plane of the figure. The x axis is parallel to the side opposite the notch and the y axis passes through the notch root. All distances are made non-dimensional through the use of a basic length. The maximum height of the specimen is taken to be ten units. Since this dimension is 0.394 in. or 10 mm, the basic length is 1 mm. Hence the boundaries of the specimen shown in Figure 27 are defined by the notch surface and the lines $x = +10$, $x = -10$, $y = +5$ and $y = -5$.

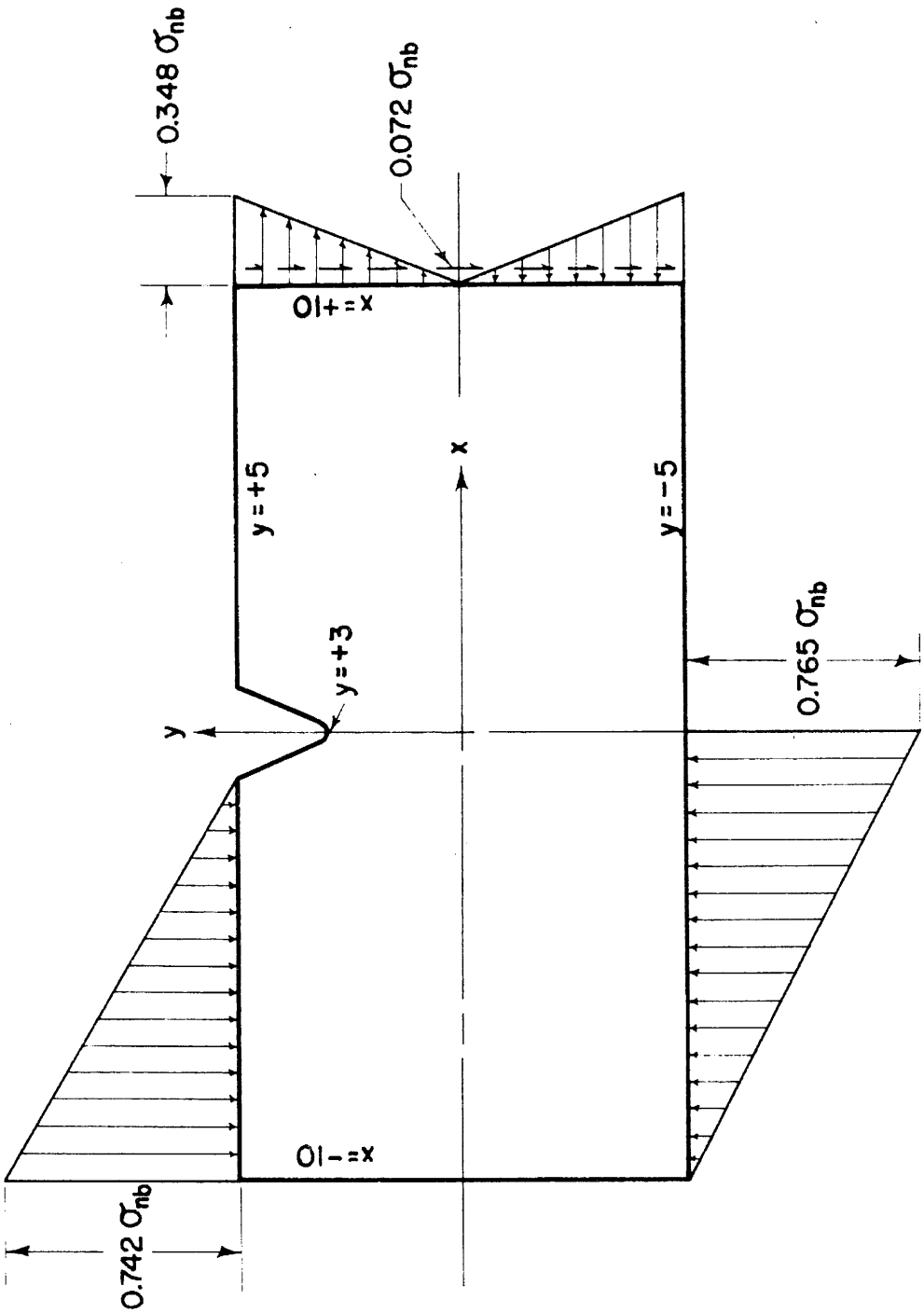

Figure 27. Model Used in Stress Analysis of Izod Test.

The Izod specimen is loaded by a force in the negative y direction applied at a distance from the notch of 0.87 in. or about 22 mm as shown in Figure 26. Reaction forces also exist. These forces are transmitted to the specimen by the clamping mechanism. Thus the boundary conditions on the Izod specimen may be described as an applied force in the negative y direction at the position $x = +22$, $y = +5$ and distributed clamping forces acting on the surfaces $y = +5$, $y = -5$ and $x < 0$.

The applied force is assumed to give rise to shear forces that are parabolically distributed in the y direction at the position $x = +10$. The moment forces on the edge $x = +10$ are assumed to be linearly distributed in accordance with the simple beam theory. The magnitude of the bending stresses at $x = +10$ is determined from the magnitude of the moment produced by the loading force at $x = +22$. The clamping forces are assumed to be linearly distributed as shown in Figure 27.

The equations of static equilibrium are satisfied, provided the distributed boundary forces have the magnitudes indicated in Figure 27. These boundary forces have been put in terms of the nominal bending stress, σ_{nb}, which is taken to be the bending stress at the notch root, based on simple beam theory and the minimum section dimensions of the Izod specimen.

The boundary conditions of the problem specify the values of the stress function, Ψ, and the first derivatives of the stress function, $\partial\Psi/\partial x$ and $\partial\Psi/\partial y$, everywhere on the boundary of the specimen. These values may be computed from the relationships listed in Appendix 1. The necessary results of these calculations are listed below where

the values of Ψ and its first derivatives are in terms of the nominal bending stress, σ_{nb}.

(1) Along the notch surface and the free portion of the surface at $y = +5$:

$$\Psi\Big|_s = -\sigma_{nb}\,(5.319 - 0.191x),$$

$$\frac{\partial \Psi}{\partial y}\Big|_s = 0, \tag{24}$$

and

$$\frac{\partial \Psi}{\partial x}\Big|_s = 0.191\sigma_{nb}.$$

(2) Along the loaded end, $x = +10$:

$$\Psi\Big|_s = -0.3409y\,(3 - .04y^2)\sigma_{nb}. \tag{25}$$

(3) Along the free portion of the surface at $y = -5$:

$$\Psi\Big|_s = \sigma_{nb}\,(5.319 - 0.191x),$$

$$\frac{\partial \Psi}{\partial y}\Big|_s = 0, \tag{26}$$

and

$$\frac{\partial \Psi}{\partial x}\Big|_s = -0.191\,\sigma_{nb}.$$

(4) Along the loaded portion of the surface at $y = -5$:

$$\Psi\Big|_s = \sigma_{nb}\left[-.363x^2\left(1 + \frac{x}{30}\right) + (5.319 - 0.191x)\right],$$

$$\frac{\partial \Psi}{\partial y}\Big|_s = 0 \tag{27}$$

(5) Along the free surface at $x = -10$:

$$\Psi\Big|_s = \text{constant} = -17.028\,\sigma_{nb},$$

$$\frac{\partial \Psi}{\partial y}\Big|_s = 0. \tag{28}$$

(6) Along the loaded portion of the surface at y = +5:

$$\Psi \Big| s = \sigma_{nb} \left[.0134x^3 + 0.041x^2 + 0.231x - 5.319 \right], \qquad (29)$$

$$\frac{\partial \Psi}{\partial y} \Big| s = 0.$$

The elastic-plastic stress solution may now be obtained for any value of the ratio between the nominal bending stress and the yield stress, σ_{nb}/σ_{yd}, by using the relaxation technique and Equations 24 through 29. Considerable labor may be saved, however, if the elasticity solution is obtained before the elastic-plastic analysis is made.

The elastic stress analysis for the plane strain specimen subjected to the loading shown in Figure 27 has been made by use of the relaxation technique described in part 3:2 of this thesis. The coarsest grid size used in this analysis has a lattice point spacing of unity (1 mm). The grid size was reduced in the region of the notch in such a manner that regions far removed from the notch have a grid size of d = 1, regions closer to the notch have a grid size of d = 1/2, then 1/4 and finally 1/8. The finest grid size (d = 1/8) corresponds to a physical dimension of 0.125 mm or about 0.005 in., which is equal to one half the root radius of curvature, ρ, of the notch. This fine a grid size enables the stresses immediately beneath the notch root to be calculated with reasonable accuracy.

The values of the elastic stress function obtained at the lattice points for the case of the specimen loaded as shown in Figure 27 are shown in Figures 28, 29, 30 and 31. Figure 28 shows the entire region within which the relaxation calculations were made, except for a sub-region near the notch root. This sub-region is shown on a progressively larger scale in Figures 29 through 31 respectively. Figure

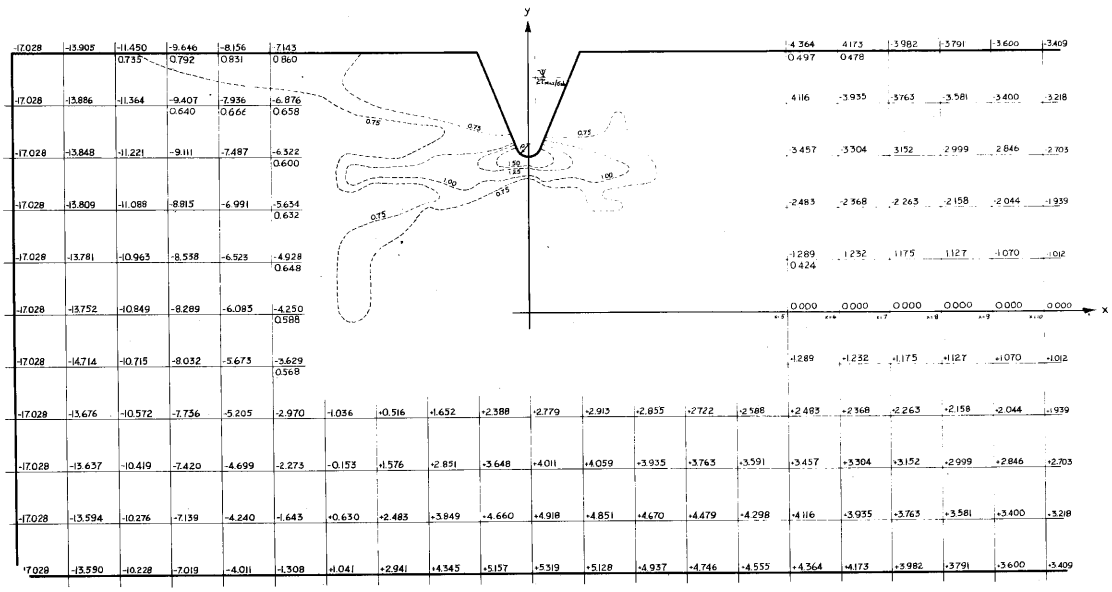

Figure 28. Relaxation Net, Grid Size d = 1, for the Elastic Izod Specimen

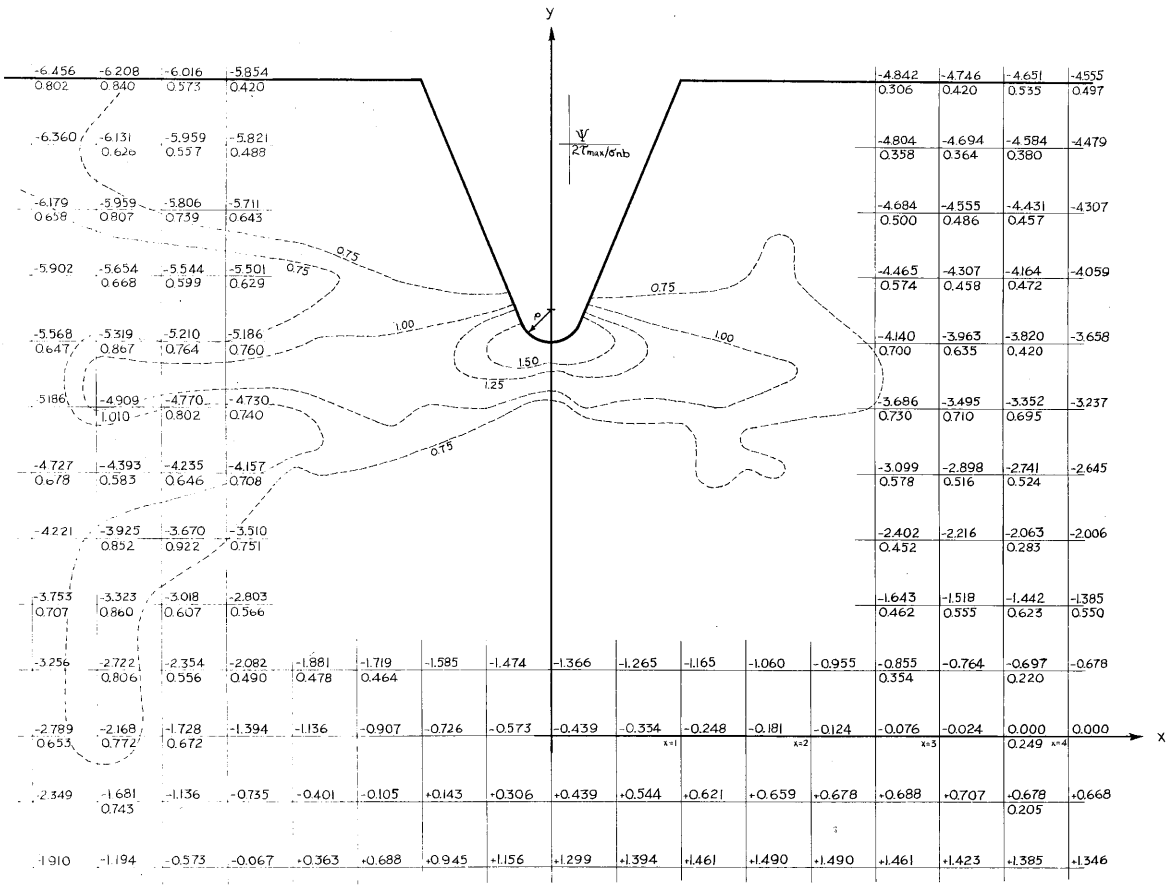

Figure 29. Relaxation Net in the Region of the Notch, Grid Size d = 1/2, for the Elastic Izod Specimen

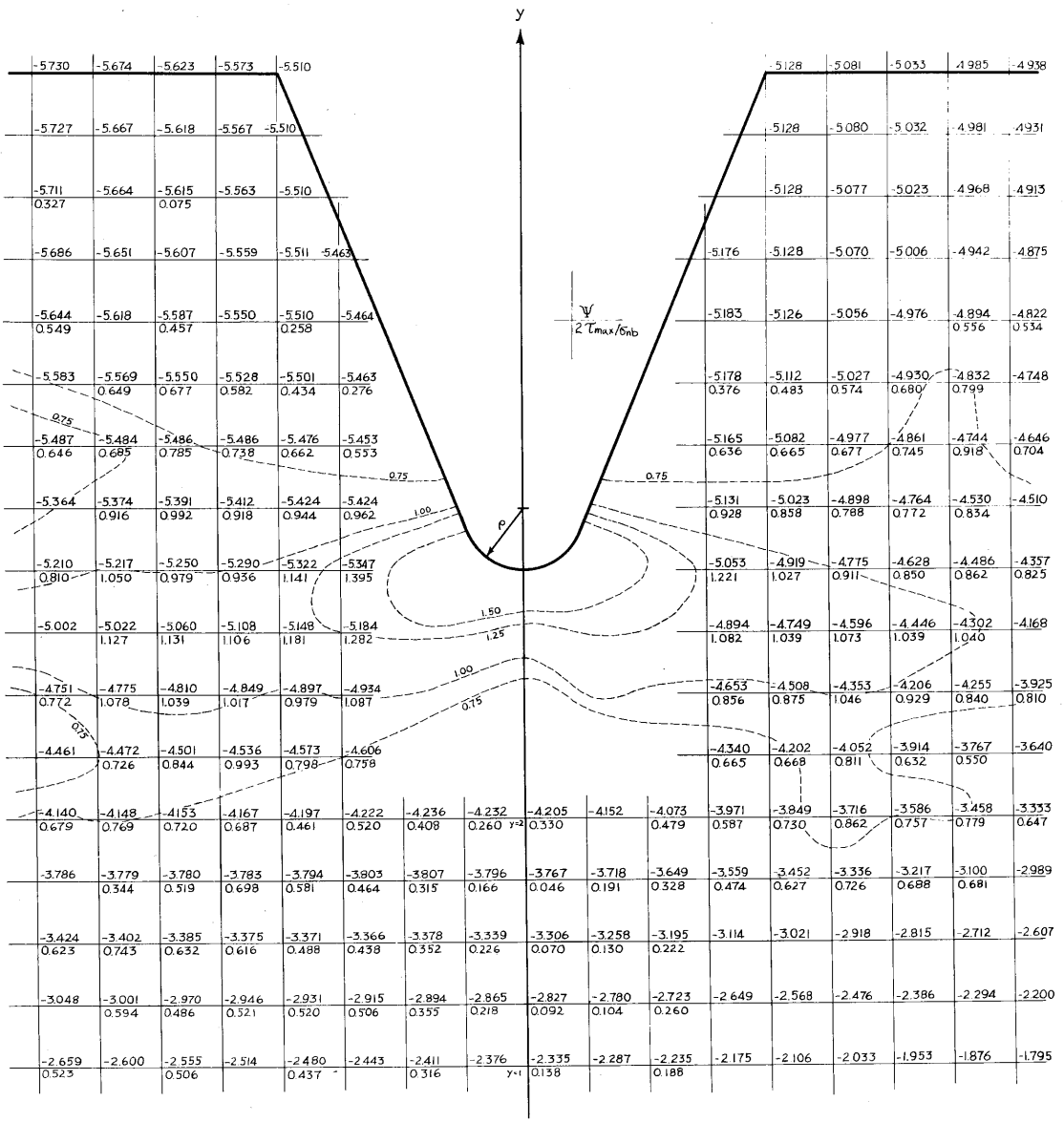

Figure 30. Relaxation Net in the Region of the Notch, Grid Size d = 1/4, for the Elastic Izod Specimen

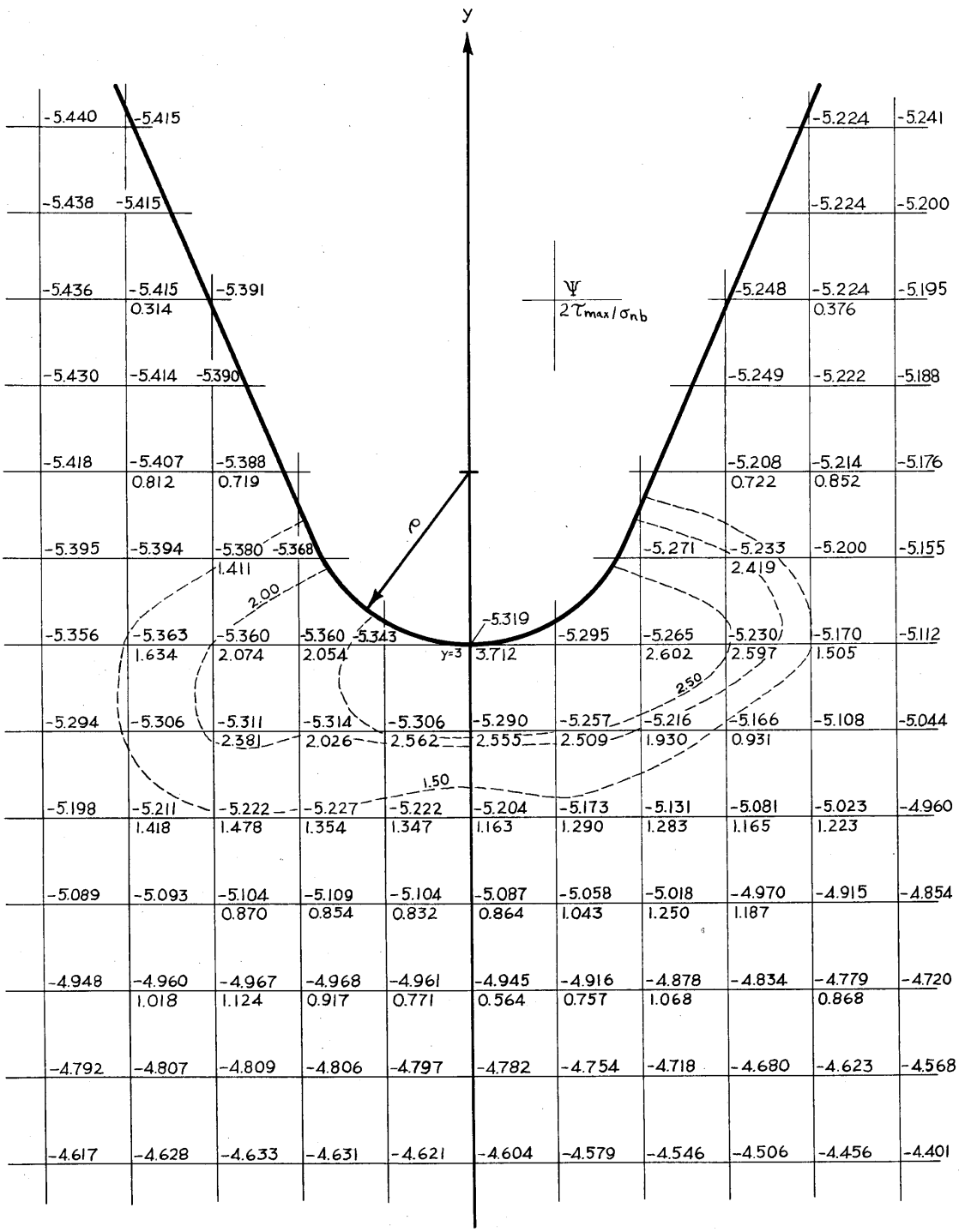

Figure 31. Relaxation Net in the Region of the Notch, Grid Size d = 1/8, for the Elastic Izod Specimen

29 shows the portion of the sub-region where the grid size is d = 1/2, Figure 30 shows the portion where d = 1/4, and finally, Figure 31 shows the region immediately beneath the notch where d = 1/8. Values of the ratio between twice the maximum shear stress and the nominal bending stress, $2\tau_{max}/\sigma_{nb}$, are shown in Figures 28 through 31, incl. The contours of constant values of this ratio are shown in Figures 28 through 31 by the dotted lines.

The stresses may be computed by using Equations 18 where now the stresses are in terms of the nominal bending stress, σ_{nb}. The stress distribution across the minimum section (x = 0), is shown in Figure 32 for the stresses σ_x and σ_y. The maximum elastic stress concentration factor is found to be $\sigma_x/\sigma_{nb} = 3.71$.

The contours of constant values of the ratio $2\tau_{max}/\sigma_{nb}$ may be used to obtain an initial approximation to the extent of the elastic-plastic boundary for a particular applied load. The assumption has been made that yielding will occur when the maximum shear stress reaches a critical value; namely, a value equal to one half the upper yield stress in simple tension, σ_{yd}. Hence points in the plastic region will have a value of unity for the ratio between twice the maximum shear stress and the upper yield stress, $2\tau_{max}/\sigma_{yd}$. Thus a particular contour of constant $2\tau_{max}/\sigma_{nb}$ will be the initial approximation to the elastic-plastic boundary, provided the load acting on the specimen, expressed as a particular value of the ratio σ_{nb}/σ_{yd}, is such that $2\tau_{max}/\sigma_{yd} = 1$. As an example, the contour $2\tau_{max}/\sigma_{nb} = 1.25$, shown in Figures 28, 29, and 30, becomes the initial approximation to the elastic-plastic boundary provided $\sigma_{nb}/\sigma_{yd} = 0.80$. The true

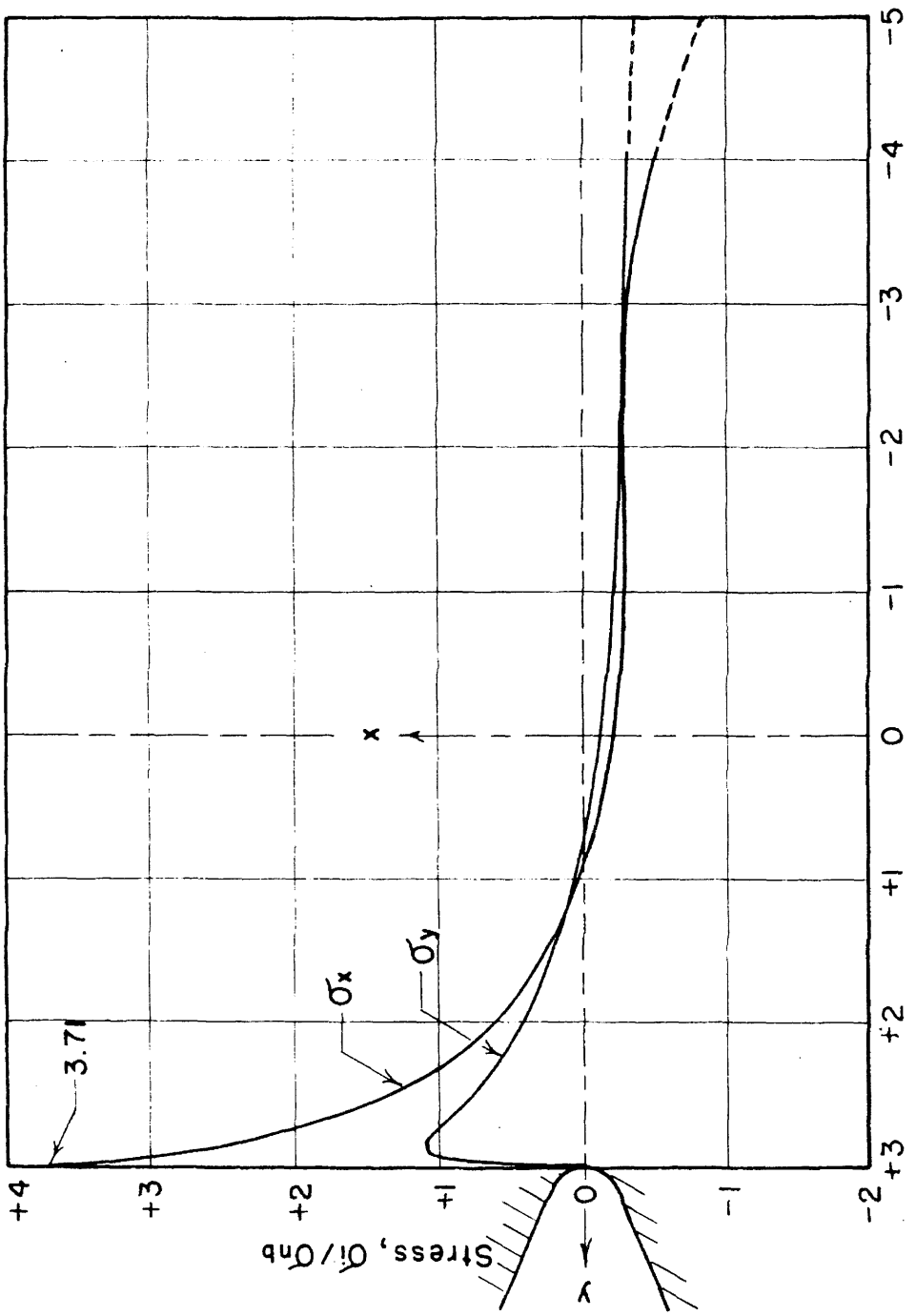

Figure 32. Elastic Stress Distribution at the Minimum Cross-Section for the Izod Specimen.

elastic-plastic boundary will, of course, be larger in extent than the one obtained from the purely elastic approximation, as has been previously pointed out.

The elastic approximation to the region of plastic deformation may be used to determine a limit on the ratio σ_{nb}/σ_{yd} for which the plastic region is confined to the notch root. Figures 28 and 29 show that the contour $2\tau_{max}/\sigma_{nb} = 0.75$ extends to the clamped surface $y = +5$, and more than midway to the surface $y = -5$. Hence, it is clear that full scale yielding will occur when the ratio between the load and the upper yield stress is such that this contour becomes the elastic approximation to the extent of the plastic region. Thus a value of the ratio $\sigma_{nb}/\sigma_{yd} > 1.33$ $(1.00/0.75 = 1.33)$ will correspond to large scale yielding. Hence, the elastic-plastic stress analysis of the Izod specimen must be applied for values of the ratio $\sigma_{nb}/\sigma_{yd} < 1.33$ until the critical value for large scale yielding is found.

The elastic-plastic analysis is made using the same assumptions and relaxation technique described previously in section 3:2. This analysis shows that the maximum value of the ratio of σ_{nb}/σ_{yd} corresponding to a stable region of plastic behavior is $\sigma_{nb}/\sigma_{yd} = 0.80$. The values of the stress function obtained at the lattice points for the case $\sigma_{nb}/\sigma_{yd} = 0.80$ are shown in Figures 33, 34, and 35. Figure 33 shows the entire region within which the relaxation calculations were made, except for a sub-region near the notch root. The grid size shown in Figure 33 is $d = 1/4$ which corresponds approximately to one root radius of curvature of the notch. The sub-region of the notch is shown on a progressively larger scale in Figures 34 and 35. These two figures contain the lattice points at spacings of $d = 1/8$ and $d = 1/16$

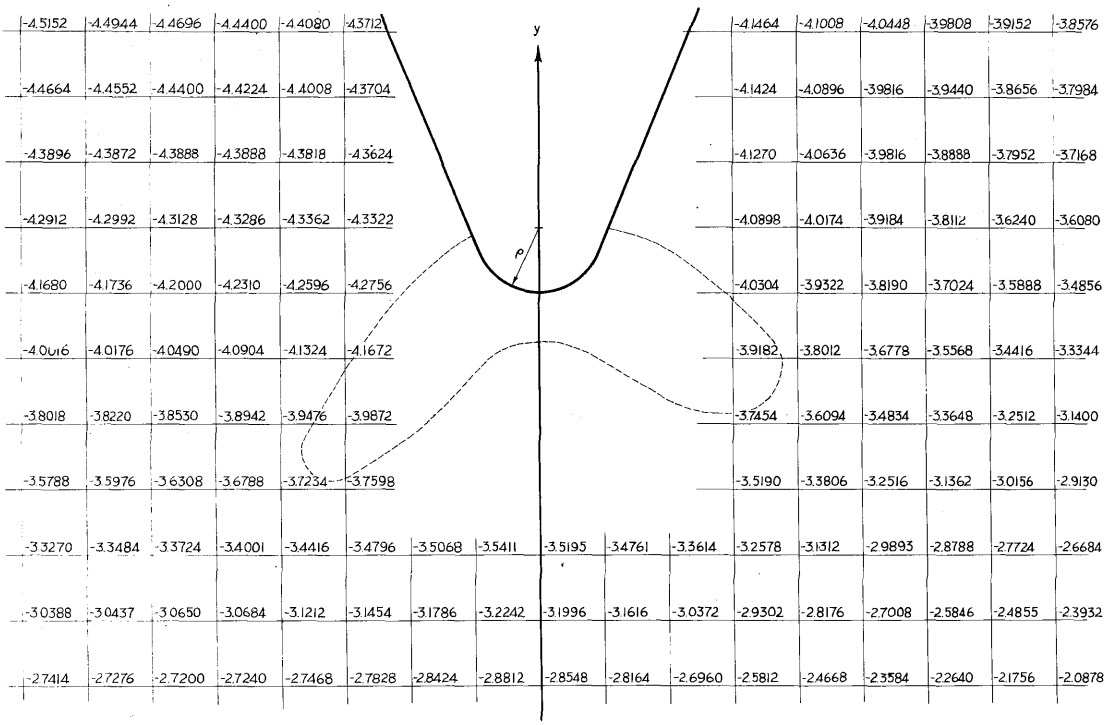

Figure 33. Relaxation Net, Grid Size d = 1/4, for the Elastic-Plastic Izod Specimen in the Case of a Load Ratio $\sigma_{nb}/\sigma_{yd} = 0.80$

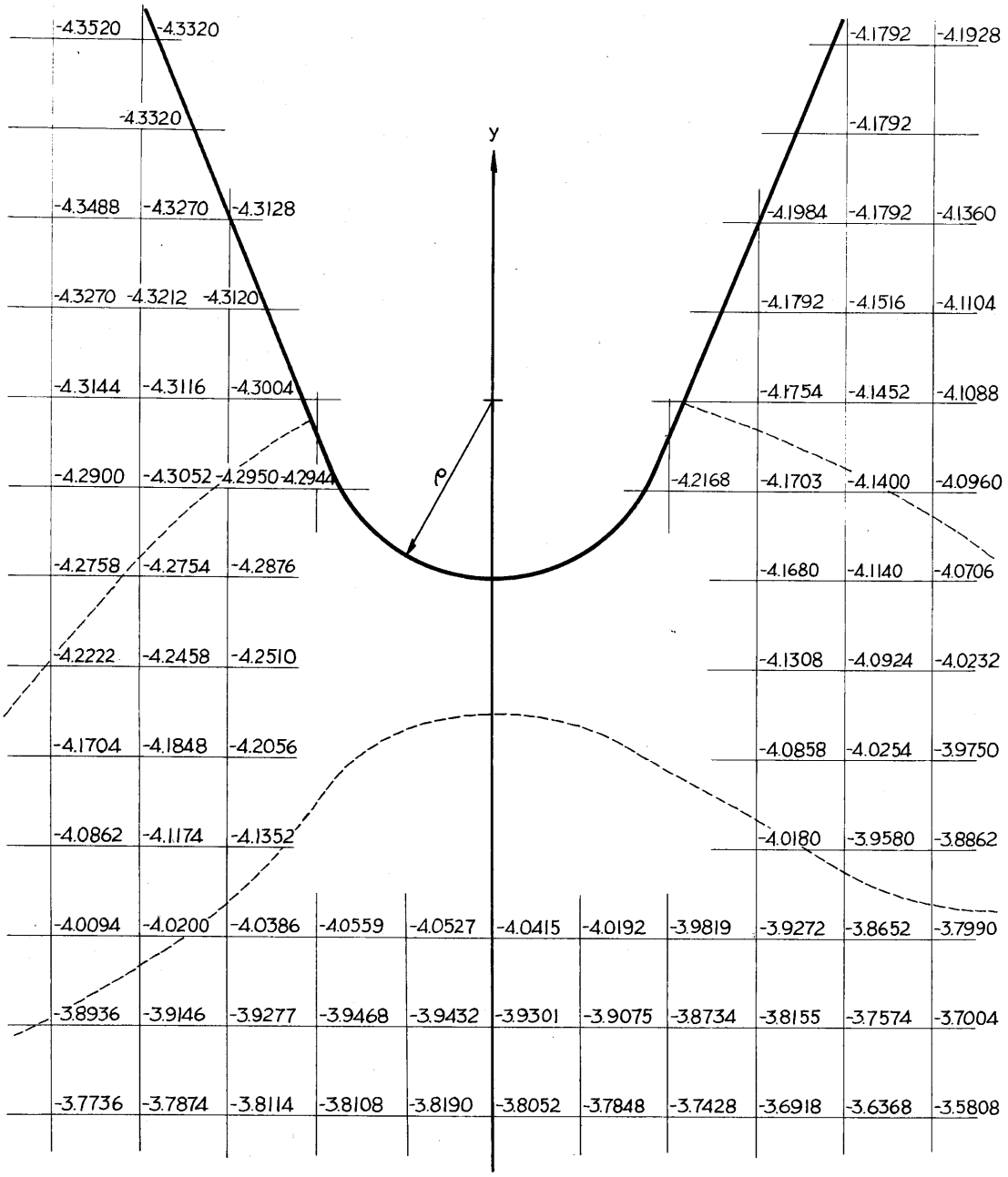

Figure 34. Relaxation Net in the Region of the Notch, Grid Size d = 1/8, for the Elastic-Plastic Izod Specimen in the Case of a Load Ratio $\sigma_{nb}/\sigma_{yd} = 0.80$

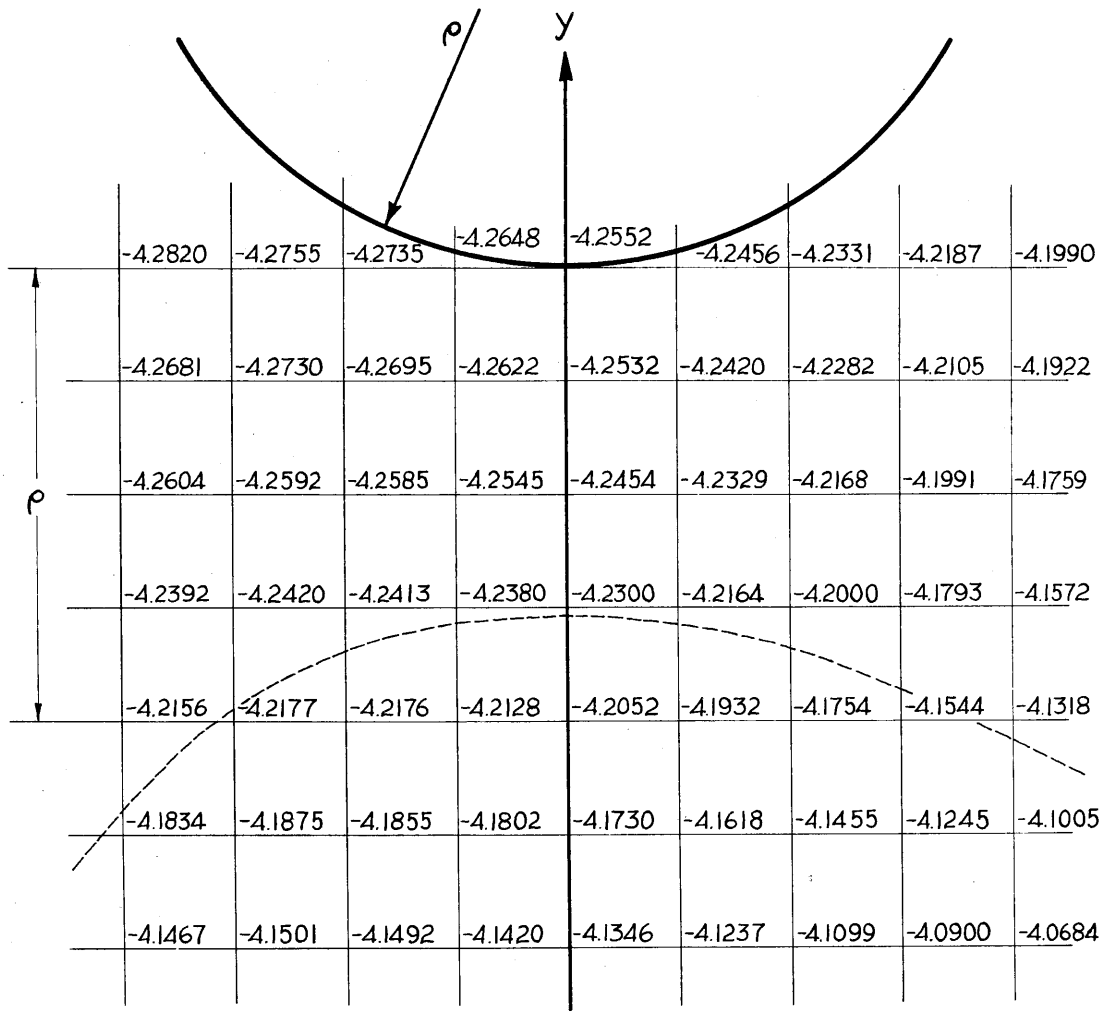

Figure 35. Relaxation Net in the Region of the Notch, Grid Size d = 1/16, for the Elastic-Plastic Izod Specimen in the Case of a Load Ratio $\sigma_{nb}/\sigma_{yd} = 0.80$

respectively. Grid spacings of d = 1/8 and d = 1/16 correspond approximately to one-half and one-fourth the root radius of curvature of the notch respectively.

The smallest grid size used in the elasticity analysis was for d = 1/8. However, in the elastic-plastic analysis for the case $\sigma_{nb}/\sigma_{yd} = 0.80$ it was found necessary to reduce the grid size to a final value of d = 1/16. The reason for this is that the stresses near the notch root change in magnitude more rapidly in the case of plastic flow as compared to the purely elastic case. Moreover, the plastic region penetrates a distance below the notch equal to about 3/16 (about 3/4 ρ) for the case $\sigma_{nb}/\sigma_{yd} = 0.80$ as may be seen from the elastic-plastic boundary shown in Figures 33, 34, and 35. Hence the errors introduced in computing the maximum tensile stress at the interface between the elastic and plastic region on the minimum section would be considerable if these calculations were based on a grid size of only 1/8.

The direct stresses, σ_x/σ_{yd} and σ_y/σ_{yd}, at the minimum cross-section are shown as a function of position near the root of the notch in Figure 36 for the case $\sigma_{nb}/\sigma_{yd} = 0.80$. The full lines represent the stresses for elastic-plastic deformation and the dashed lines show the stresses for purely elastic deformation. The maximum tensile stress, $(\sigma_a)_{max}$, in the case of elastic-plastic deformation is not strictly equal to the stress in the x direction at the elastic-plastic boundary. This is true because of the existence of a shear stress, τ_{xy}, on the minimum section of the Izod specimen. The shear stress component is negligible near the notch compared to the

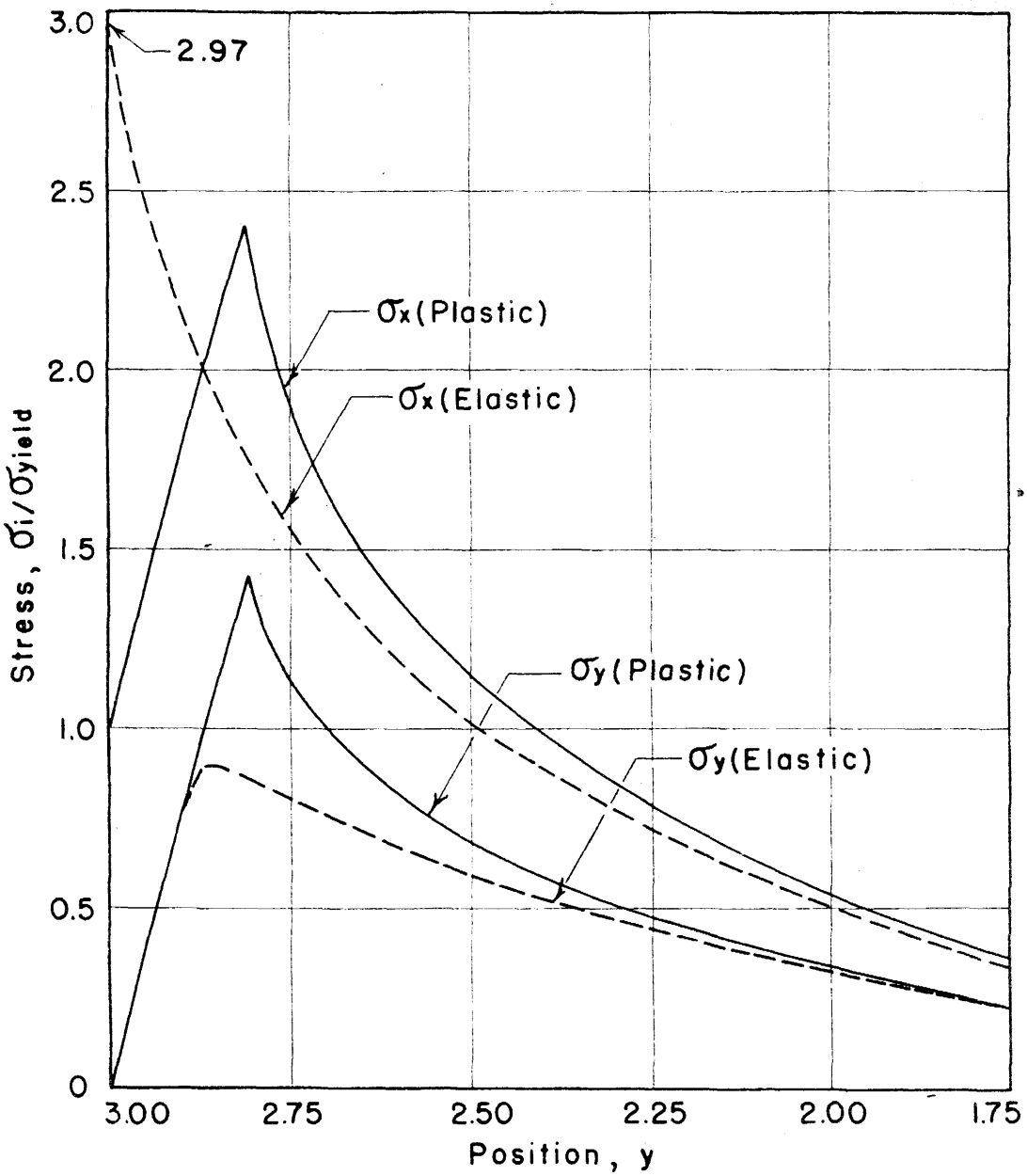

Figure 36. Elastic-Plastic Stress Distribution at the Minimum Cross-Section of the Izod Specimen for an Applied Load Ratio $\sigma_{nb}/\sigma_{yd} = 0.80$.

bending stress because of the magnitude of the lever arm through which the loading force acts. Hence, for all practical purposes, the stress distributions shown in Figure 36 are for the principal stresses.

The results of the elastic-plastic stress analysis for the Izod specimen, for the critical value of the ratio $\sigma_{nb}/\sigma_{yd} = 0.80$, may now be used to obtain the yield stress, σ_{yd}^*, corresponding to the transition between ductile and brittle behavior. This calculation may be made as follows. Figure 36 shows that the ratio between the maximum tensile stress and the yield stress has a value of $(\sigma_a)_{max}/\sigma_{yd} = 2.41$ when the ratio between the nominal bending stress and the yield stress, σ_{nb}/σ_{yd}, attains the critical value of $\sigma_{nb}/\sigma_{yd} = 0.80$. However, in accordance with the results of the previous section of this thesis, the transition from ductile to brittle behavior in the steel investigated, will occur for the critical value of σ_{nd}/σ_{yd} at the instant $(\sigma_a)_{max} = 210,000$ lb/in^2. Thus the transition yield stress for the Izod specimen is

$$\sigma_{yd}^* = (\sigma_a)_{max} / \left[(\sigma_a)_{max}/\sigma_{yd}\right]_{crit} = 210,000/2.41$$

or about 87,200 lb/in^2.

The transition temperature may now be computed from previous results presented in this thesis provided that the rate of stress application at the elastic-plastic boundary is known. The rate of stress application may be computed as follows. The elastic deflection beneath the striking hammer is assumed to be well approximated by the elementary cantilever beam formula

$$\delta_e = \frac{P\ell^3}{3EI} \qquad (30)$$

where δ_e = the elastic deflection beneath the striking hammer,

P = the instantaneous force transmitted to the Izod specimen by the impact hammer,

E = Young's modulus for mild steel and is assumed to be 30×10^6 lb/in.^{2},

ℓ = the distance from the specimen clamps to the point of load application and is taken to be $\ell = 0.87$ in. or about 22 mm,

and I = the moment of inertia of the maximum cross-section of the Izod specimen about the z axis.

The nominal bending stress, σ_{nb}, may be put in terms of the elastic deflection, δ_e, as follows. The nominal bending stress, σ_{nb}, may be written as

$$\sigma_{nb} = \frac{M}{Z'} \tag{31}$$

where $M = P\ell$ = the moment at the minimum section produced by the instantaneous loading force, P,

and Z' = the section modulus of the minimum section of the specimen.

Combining Equations 30 and 31 and substituting the dimensions shown in Figure 26, one obtains

$$\sigma_{nb} = 0.367 \times 10^8 \, \delta_e \text{ lb/in.}^2 \tag{32}$$

where δ_e is to be given the units of in.

The assumption is made that the load, P, is a monotonically increasing function of time, hence Equation 32 may be written as

$$\dot{\sigma}_{nb} = 0.367 \times 10^8 \dot{\delta}_e \text{ lb/in.}^2 \text{ sec} \tag{33}$$

where $\dot{\sigma}_{nb}$ = the time rate of change of the nominal bending stress, and

$\dot{\delta}_e$ = the time rate of change of the elastic deflection beneath the impact hammer.

The assumption used in section 3:6 of this thesis relating the rate of maximum stress rise at the elastic-plastic boundary to the rate of nominal stress application will also be used in the analysis of the Izod specimen. Hence the ratio between the maximum rate of stress application at the elastic-plastic boundary and rate of nominal bending stress application, $\dot{\sigma}_a / \dot{\sigma}_{nb}$, is set equal to the elastic stress concentration factor, k. Substitution of the value of k = 3.71 found from the elasticity analysis of the Izod specimen into Equation 33 gives

$$\dot{\sigma}_a = 1.36 \times 10^8 \dot{\delta}_e \text{ lb/in.}^2 \text{ sec} . \qquad (34)$$

The value of the rate of elastic deflection beneath the striking hammer may be computed and hence Equation 34 may be solved for $\dot{\sigma}_a$ as follows. The assumption will be made that the velocity of the striking hammer, V, is equal to the sum of the rate of elastic deformation, $\dot{\delta}_e$, and the rate of plastic deformation, $\dot{\delta}_p$, at the point of impact of the striking hammer. The velocity of the striking hammer, V, may be computed from compound pendulum formulae. This requires a knowledge of the length from the pivot point to the point of impact on the hammer, the free period of the pendulum and the initial angle through which the pendulum swings. This calculation shows that the impact velocity of the hammer is 11.3 ft/sec or 135.5 in./sec. The amount of plastic deformation beneath the hammer, δ_p, was measured for several of the Izod specimens fractured near the transition temperature. The results show that the plastic deformation, δ_p, is

about 2×10^{-3} in. This value of plastic deformation is of the same order of magnitude as the elastic deflection, δ_e. This may be seen by substituting the ratio $\sigma_{nb}/\sigma_{yd} = 0.80$ into Equation 32 with the value of the yield stress taken to be $\sigma_{yd} = 87,200$ lb/in^2. Thus, from the foregoing, and assuming that the plastic deformation increases linearly with load, $V = \dot{\delta}_e + \dot{\delta}_p \approx 2\dot{\delta}_e = 135.5$ in./sec. Hence Equation 34 yields the result that $\dot{\sigma}_a \approx 9.2 \times 10^9$ lb/in.^{2} sec.

The transition temperature for the Izod test may now be computed from the previously derived relation between the rate of stress application, temperature, and upper yield stress. This calculation may be made since two of the three variables are known; namely, the rate of stress application ($\dot{\sigma}_a = 9.2 \times 10^9$ lb/in.^{2} sec), and the upper yield stress at transition ($\sigma_{yd}^* = 87,200$ lb/in.^{2}).

The dislocation theory of the yield mechanism appears to break down for stress rates greater than about 10^7 lb/in.^{2} sec, as described previously. The rate of stress application in the Izod test is almost one thousand times this rate. Hence, direct calculation of the transition temperature cannot be made accurately. The assumption will be made that the upper yield stress may be obtained for stress rates greater than 10^7 lb/in.^{2} sec by linear extrapolation of the relation between upper yield stress and the logarithm of the stress rate obtained from Equation 6 for the range of stress rates from 10^2 to 10^7 lb/in.^{2} sec. This procedure was followed with the result that a temperature of about 50° F (10° C) corresponds to an upper yield stress of 87,200 lb/in.^{2} when the rate of stress application is 9.2×10^9 lb/in.^{2} sec. Thus the predicted transition temperature for the standard Izod tests of the steel employed in this investigation is 50°F (10°C).

4:3 Equipment and Test Procedure

An experimental determination of the transition temperature was made so that the prediction could be checked. This experimental determination was made by performing standard notched bar Izod impact tests on the annealed mild steel. The Izod tests were made at temperatures ranging from -56° F (-48.9° C) to 300° F (148.9° C). The means of obtaining the test temperatures may be illustrated by reference to several examples. For instance, the test temperature of -56° F (-48.9° C) was achieved by submerging both the clamps and the specimen in a mixture of dry ice and alcohol. The clamps which contained the specimen were left in the mixture until a temperature slightly less than -56° F (-48.9° C) was obtained. The clamps and the specimen were then quickly transferred to the testing machine and the hammer was then released. The test temperature of 300° F (148.9° C), was achieved by heating the specimen and clamps while they were in place on the testing machine. This was accomplished by using heat lamps arranged in parallel rows, one row of lamps on either side of the machine.

The temperature was measured by means of a copper-constantan thermocouple. The thermocouple was attached to the specimen at a position slightly above the clamping blocks on the side of the specimen opposite the notch. The test temperature was taken to be the specimen temperature, as determined from the thermocouple, immediately prior to the release of the hammer.

The position of the elastic-plastic boundary was determined experimentally for the Izod specimens tested at temperatures of 25° F (-3.9° C) and 50° F (10° C). The fractured specimens were

sectioned in half along the longitudinal plane perpendicular to the bending axis. The specimens were then mounted in lucite. The preparation of the mounted specimens and the determination of the elastic-plastic boundary by micro-hardness measurements were accomplished in the same manner as described previously in section 3:4 of this thesis.

4:4 Experimental Results

The experimentally determined relationship between the energy absorbed by the Izod specimens and the temperature of the test is shown in Figure 37. The experimental results are given by the plotted points and the average trend of these points is represented by the full line. These results show that the amount of energy absorbed in fracturing varies from a minimum of about 2 ft lb at a temperature of 0° F (-17.8° C) to a maximum of about 66 ft lb at a temperature of 240° F (115.6° C). The 15 ft lb level of absorbed energy occurs at a temperature of about 32° F (0° C).

The results of the surveys of micro-hardness on the cross sections of the Izod specimens fractured at temperatures of 25° F (-3.9° C) and 50° F (10° C) are shown in Figures 38 and 39 respectively. The boundary between the regions of elastic and plastic behavior are shown by the full lines in Figures 38 and 39. The elastic-plastic boundaries were determined by the micro-hardness readings in the same manner as described previously in sec. 3:5 of this thesis. The experimental elastic-plastic boundaries shown in Figures 38 and 39 are based on the results of about 100 hardness readings in each case.

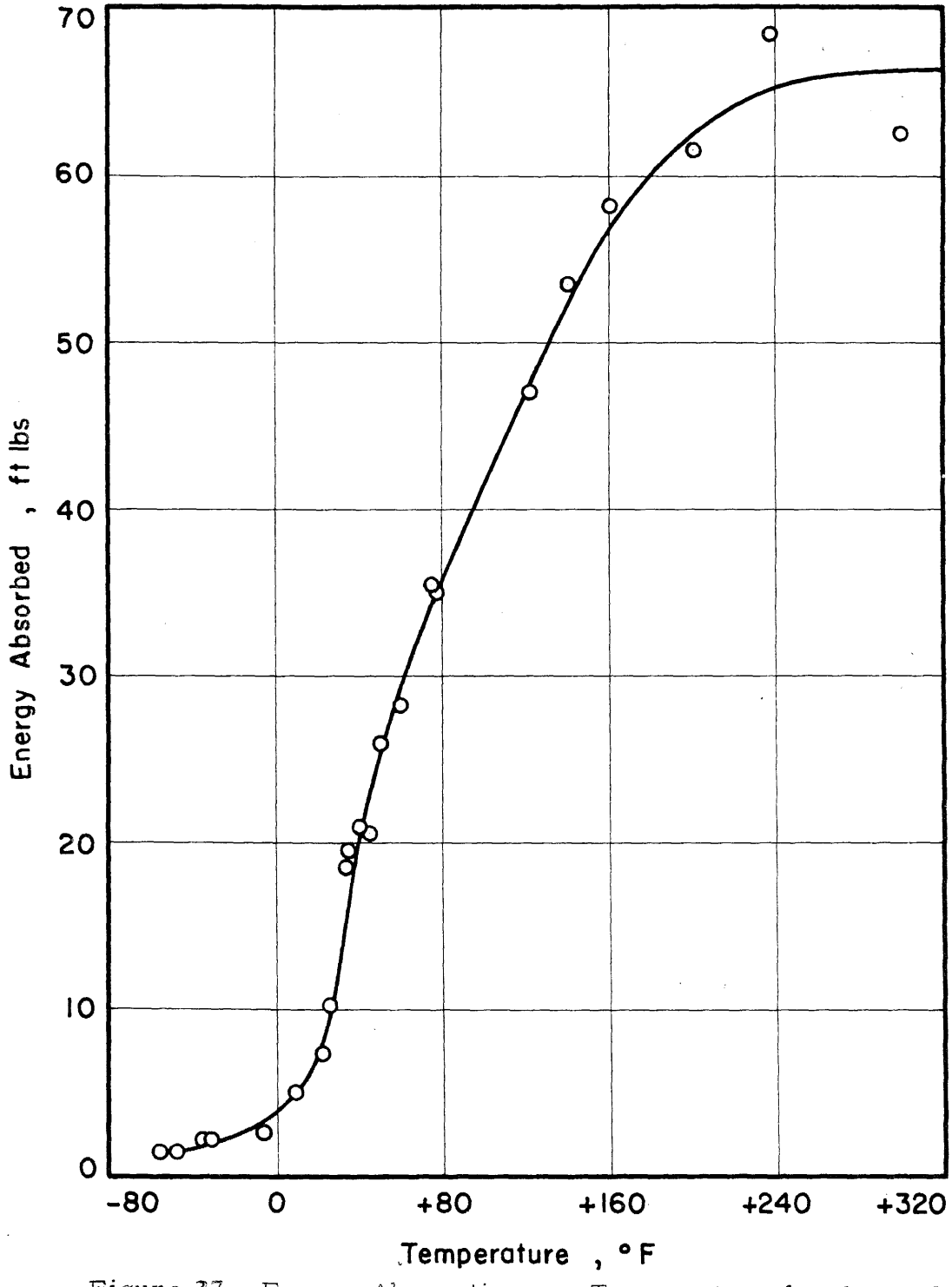

Figure 37. Energy Absorption vs. Temperature for the Izod Test.

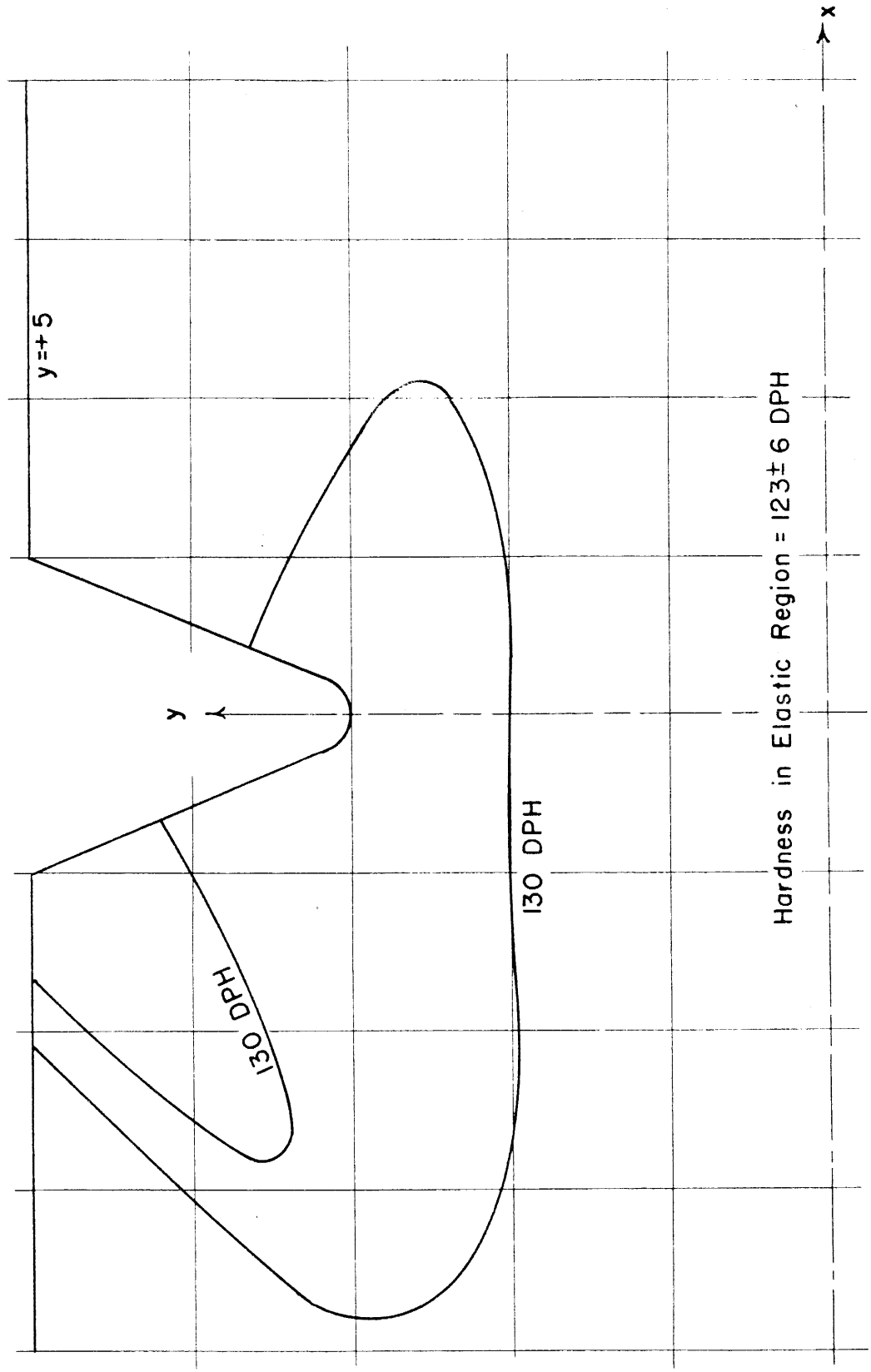

Figure 38. Elastic-Plastic Boundary for an Izod Test at a Temperature of +250 F (-3.9° C).

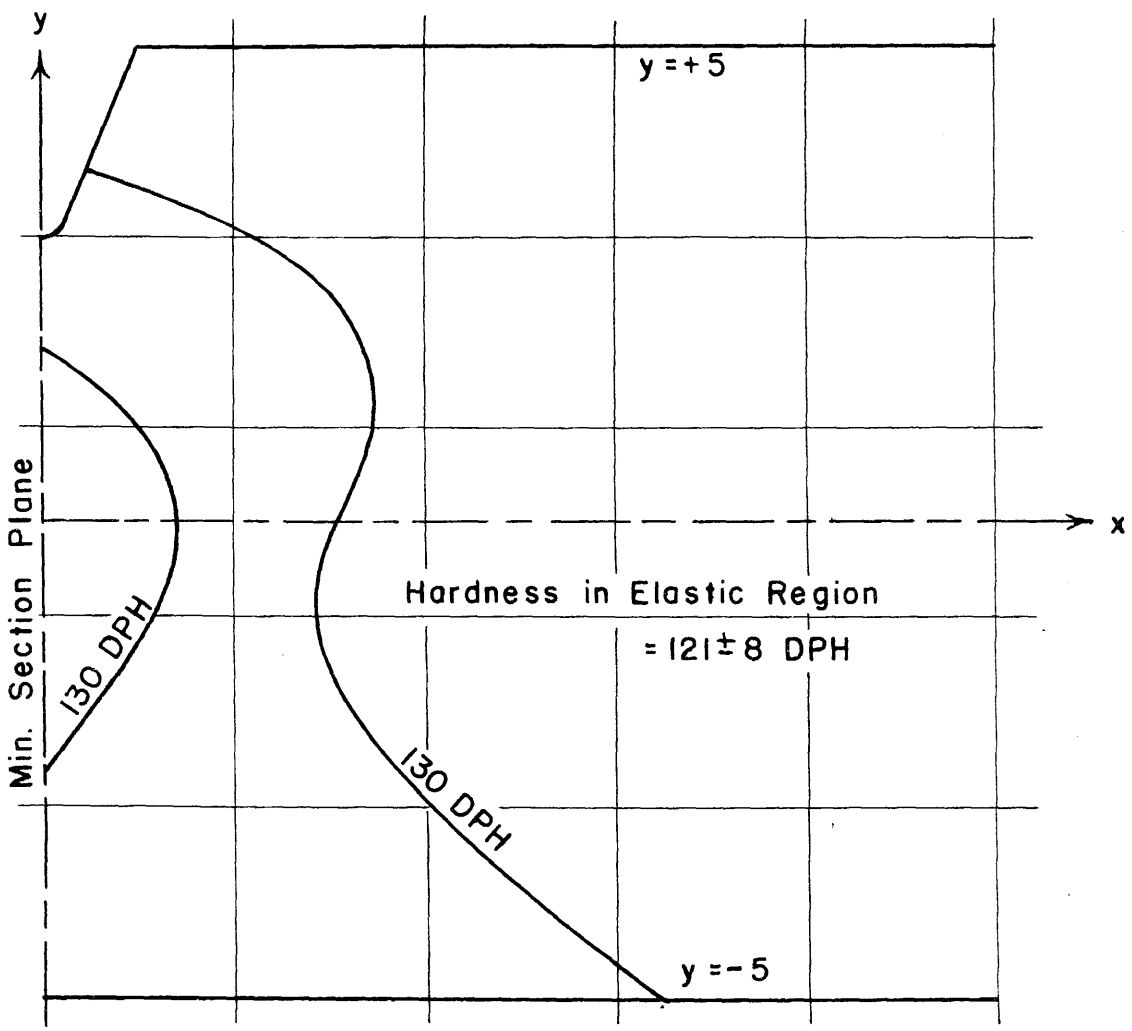

Figure 39. Elastic-Plastic Boundary for an Izod Test at a Temperature of +50° F (+10° C).

4:5 Discussion

The conventional transition temperature for the Izod impact test is defined as being the temperature corresponding to a given amount of energy absorption of the Izod specimen. The amount of absorbed energy at the transition temperature is usually taken to be 15 ft lb in the case of materials such as mild steel. The experimental results of the Izod test for the present investigation indicate that the conventional transition temperature is 32° F (0° C). Thus, the predicted value of 50° F (10° C) for the transition temperature is slightly higher than the value obtained in the conventional manner. However, the agreement between the theory and experiment is surprisingly good, in view of the wide range of temperatures over which the absorbed energy changes (0° F (-17.8° C) to 240° F (115.6° C)).

The hardness surveys on fractured Izod specimens also indicate that the predicted transition temperature is too high. Figure 39 shows that for a temperature of 50° F (10° C) plastic deformation has proceeded completely across the minimum section of the specimen. This result clearly shows that the transition temperature is actually less than 50° F (10° C). Figure 38 shows that for a temperature of 25° F (-3.9° C), plastic deformation is substantially confined to the immediate vicinity of the root of the notch. A small region of plastic deformation has progressed to the clamped surface of the specimen nearest the notch in the case of the test at a temperature of 25° F (-3.9° C). The shape of the regions of plastic deformation indicate, however, that the transition temperature is close to 25° F (-3.9° C). Thus the hardness surveys show

that the transition temperature defined by the extent of the region of plastic deformation is in very close agreement with the transition temperature defined by the absorption of 15 ft lb of energy.

These considerations indicate that the discrepancy between the predicted transition temperature and the 15 ft lb transition temperature is a result of an error in estimating the upper yield stress for the stress rate pertinent to the Izod test. The fact that such an error exists is not surprising in view of the means used to estimate the upper yield stress at high rates of loading such as are involved in the Izod test. Unfortunately, the yield behavior of mild steel is in doubt at rates greater than about one thousandth of the loading rate of the Izod test. Apparently this difficulty can only be resolved by a refinement of the experimental technique allowing the attainment of higher rates of loading.

Another source of the discrepancy between the predicted and experimental values of the transition temperature is the fact that the stress analysis does not account for all of the plastic deformation which occurs in the Izod specimen. For example, the analysis does not include the effect of the plastic deformation occurring in regions adjacent to the lateral surfaces of the specimen. This plastic deformation will account for some of the energy absorbed by the Izod specimen in fracturing. The existence of this plastic deformation would tend to lower the transition temperature from that predicted on the basis of the rather simple model shown in Figure 27.

4:6 Summary and Conclusions

A theoretical prediction for the transition temperature of the Izod impact test of an annealed mild steel has been made. This prediction is based on the results of an elastic-plastic stress analysis and the results of the yielding and brittle fracture behavior of this steel determined previously. The analysis shows that a transition from ductile to brittle behavior in the Izod test should occur at a temperature of 50° F (10° C).

An experimental investigation has been made on Izod specimens in order to test the results of the theoretical analysis. The experimental investigation shows that the transition temperature is very nearly 25° F (-3.9° C). The discrepancy between the theoretical and experimental values of the transition temperature is thought to be the result of two main factors. The first of these is an inadequate method of determining the yield stress for very high rates of load application, such as exist in the Izod test. The second is the fact that the theory does not account for all of the plastic deformation known to occur in the Izod test.

GENERAL SUMMARY AND CONCLUSIONS

The initiation of brittle fracture and the transition between ductile and brittle behavior of an annealed mild steel has been investigated. This investigation includes a determination of the interrelationship between the rate of stress application, temperature and the state of stress beneath a notch which governs the initiation of brittle fracture in notched tensile specimens. The investigation takes into account the limited plastic deformation beneath a notch, known to occur in cases involving brittle type failures.

An elastic-plastic stress analysis of the notched tensile specimen used in this investigation has been made. The results of this analysis allow the true state of stress beneath the notch to be computed at the instant of initiation of brittle fracture, provided certain information is known. First, the nominal stress to produce brittle fracture in the notched tensile specimens must be known as a function of the rate of stress application and the test temperature. Second, the upper yield stress of the steel must be known for the same rates and temperatures.

A theoretical and experimental investigation was conducted to determine the upper yield stress of the steel as a function of rate of stress application and temperature. The theory presented is based on a dislocation model of a yield nucleus and previously existing data obtained in tests to determine delay time of yielding at constant stress. The theoretical expression for the yield stress as a function of rate and temperature is found to agree very well with the experimental results within the ranges of temperature and stress rates investigated.

The nominal stress at the instant of brittle fracture in the notched tensile specimens was determined experimentally as a function of stress rate for temperatures of -110° F (-79° C) and -200° F (-129° C). An experimental investigation conducted on notched specimens that had fractured in a brittle manner shows good agreement with the theoretical prediction of the yielding behavior of these specimens.

The true tensile stress at the position and instant of initiation of brittle fracture in the notched tensile specimens has been determined by combining the experimental results with the stress analysis. The results show that brittle fracture in the mild steel of this investigation is initiated when a critical tensile stress of about 210,000 lb/in.^{2} is reached. This value is found to be independent of both the rate of stress application and the test temperature. Also, it is shown that general yielding, and hence ductile behavior, occurs if a critical value of the ratio between the nominal stress and the upper yield stress is exceeded.

The results obtained from the investigation of the yielding and the brittle fracture behavior in mild steel are shown to be applicable to a case of practical engineering importance. This is accomplished by applying the results to the prediction of the transition temperature of the mild steel when it is used in the standard Izod impact test. The transition temperature so obtained is compared with experimental results and it is found that the predicted transition temperature is slightly higher than that found by experiment. The slight discrepancy between theory and experiment is explained in the light of the assumptions made in the theoretical analysis.

The following general conclusions can be made on the basis of the results presented in this thesis:

1) Brittle fracture in notched specimens of mild steel is initiated when a critical tensile stress is attained. This critical tensile stress is reached after limited plastic deformation has occurred beneath the notch. The tensile stress is a maximum at the interface between the regions of elastic and plastic behavior directly beneath the notch, presumably at the position where the brittle crack originates.

2) The occurrence of general yielding and hence ductile behavior is governed by the applied load and the upper yield stress, as determined from simple tension tests. Apparently in the case of yielding beneath notches, full scale or general yielding occurs in an abrupt manner when a critical value of the ratio between the nominal applied stress and the upper yield stress is exceeded.

3) A transition from ductile to brittle behavior will occur when two conditions are simultaneously satisfied. First, the critical value of the ratio between the nominal stress and upper yield stress (to produce general yielding) is reached. Second, this occurs at the instant the critical value of the tensile stress to produce brittle fracture is attained. Hence the ability of a material to exhibit a transition temperature is due to the dependence of the upper yield stress on the rate of stress application and temperature.

4) The rate and temperature dependence of the upper yield stress has been shown to explain the transition phenomenon. However, the rate and temperature effect on the upper yield stress has been quantitatively explained on the same basis as the delayed yield phenomenon. The latter is observed to occur in the same metals that exhibit a transition temperature. Hence, it is in this manner that delayed yielding and ductile to brittle transition are connected.

5) Finally, as a consequence of this investigation, it is concluded that only those materials which exhibit a distinct yield point will also exhibit a clear transition from ductile to brittle behavior. This latter conclusion has not been directly verified, but to the best of the author's knowledge it agrees with known experimental results.

Further investigations are needed in order to obtain a complete understanding of the brittle fracture phenomenon. Investigations similar to the one presented in this thesis should be undertaken for materials other than mild steel. Also, a fundamental or atomistic understanding of the initiation and propagation of a brittle crack is needed.

APPENDIX

1. Boundary Conditions on the Stress Function and its Derivatives for Conditions of Plane Strain

A portion of the boundary of a material is indicated by the surface, s, shown in Figure 40. Let the traction forces on the surface acting in the x and y direction be denoted by X and Y, respectively. Consider an element of the material bounded by the sides dx, dy and an increment of the surface, ds. The equilibrium of this element requires that the following relations are satisfied:

$$dX = -\sigma_x dy + \tau_{xy} dx$$
$$dY = \sigma_y dx - \tau_{xy} dy \quad , \tag{A1}$$

where

dX = the increment of the traction force in the x direction along the surface increment ds,

dY = the increment of the traction force in the y direction along the surface increment ds,

σ_x = the direct stress on the positive x face of the element in the positive x direction,

σ_y = the direct stress on the positive y face of the element in the positive y direction,

and τ_{xy} = the shear stress which is taken to be positive if it acts on the positive x face of the element in the positive y direction.

The stresses may be expressed in terms of derivatives of the stress function, Ψ, by means of Equation 9 which shows that

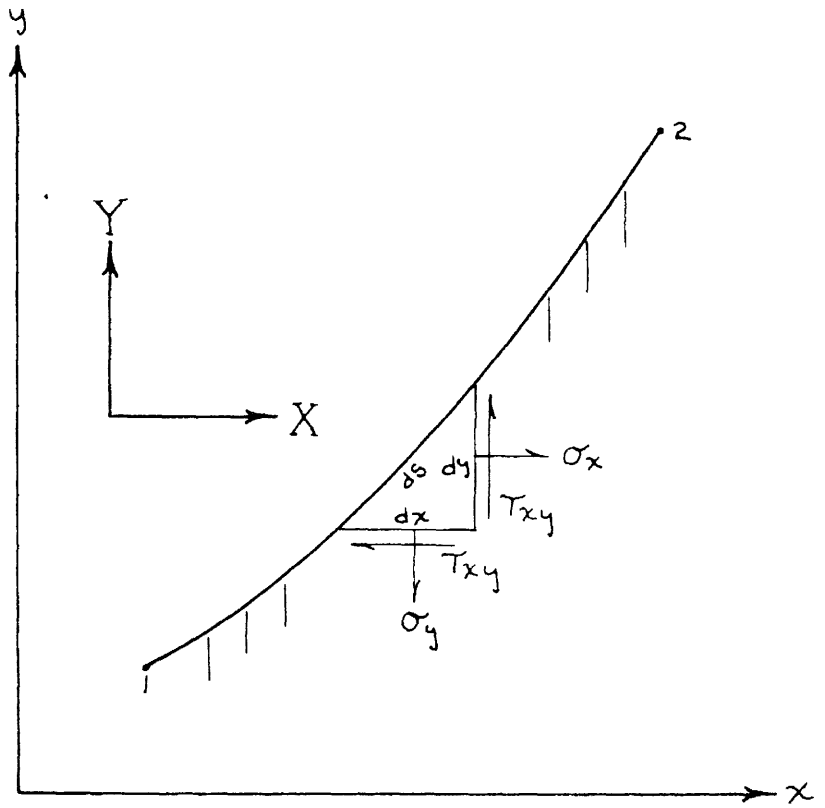

Figure 40., Typical Portion of a Loaded Boundary

for plane strain

$$\sigma_y = \frac{\partial^2 \Psi}{\partial x^2}, \qquad \sigma_x = \frac{\partial^2 \Psi}{\partial y^2}, \quad - \tau_{xy} = \frac{\partial^2 \Psi}{\partial x \partial y} .$$

Hence Equation A1 may be expressed in the form

$$\begin{aligned} dX &= - \left(\frac{\partial^2 \Psi}{\partial y^2}\right) dy - \left(\frac{\partial^2 \Psi}{\partial x \partial y}\right) dx = -d \left(\frac{\partial \Psi}{\partial y}\right) \\ dY &= \left(\frac{\partial^2 \Psi}{\partial x^2}\right) dx + \left(\frac{\partial^2 \Psi}{\partial x \partial y}\right) dy = d \left(\frac{\partial \Psi}{\partial x}\right) , \end{aligned} \tag{A2}$$

where $d(\partial \Psi / \partial y)$ = the total derivative of the partial derivative of the stress function with respect to y,

and $d(\partial \Psi / \partial x)$ = the total derivative of the partial derivative of the stress function with respect to x.

Equation A2 may be integrated between the points 1 and 2 on the boundary surface S shown in Figure 40. This integration yields the following relations:

$$\begin{aligned} X_{12} &= \frac{\partial \Psi}{\partial y}\bigg|_1 - \frac{\partial \Psi}{\partial y}\bigg|_2 \\ Y_{12} &= \frac{\partial \Psi}{\partial x}\bigg|_2 - \frac{\partial \Psi}{\partial x}\bigg|_1 , \end{aligned} \tag{A3}$$

where X_{12} = the integrated traction force in the x direction between the points 1 and 2 on the boundary surface S,

Y_{12} = the integrated traction force in the y direction between the points 1 and 2 on the boundary surface S,

and the quantities on the right of Equation A3 are to be interpreted as being evaluated at the particular point 1 or 2.

The change in the stress function, Ψ, between points 1 and 2 may be calculated on the surface S provided the first derivatives of the stress function and the traction forces on the boundary are known. The total derivative of the stress function, $d\Psi$, may be written as

$$d\Psi = \frac{\partial \Psi}{\partial x} \frac{dx}{ds} ds + \frac{\partial \Psi}{\partial y} \frac{dy}{ds} ds .$$

The total derivative of the stress function may be integrated by parts with the result

$$\Psi_2 - \Psi_1 = x_2 \frac{\partial \Psi}{\partial x}\bigg|_2 - x_1 \frac{\partial \Psi}{\partial x}\bigg|_1 + y_2 \frac{\partial \Psi}{\partial y}\bigg|_2 - y_1 \frac{\partial \Psi}{\partial y}\bigg|_1 - \int_1^2 [xY - yX]\, ds, \tag{A4}$$

where x_1 and x_2 = the values of the coordinate x evaluated at the points 1 and 2 respectively,

y_1 and y_2 = the values of the coordinate y evaluated at the points 1 and 2 respectively,

and the integral appearing in the equation is to be integrated between the limits corresponding to the coordinates of points 1 and 2.

The integral appearing in Equation A4 is merely the moment about the origin of coordinates produced by the traction forces between points 1 and 2 in Figure 40. Hence if the traction forces are known and if the values of the stress function and its first derivation are known at point 1, the values of the stress function and its first derivatives at the point 2 may be computed by means of Equations A3 and A4.

As an example, consider the case of a free boundary. The traction forces, in this case, are zero. Hence Equation A3 yields the result

$$\left.\frac{\partial \Psi}{\partial y}\right|_1 = \left.\frac{\partial \Psi}{\partial y}\right|_2 = \text{constant} = C_1$$

$$\left.\frac{\partial \Psi}{\partial x}\right|_1 = \left.\frac{\partial \Psi}{\partial x}\right|_2 = \text{constant} = C_2 \, .$$

Equation A4 may then be used with the result

$$\Psi_2 = \Psi_1 + (x_2 - x_1)C_2 + (y_2 - y_1)C_1 \, .$$

The value of the stress function and its derivation at the point 1 may be arbitrarily chosen. This selection should be done in such a way as to simplify the boundary condition as much as possible so as to simplify the use of the relaxation method in the solution to the problem.

2. Summary of the Results of Neuber's Elastic Stress Analysis

(a) Plane Hyperbolic Notch in Tension

Neuber's results (23) are most conveniently expressed in terms of ellipsoidal coordinates, which are related to the x, y coordinates shown in Figure 6 by the relations

$$\frac{x}{a} = \sinh u \, \frac{\cos v}{\sin v_o} \qquad (A5)$$

$$\frac{y}{a} = \cosh u \, \frac{\sin v}{\sin v_o} \, .$$

The surfaces v = constant are hyperbolas whose axes coincide with the axes of the hyperbola forming the notch surface. The notch

surface is given by the surface $v = v_o$. The angle v_o is the angle between the x axis and the asymptote to the notch surface. The surfaces u = constant are ellipses which are orthogonal to the surfaces v = constant. The degenerate ellipse u = 0 coincides with the plane of the minimum section x = 0. The radius of curvature at the root of the notch, ρ, is given by the expression

$$\rho = \frac{a}{\tan^2 v_o} \quad . \tag{A6}$$

The stress function, Ψ, is given by

$$\Psi = - \frac{a^2 \sigma_n}{\sigma_{yd}} \left[1 - \cosh u \, \frac{(v \sin v + \sin^2 v_o \cos v)}{(v_o \sin v_o + \sin^2 v_o \cos v_o)} \right] \tag{A7}$$

where σ_n is the nominal or average stress on the minimum cross-section. The stresses are given by:

$$\sigma_u = \frac{A}{h^2} \cosh u \cos v \left(2 + \frac{\cos^2 v_o - \cos^2 v}{h^2}\right) \tag{A8}$$

$$\sigma_v = \frac{A}{h^4} \cosh u \cos v \, (\cos^2 v - \cos^2 v_o) \tag{A9}$$

$$\tau_{uv} = \frac{A}{h^4} \sinh u \sin v \, (\cos^2 v_o - \cos^2 v) \tag{A10}$$

where

$$h^2 = \sinh^2 u + \cos^2 v \, ,$$

and

$$A = \frac{\sigma_n \sin v_o}{(v_o + \sin v_o \cos v_o)} \quad .$$

(b) An Hyperboloid of Revolution Subjected to Axial Tension

The results are again most conveniently expressed in terms of ellipsoidal coordinates related to the x, y coordinates by the relations

$$\frac{x}{a} = \sinh u \frac{\cos v}{\sin v_o}$$

$$\frac{y}{a} = \cosh u \frac{\sin v}{\sin v_o} \cos w \ , \tag{A11}$$

where a, u, v, and v_o have the same meaning as described for the plane hyperbolic notch, and the surface w = constant are planes containing the axis of rotational symmetry.

The intersection of planes w = constant with the external surface of the body are hyperbolas whose asymptotes make angles of v_o with the axis of rotational symmetry of the body.

The elastic stresses are given by

$$\sigma_u = \frac{1}{h^2}\left\{A\tanh^2 u + B\frac{\cos v}{\cosh^2 u} + C\left[-2-\alpha+\frac{1}{\cosh^2 u}\right]\cos v\right\} + \frac{\cos v}{h^4}\left\{-A+B+C\cos^2 v\right\} \tag{A12}$$

$$\sigma_v = \frac{1}{h^2}\left\{-A\frac{\cos v}{(1+\cos v)} + (\alpha-1)C\cos v\right\} + \frac{\cos v}{h^4}\left\{A-B-C\cos^2 v\right\} \tag{A13}$$

$$\sigma_w = \frac{1}{h^2}\left\{A\left[-\tanh^2 u + \frac{\cos v}{(1+\cos v)}\right] - B\frac{\cos v}{\cosh^2 u} + C\left[\alpha-1-\frac{1}{\cosh^2 u}\right]\cos v\right\} \tag{A14}$$

$$\tau_{uv} = \frac{1}{h^2}\tanh u \sin v\left\{-\frac{A}{(1+\cos v)} + (\alpha-1)C + \frac{1}{h^2}\left[-A+B+C\cos^2 v\right]\right\} \tag{A15}$$

and

$$\tau_{vw} = \tau_{uw} = 0 \qquad \text{(A16)}$$

where $A = (a-1)(1 + \cos v_o)C$,

$$B = A - C \cos^2 v_o ,$$

$$C = -\frac{\sigma_n}{2} \frac{(1 + \cos v_o)}{[1+(2-a)\cos v_o + \cos^2 v_o \ ]} ,$$

σ_n = average stress over the minimum cross-section,

$a = 2(1 - \nu)$, where ν = Poisson's ratio,

and

$$h^2 = \sinh^2 u + \cos^2 v .$$

The stresses acting on the minimum section are obtained by setting $u = 0$ in Equations A12 through A16. For this case σ_u becomes the axial tension stress, σ_z, σ_v the radial stress, σ_r, and σ_w the circumferential stress σ_θ. The shear stress is zero on this section.

3. Details of Notch Shape Measurement and the Determination of the Root Radius of Curvature

An optical comparator was used to obtain measurements of the shape of the hyperboloid cross-section of several of the notches produced. The x and y coordinates of the notch surface could be obtained to within 0.0001 in. with this instrument. A comparison between the shape of the ideal notch for a value of $a/\rho = 15$ and $a = 0.150$ in. with measurements of an actual notch is given in

Figure 16. The deviation of the actual notch shape from the ideal or theoretical shape is due primarily to the finite thickness of the edge of the grinding wheel used to generate the notches.

The critical characteristic of the notch shape which determines how closely the maximum concentrated stress in the specimen approximates the theoretical value for the ideal notch is the root radius of curvature of the notch, ρ. A special method of plotting the results of the measurements of actual notch shapes was employed to determine this radius of curvature. This method is based upon the following geometrical considerations. The radius of a circle which passes through the three points ($y = a$, $x = 0$), ($y = y_1$ $x = x_1$), and ($y = y_1$, $x = -x_1$) on the actual notch contour is given by

$$r_1 = \frac{(y_1-a)^2 + x_1^2}{2(y_1-a)} \tag{A17}$$

The equation of the ideal notch contour is

$$y^2 - x^2 \tan^2 v_o = a^2 \tag{A18}$$

which may be shown from Equation A11 for the case $w = 0$ and $v = v_o$. Thus the radius of such a circle in the case of an ideal hyperbolic notch would be

$$r = \frac{1}{2}(y - a) + \frac{1}{2}\frac{(y + a)}{\tan^2 v_o} \tag{A19}$$

which may be shown by eliminating x from Equation A17 by the use of Equation A18. In the limit as $y \to a$, r goes to the radius of curvature, ρ, at the root of the notch, given by Equation A6.

Measured values of the coordinates x, y, of the notch shape were used to compute the radii, r_1, for small values of $(y_1 - a)$, using Equation A17. These values for r_1 were then plotted as a function of $(y_1 - a)$. The value of r_1, obtained by extrapolating the straight line of best fit with the plotted points is then the actual root radius of curvature of the notch, ρ.

REFERENCES

1. Shank, M. E., "Brittle Failure of Steel Structures - Theory, Practice and Future Prospects", Metal Progress, Vol. 66, 1954, No. 3, p. 83; No. 4, p. 120; Vol. 67, 1955, No. 6, p. 111.

2. Wood, D. S., and Clark, D. S., "The Influence of Stress and Temperature on the Time for the Initiation of Plastic Deformation in an Annealed Low Carbon Steel", First Technical Report under Contract N6onr-24418, Project Designation NR031-285, California Institute of Technology, June 1949.
Also:
Wood, D. S., and Clark, D. S., "The Influence of Temperature Upon the Time Delay for Yielding in Annealed Mild Steel", Trans. Amer. Soc. for Metals, Vol. 43, p. 571, 1951.

3. Wood, D. S. and Clark, D. S., "Delayed Yielding in Annealed Mild Steel with Special Reference to Yielding at Low Temperature", Fourth Technical Report submitted to Office of Naval Research, Contract N6onr-24418, Project Designation NR031-285, California Institute of Technology, December 1951.

4. Hendrickson, J. A., Wood, D. S., and Clark, D. S., "The Initiation of Discontinuous Yielding in Ductile Molybdenum", Ninth Technical Report Submitted to Office of Naval Research, Contract N6onr-24418, Project Designation NR031-285, California Institute of Technology, October 1954.
Also:
Hendrickson, J. A., Wood, D. S., and Clark, D. S., "The Initiation of Discontinuous Yielding in Ductile Molybdenum", Trans. Amer. Soc. for Metals, Vol. 48, p. 540, 1956.

5. Kramer, I. R. and Maddin, R., "Delay Time for the Initiation of Slip in Metal Single Crystals", Jour. of Met., Vol. 4, p. 197, 1952.

6. Tien-Shih Liu, Kramer, I. R. and Steinberg, M. A., "The Delay-Time Phenomenon in Metal Single Crystals", Acta Metallurgica, Vol. 4, No. 4, p. 364, July 1956.

7. Felbeck, D. K. and Orowan, E., "Experiments on Brittle Fracture of Steel Plates", The Weld. Journ. Res. Supp., Vol. 34, No. 11, p. 570-s, November 1955.

8. Morrison, J. L. M., "The Influence of Rate of Strain in Tension Tests", The Engineer, Vol. 158, p. 183, 1934.

9. Wood, D. S. and Clark, D. S., "Delayed Yield in Annealed Steels of very Low Carbon and Nitrogen Content , Second Technical Report under Office of Naval Research, Contract N6onr-24418, Project Designation NR031-285, California Institute of Technology, August 1950.

10. Vreeland, T., Jr., Wood, D. S. and Clark, D. S., "Pre-Yield Plastic and Anelastic Microstrain in Low-Carbon Steel", Sixth Technical Report under Office of Naval Research, Contract N6onr-24418, Project Designation NR031-285, California Institute of Technology, September 1952.
Also:
Vreeland, T., Jr., Wood, D. S. and Clark, D. S., "Pre-Yield Plastic and Anelastic Microstrain in Low-Carbon Steel", Acta Metallurgica, Vol. 1, p. 414, July 1953.

11. Vreeland, T., Jr., and Wood, D. S., "A Comparison between Dislocation Theory and Experimental Measurements of Delayed Yield in Steel", Eighth Technical Report under Office of Naval Research, Contract N6onr-24418, Project Designation NR031-285, California Institute of Technology, April 1954.

12. Cottrell, A. H. and Bilby, B. A., "Dislocation Theory of Yielding and Strain Aging of Iron", Proc. Phys. Soc., London, Part A., Vol. 62, p. 49, 1949.

13. Frank, F. C. and Read, W. T., "Multiplication Process for Slow Moving Dislocations", Phys. Rev., Vol. 79, p. 722, 1950.

14. Cottrell, A. H., "The Yield Point in Single Crystal and Polycrystaline Metals", Symposium on the Plastic Deformation of Crystalline Solids, Mellon Institute, 1950.

15. Vreeland, T., Jr., Wood, D. S. and Clark, D. S., "A Study of the Mechanism of the Delayed Yield Phenomenon", Third Technical Report under Office of Naval Research, Contract N6onr-24418, Project Designation NR031-285, California Institute of Technology, September 1951.
Also:
Vreeland, T., Jr., Wood, D. S., and Clark, D. S., "A Study of the Mechanism of the Delayed Yield Phenomenon", Trans. Amer. Soc. for Metals, Vol. 45, p. 620, 1953.

16. Hendrickson, J. A., Wood, D. S., and Clark, D. S., "The Influence of Temperature on Pre-Yield Plastic and Anelastic Microstrain in Low-Carbon Steel", Tenth Technical Report under Office of Naval Research, Contract N6onr-24418, Project Designation NR031-285, California Institute of Technology, June 1955.
Also:
Hendrickson, J. A., Wood, D. S., and Clark, D. S., "The Influence of Temperature on Pre-Yield Plastic and Anelastic Microstrain in Low-Carbon Steel", Acta Metallurgica, Vol. 4, p. 593, November 1956.

17. Fisher, J. C., "Application of Cottrell's Theory of Yielding to Delayed Yielding in Steel", Trans. Amer. Soc. for Metals, Vol. 47, p. 451, 1955.

18. Köster, W., "Die Temperaturäbhangigkeit des Elastizitatsmoduls Reiner Metalle", Zeitschrift für Metalkunde, Vol. 39, p. 1, 1948.

19. Yokobori, T., "The Cottrell-Bilby Theory of Yielding in Iron", Phys. Rev., Vol. 88, Series 2, p. 1423, 1952.

20. Campbell, J. D., "The Dynamic Yielding of Mild Steel", Acta Metallurgica, Vol. 1, p. 706, November 1953.

21. Cottrell, A. H., "Dislocations and Plastic Flow in Crystals", Oxford at the Clarendon Press, p. 142, 1953.

22. Crussard, et al., "A Study of Impact Test and the Mechanics of Brittle Fracture", Journ. of the Iron and Steel Inst., Vol. 183, Part 2, p. 146, June 1956.

23. Neuber, H. (Berlin: Julius Springer, 1937). "Theory of Notch Stresses: Principles for Exact Stress Calculations". David Taylor Model Basin Trans. No. 74.

24. Southwell, R. V., "Relaxation Methods in Theoretical Physics", Oxford at the Clarendon Press, 1946.

25. Allen, D. N. de G., and Southwell, Sir Richard, "Relaxation Methods Applied to Engineering Problems; XIV. Plastic Straining in Two-Dimensional Stress-Systems", Roy. Soc. of London-Phil. Trans. Series A, Vol. 242, p. 379, 1949.

26. Hill, R., "The Mathematical Theory of Plasticity", Oxford, p. 245, 1950.